3-17-2008

An Experimental Technique for Developing Intermediate Strain Rates in Ductile Metals

Hugh E. Gardenier IV

An Experimental Technique for Developing Intermediate Strain Rates in Ductile Metals

THESIS

Hugh E. Gardenier IV, Captain, USAF

AFIT/GAE/ENY/08-M10

DEPARTMENT OF THE AIR FORCE
AIR UNIVERSITY

AIR FORCE INSTITUTE OF TECHNOLOGY

Wright-Patterson Air Force Base, Ohio

The views expressed in this thesis are those of the author and do not reflect the official policy or position of the United States Air Force, Department of Defense, or the United States Government.

AFIT/GAE/ENY/08-M10

An Experimental Technique for Developing Intermediate Strain Rates in Ductile Metals

THESIS

Presented to the Faculty

Department of Aerospace Engineering

Graduate School of Engineering and Management

Air Force Institute of Technology

Air University

Air Education and Training Command

In Partial Fulfillment of the Requirements for the

Degree of Master of Science in Aeronautical Engineering

Hugh E. Gardenier IV, B.S.E.M.

Captain, USAF

March 2008

AFIT/GAE/ENY/08-M10

An Experimental Technique for Developing Intermediate Strain Rates in Ductile Metals

Hugh E. Gardenier IV, B.S.E.M.
Captain, USAF

Approved:

/signed/	17 Mar 2008
Anthony N. Palazotto, PhD (Chairman)	date
/signed/	17 Mar 2008
William P. Baker, PhD (Member)	date
/signed/	17 Mar 2008
Robert A. Brockman, PhD (Member)	date

Abstract

Quantifying the strain-rate sensitive dynamic properties of structural materials is an important area of research in the solid mechanics field. Property evaluation is typically accomplished using dynamic tests which involve rapid loading or impact of specimens. In these tests, inertial forces and wave propagation make it difficult to accurately record the material response to a loading condition at an equivalent location. Furthermore, these tests typically generate high strain rates (in excess of $10^3\ s^{-1}$) and an experimental method for generating rates of strain in the intermediate strain rate regime which is relatively simple, low cost, and reliable is still lacking. This research effort develops an experimental technique for generating tensile plastic strain rates up to $10^2\ s^{-1}$ in ductile metals. The technique relies on an impact from a load cell instrumented drop weight machine capable of delivering a suitable impact velocity and energy to globally deform a slotted beam specimen. At impact, a state of plastic uniaxial tensile stress is created in the ligament underneath a slot. The ligament is instrumented with an electrical-resistance strain gauge, and the strain history from the gauge is measured and stored in a digital oscilloscope. The Johnson-Cook constitutive equation is assumed to reflect the material behavior and its parameters are determined through a matching of the experimental strain history with a finite element simulation.

Acknowledgements

I would like to express my sincere appreciation to my thesis advisor, Dr. Anthony Palazotto, for his unwavering support and dedication to the completion my thesis. His knowledge and support proved to be invaluable for my success. Next, I would like to thank Kevin Poormon and the Impact Physics Team at the University of Dayton Research Institute for their help in developing a measurement system for this research. I would also like to thank the folks at the AFRL Structural Science Center including Brian Smyers and Richard Wiggins for their dedication and assistance in operating and maintaining the Dynatup throughout these tests. Furthermore, I would like to express my thanks and appreciation to Capt Reid Larson for his help during this research. His hard work and insight were invaluable to the success of this work. Last, but not least, I would like to thank my parents, brother, and most of all my wife for their endless hours of motivation, support, and help.

Hugh E. Gardenier IV

Table of Contents

Page

List of Figures

List of Tables

List of Symbols

List of Abbreviations

An Experimental Technique for Developing Intermediate Strain Rates in Ductile Metals

I. Introduction

1.1 Introduction to Slotted Beam Technique

The threat of impact to aircraft or spacecraft, in light of the Space Shuttle Columbia disaster and the always existent possibility of bird impact or turbine engine blade separation, places increased demands on aerospace structural materials [35] [7]. Impact loading conditions dynamically load a structure and typically result in yielding of the material and plastically deform the structure [51]. In an effort to quantify the point at which yielding occurs and the magnitude of resulting plastic deformation, research has been undertaken to quantify a material's dynamic mechanical properties [33]. However, while quasi-static testing has been used extensively to determine mechanical properties such as Young's Modulus, yield strength, ultimate strength, and elongation at failure, methods to quantify the affect of dynamic loading on the mechanical properties of structural materials are not as well developed. The dynamic properties of a material may be significantly different than the well documented quasi-static properties, and in aerospace structural design quantifying the dynamic behavior of structural materials is essential in predicting the structural response when impacted [10]. While not as established as quasi-static testing, dynamic or impact testing is an important technique for quantifying the dynamic mechanical properties of structural materials, making impact testing an important technique in the study of a material's dynamic behavior [10].

1.1.1 Impact. Impact is characterized by very rapid loading conditions which may cause rate-dependent plastic behavior in a structural material, behavior which cannot be quantified in the static or quasi-static material testing [19]. It has been recognized that the mechanical behavior of materials under conditions of rapid loading and impact differs significantly from the response to static load application [10] [19] [33]. At impact, the rate of loading is many times faster than that of quasi-static loading conditions and the characteristic time of the dynamic event is much smaller than the quasi-static test. These two characteristics of impact create a fundamental difference between the the quasi static loading condition and the dynamic loading condition. In quasi-static loading it can be assumed that the stresses acting on the body are very close to static equilibrium, such that a summation of the forces acting on the body would be close to zero and the state of stress within the body is approximately constant [33]. This assumption cannot be made in the dynamic loading condition, and at a high rate of loading the stress acting at one part of the body has not yet been experienced by other parts of the body and travels through the body in the form of waves [33]. This difference between quasi-static and impact conditions make it much more difficult to quantify the mechanical behavior of materials at high rates of loading.

1.1.2 Impact Testing. Significant work in the field of impact testing did not begin until the end of World War II when the discovery of loading rate dependence on mechanical properties sparked interest in the study of rate dependent behavior [10] [33]. Since this discovery, impact testing has received a great deal more attention, with the majority of impact tests conducted to serve one of three purposes [19];

1. To provide criteria for the selection of engineering materials for service conditions involving dynamic loads
2. To yield further information about the fundamental mechanisms producing plastic deformation, flow, and fracture

3. To establish dynamic stress-strain relations which permit an explicit comparison with the corresponding properties in static loading tests where strain rates are normally of the order of $10^{-3}\,s^{-1}$

However, reliable test techniques over a wide range of strain rates are not fully developed [5]. Two major difficulties in the development of impact tests are the increased significance of inertial forces and wave propagation, both of which make the accurate measurement of load and deformation at an equivalent point on a specimen challenging. Inertial forces are forces created by the acceleration of the mass of a body. At low rates of loading the inertial forces can be assumed to negligible due to the small accelerations created by loading the specimen slowly. However, in impact testing a specimen will be rapidly accelerated when impacted or rapidly loaded by a test apparatus. At strain rates of $10^2\,s^{-1}$ and above, the inertial forces can no longer be neglected and must be accounted for in the collection of load data. In elevated strain rate tests, large transient oscillations in measurement equipment are generated due to inertial effects at impact, making it difficult to measure both the yield point and the low-strain behavior in the specimen [22] [19]. Furthermore, at higher rates of loading the stresses are no longer constant throughout the specimen but rather travel through the specimen in the form of waves. Depending on the magnitude of the loading and the size and geometry of the specimen, different types of waves and wave velocities will be generated, which must be taken into account for accurate load and elongation measurements. Wave propagation effects become important above strain rates of $10^2\,s^{-1}$ and must be considered since the state of stress in a specimen can no longer be assumed as constant [36].

In impact testing, energy, velocity, and strain rate are all important characteristics in defining an impact condition. The kinetic energy equation is an established relationship in impact problems due to the relation of energy to the velocity of the impactor [33]. Kinetic energy is defined as,

Table 1.1: Characteristics of Low and High Velocity Impact [36]

	LOW VELOCITY	**HIGH VELOCITY**
Extent of Deformation	Global	Local
Loading/Response Time	Milliseconds-Seconds	Sub-milliseconds
Strains	0.5-10%	$> 60\%$
Strain Rates	10^{-2} - 10^{1} s^{-1}	$> 10^{3}$ s^{-1}

$$E = \frac{1}{2}mv^2 \tag{1.1}$$

where E is the kinetic energy, m is the mass of the impactor, and v is the velocity of impactor. Clearly it can be observed that the kinetic energy of the impactor increases with the square of its velocity. Velocity therefore has a significant effect on the force of the impact [33]. Impact tests such as the Charpy Impact tests are purely comparative tests which use energy to fracture a specimen as the primary criterion in each test [19]. The energy equation illustrates that energy will be dependent on both the mass and velocity of the object and often the impact condition will be defined only by velocity in two categories, low velocity and high velocity. Table 1.1 summarizes the differences between these two categories.

Velocity of the impactor will affect the extent of deformation at impact; low velocities will result in global deformation and high velocities will result in less global deformation and more local deformation. The effects of velocity on the extent of deformation of a cantilevered beam impacted at its free end are shown in Figure 1.1 [36]. Evidently, as the velocity of the impactor increases, the area in the immediate vicinity of the impact site is subjected to an increasing amount of local deformation while the rest of the beam experiences a decreasing amount of global deformation further away from the impact site.

As velocity is increased the local strain rates continue to increase until material separation results and the beam is perforated by the projectile. Local deformation is a characteristic of both low and high velocity impact while global deformation

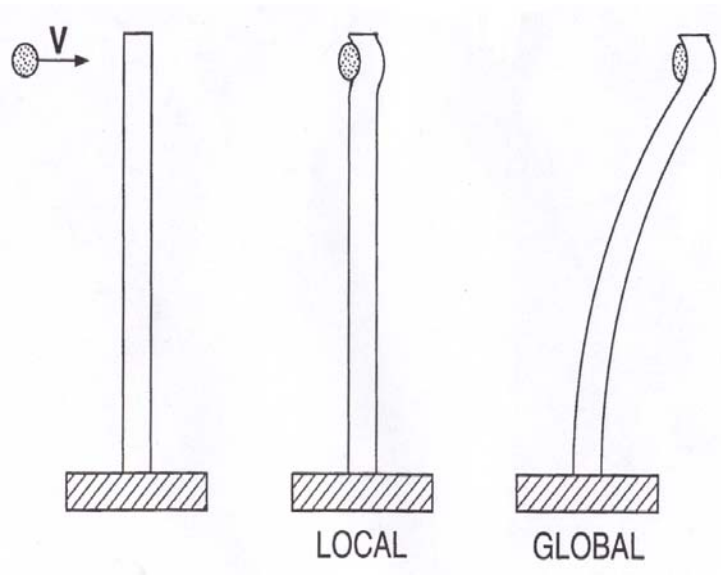

Figure 1.1: Local and Global Response of a Cantilevered Beam to Impact [36]

is exclusive to low velocity impact. The range of strain rates for different loading conditions for both low velocity and high velocity and additional phenomenological characteristics are defined in Table 1.1. Strain rate can also be an appropriate measure to characterize the rate of loading in impact tests, and it is commonly used to characterize the rate of loading in tests like the Split Hopkinson Pressure Bar (SHPB) test. When using strain rate to characterize the rate of loading, velocity remains a primary factor in the magnitude of strain rates generated at impact.

As strain rate increases, the mechanical properties of most materials demonstrate a behavior that is strain rate dependent [19]. Quantifying this strain rate dependence is necessary in determining the dynamic plastic behavior of structures. The intermediate strain rate range, 10 s^{-1} to 100 s^{-1}, is the range in which rate dependence effects begin to emerge and therefore is an important region of study for materials research [10] [16]. Furthermore, the intermediate strain is of significance in some metal processing applications and therefore is an important strain rate range for industrial and machining operations [51]. Strain rate effects are not captured by the static stress strain curve, so stress strain curves developed from load and elonga-

tion data measured from rapid loading and impact testing methods are necessary to reveal these effects. An investigation of mechanical properties at different strain rates with a number of experimental of methods must be made to quantify a material's dynamic behavior. Depending on the objective, the most appropriate experimental method can be selected to satisfy the purpose of the material investigator. However, the investigator must clearly understand both the objective and the limitations of the impact test being used. For example, a fundamental problem with some impact tests including the Charpy Impact test is that recorded data provides properties of little or no value in the development of the rate dependent constitutive relationships. Instead these tests provide qualitative data for researchers to determine the survivability of materials under certain conditions or quantitative data, which has little application outside of the specific testing application [19]. Other tests have been developed to provide quantitative data about the loading and elongation of a specimen. In these tests, great care must be taken to account for the effects of dynamic loading to ensure the accurate measurement of load and elongation at an equivalent location. One major difficulty in these dynamic tests is analyzing the state of stress in the test specimen. Commonly, the test setup is created such that a one-dimensional state of stress dominates the test specimen and the stress state becomes much less complex than a two or three dimensional stress state. This is the primary driver for the axial impact of rods in the SHPB test. The stress waves propagated during this test are assumed to travel longitudinally through the bars, which allows for the assumption of a uniaxial stress state in the specimen and the usage of the one-dimensional wave equation in the analysis of experimental data. As strain rates increase, the state of stress in the test specimen may become so complex that it is no longer appropriate to assume a state of uniaxial stress and a more appropriate assumption is a state of uniaxial strain [23]. Understanding the state of stress in the specimen is an important consideration in impact testing and will constrain the types of impact conditions which can be tested [23].

In the process of quantifying the mechanical properties of a material, it is typically desired to develop a constitutive relationship which predicts the material behavior under any state of loading. A constitutive model typically contains some general form of the constitutive equation with material dependent constants, which are determined experimentally at a range of loading conditions and then published in the literature. Some of the more commonly documented metals and metal alloys, include aluminum, titanium, and steel. These metals and alloys have many aerospace structural applications which makes the quantification of their mechanical properties important to both researchers and aerospace designers. Furthermore, these metals and alloys exhibit a significant degree of ductility, a measure of the materials ability to absorb energy. In impact, ductility is an important material property because of the significant plastic deformations which will result before material fracture in a ductile material [51]. In application, the use of plastic design methods in structural engineering has led to the requirement that the plastic behavior of structural elements must be understood and an awareness of the micro-mechanisms responsible for the macroscopic plastic behavior of these metals is important in structural design [10].

1.1.3 Experimental Methods. Experimental methods are necessary which can measure the material response at elevated loading rates. The requirements placed on the measurement equipment in these methods are important factors to consider. The objective of experimental measurement is to assign a measured value to some physical variable, thus characterizing the response of a system to an input. Depending on the objective of the test, an appropriate measurement system must be developed to collect the specimen response for further analysis. A diagram of the components of a general measurement system is contained in Figure 1.2 [45].

Most measurement systems contain a sensor, a transducer, a conditioner and amplifier, and a data acquisition device. A sensor by definition is a device which measures the physical quantity and converts it into a signal which can then be measured [17]. Signals are usually generated in three forms: electrical, mechanical, or

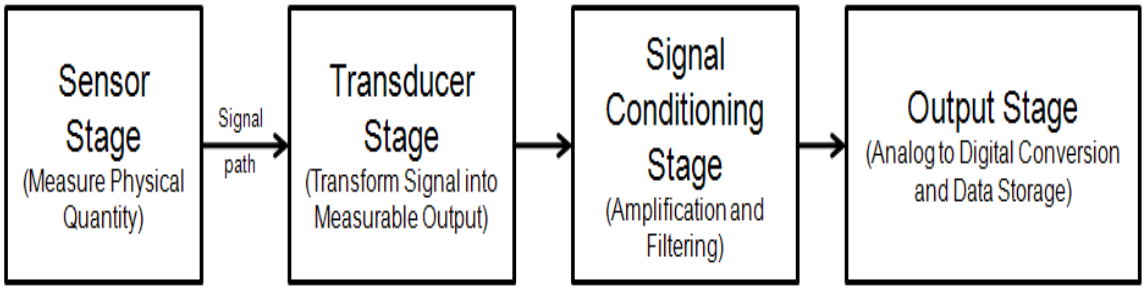

Figure 1.2: Components of a General Measurement System [45]

optical. The device which transforms the signal into a measurable output is the transducer. A sensor and transducer may be separate elements or they may be embedded together into one unit. Sensor selection begins with an examination of the sensor's input/output characteristics. These characteristics include operational bandwidth, frequency response, sensor sensitivity and accuracy, voltage supply requirements, physical dimensions, weight, material, type of output, and cost. Transducer selection must be made with a consideration for the physical variable which is to be measured, the environment in which the physical variable is to be measured, and the output of the transducer. A common sensor/transducer combination used to measure the strain in a specimen is the electrical resistance strain gage combined with a Wheatstone bridge. Depending on the transducer used in testing, conditioning equipment may be necessary to amplify the output of the transducer. This is the case with the low magnitude output of strain gages and an amplifier is generally needed to boost the magnitude of the voltage signal so that it may be measured. An important consideration in the selection of conditioning equipment for some tests is the frequencies of any measured signals. This is important in an attempt to prevent the filtering of desired frequencies, while at the same time maintaining the capability to filter undesired frequencies. This consideration is not as important for impact experiments, since all the frequencies of the specimens are excited at impact and therefore filtering of the impulse signal is not appropriate. Finally, the rate at which data can be sampled by the data acquisition device during an experiment is important in providing an accurate view of the

actual physical condition of the specimen. If the rate of data sampling is too slow then all of the characteristics of the specimen response may not be collected and an accurate picture of the physical situation may not be collected. This phenomenon is exacerbated by the brief duration of an impact event, and makes the capability to sample data at a high rate important in impact experiments. Digital oscilloscopes, which can typically sample at rates over 1 $\frac{GS}{s}$ or giga-samples per second, are used to acquire data in impact tests [19] [2]. If data cannot be sampled at a fast enough rate then valuable signal information will be lost in the sampling of the analog signal and conversion to digital data.

1.1.4 Slotted Beam Technique. Current impact test methods for characterizing the dynamic material response require extensive test equipment and can be expensive to perform [29]. These tests include SHPB test at high strain rates and servo-hydraulic and pneumatic machines at intermediate strains. The ability to investigate the dynamic response of structural metals with a relatively inexpensive test apparatus and a simple test procedure would fulfill a significant need in the study of dynamic material behavior [47]. In an effort to create this capability, a new experimental method for developing a state of uni-axial tensile stress at elevated strain rates in ductile metals has been created. This experimental method relies on a transverse impact from a load cell instrumented, drop weight apparatus at the center of a slotted beam specimen subjected to a fixed-fixed boundary condition, and ABAQUS, a three dimensional finite element program. At impact, a sufficient amount of energy is delivered to plastically deform the metal beam specimen. Before testing, a slot is machined in the beam through Electrical Discharge Machining EDM. The EDM process removes material directly below the impact site leaving a slot in the beam specimen and a thin ligament at the bottom of the beam. The slot and the development of plastic hinges at the center and boundaries of the beam during impact stretch the ligament resulting in a state of uniaxial tensile stress. Figure 1.3 provides a schematic of the slotted beam and identifies the location of the uni-axial tensile stress.

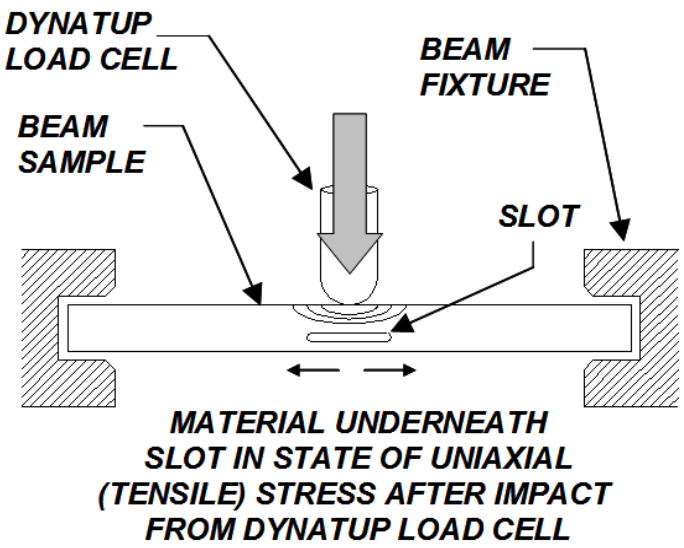

Figure 1.3: Development of Uni-Axial Tensile Stress in Slotted Beam [29]

Instrumenting this location with an electrical resistance strain gage allows the measurement of strain data as the specimen globally deforms and provides a history of the material response to rapid loading. The rate of loading is controlled by increasing or decreasing the velocity of the tup. The strain history at the ligament and impact energy at the top surface of the beam are known for each test, however the stress at the location where the strain history is recorded can not be quantified experimentally. The development of a relationship between the loading at the top of the beam and the stress at the ligament would be complex and difficult to develop due to the complex states of stress in the vicinity of the slot in the beam [4]. Instead a finite element model of the beam impact is developed and the model's output of strain history at the equivalent location as the location measured on the slotted beam can be collected. The finite element method has proven to be a useful tool in the characterization and prediction of material behavior under a wide range of loading conditions [51]. Assuming a constitutive model for the finite element solution, the material constants for the model are determined from the experimental data through a curve fitting procedure. The determined constants are then input into the finite element model

in an attempt to match the experimental strain histories at different strain rates and different states of stress, and an iterative technique is carried out to establish the constants for the associated stress fields. The Johnson and Cook constitutive model defined as [33],

$$\sigma_{eff} = \left(A + B\varepsilon_p^n\right)\left(1 + C\, ln\, \dot{\varepsilon}^*\right)\left(1 - T^{*m}\right) \tag{1.2}$$

where σ_{eff} and ε_p are effective stress and equivalent plastic strain respectively, $\dot{\varepsilon}^*$ $= \dot{\epsilon}/\dot{\epsilon}_0$ is the dimensionless reference plastic strain rate for $\dot{\epsilon}_0 = 1.0$ s^{-1}, and A, B, C, n, and m are material constants. The component of the equation containing T^* incorporate the effects of temperature on the mechanical properties of the material, and for these experiments the effects of temperature are neglected since they will be conducted at room temperature so that the constitutive model in the finite element solution assumes the following form,

$$\sigma_{eff} = \left(A + B\epsilon_p^n\right)\left(1 + C\, ln\, \dot{\epsilon}^*\right) \tag{1.3}$$

where the variables defined previously remain the same but the material constants are reduced to A, B, C, n. The Johnson-Cook equation is a highly useful constitutive model and one of the most widely used equations for constitutive modeling of visco-plastic behavior [33]. Once the material constants for the Johnson-Cook equation are determined and validated at different stress states, dynamic stress-strain curves can be generated.

The objective of this research is to develop the slotted beam technique into a reliable and simple experimental technique for generating a uniaxial tensile state of stress at intermediate strain rates. Then with the aid of a finite element solution generate coefficients for the Johnson-Cook equation for each material tested. The first step in this research is a thorough understanding of impact and impact testing in an effort to correctly select test and measurement equipment capable of measuring the

material response under impact conditions. This also requires an understanding of different types of transducers and data acquisition equipment in an attempt to select the equipment which provides a balance between reliability, cost, and performance. The next step is develop the experimental technique so that experimental data will be collected accurately, and the possibility of noise and error are minimized. In addition, the development of a technique which is easily reproduced is important. Finally, a numerical method will be used to take the experimental data collected and generate a constitutive relationship for three different metals; 1018 Steel, 2024 Aluminum alloy, and Commercially Pure (CP) Titanium.

The remainder of this document is organized such that Chapter 2 presents a detailed discussion of past and present impact test techniques, the issues involved in impact testing, and the experimental equipment which can be used to measure physical characteristics during impact conditions. Following this discussion, Chapter 3 provides the details of the slotted beam experiments including the test equipment used and the procedure for executing all of the tests. Chapter 4 provides the results of the slotted beam experiments including experimental data, finite element model outputs, and the determination of constitutive models for the materials tested. Chapter 5 will present the conclusions gathered from the slotted beam experiments and recommendations for future research using this test apparatus.

II. Theory and Background

2.1 Theory and Background for Slotted Beam Technique

This chapter examines the theory and background for the slotted beam technique to determine the most important issues to consider for experimentation. First, a general overview of impact, emphasizing the differences between quasi-static loading conditions and dynamic loading conditions will be discussed. Then, the impact phenomenon associated with the intermediate strain-rate range will be addressed, which will lead into a conversation of rate-dependent behavior and dynamic plasticity. Next, there will be a theoretical discussion of the transverse impact of a beam, which will be followed by a presentation of past and present impact experimental methods. This dialogue will be limited to methods which are applicable to impact testing in the intermediate strain rate range, in an attempt to provide a broad description of the test methods which are currently available. The chapter will conclude with a description of specific test equipment which is presently used in testing at impact conditions to provide background on the types of test equipment available for use in the slotted beam experimental method.

2.1.1 Impact. The slotted beam relies on the transverse impact from a weighted tup to rapidly load the ligament at the bottom of the specimen in tension. The physical phenomena involved when two bodies collide, *impact*, is fundamentally different than quasi-static loading. In quasi-static loading the assumption of a constant state of stress throughout the majority of the specimen is well accepted [49]. However, when a body is stressed by a suddenly applied load i.e. impact, the deformations and stresses will not be immediately transmitted to all parts of the body, and remote portions of the body will remain undisturbed for some time [23]. Instead of a constant stress in the specimen, the stress travels through the specimen in the form of waves. The sudden or impulsive loading required to create dynamic loading conditions may be generated by a sharp mechanical blow, an explosive's detonation, or impact of a projectile; but regardless of the method of application, the generated stress disturbances have the same properties [23]. This fundamental difference between how stress

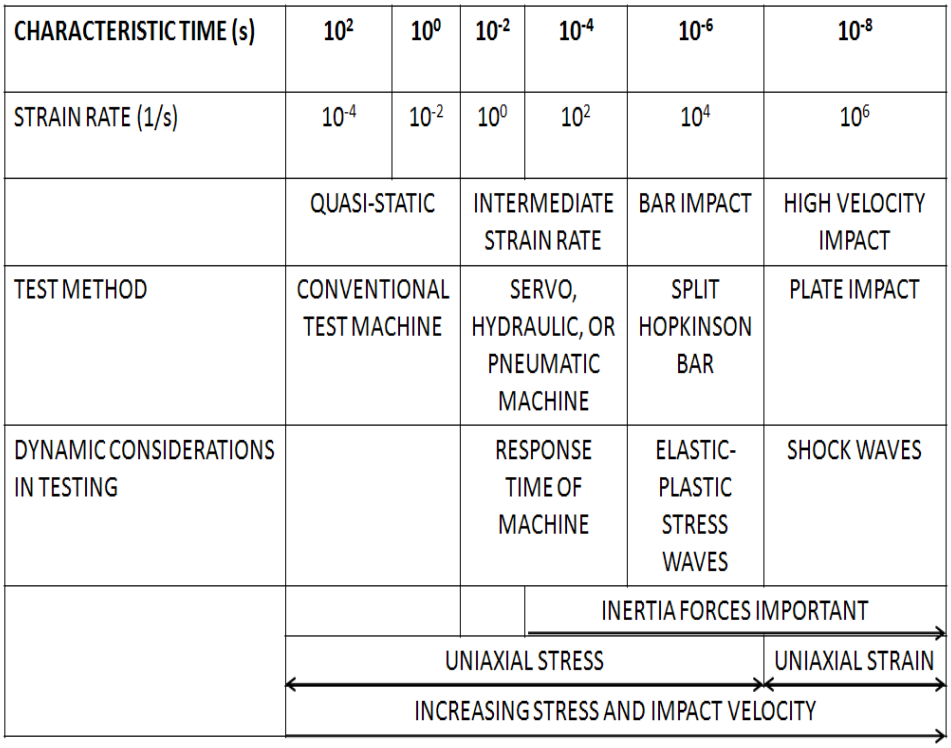

Figure 2.1: Characteristics of Increased Rate of Loading [36].

travels through a body at various rates of loading makes it important to consider the different characteristics associated with the increased rate of loading. Figure 2.1 [36] adapted from a table in Dr. Theodore Nicholas' short course presentation on impact details the characteristics associated with different rates loading as a function of the characteristic time in which the load is applied.

Figure 2.1 illustrates that the quasi-static loading condition covers only a small range of possible loading rates, 10^{-2} to 10^{0}, and makes it clear that mechanical properties obtained from quasi-static tests may not be appropriate for predicting a material's behavior under dynamic loading conditons [19]. Furthermore, Figure 2.1 defines the strain rate ranges for a wide range of loading rates, including what can be defined as the intermediate strain rate range. A study of the characteristics associated with each strain rate range is necessary to develop a successful experimental method at each rate of loading. Important factors in the intermediate strain rate range which differentiate it from both the quasi-static strain rates and higher velocity impacts are

the testing method and the dynamic considerations of the test machine. These two points will be addressed during the discussion of the experimental methods and test equipment later in this chapter. Another important characteristic of the intermediate strain rate range, especially as the rate of loading increases to the millisecond range, is the increase in the importance of inertial forces. Inertial forces, or the forces caused by the rigid body acceleration of the specimen from an at rest position to a velocity near that of the impacting projectile, affect experimental testing as the dynamic loading of the specimen is measured [22]. The inertial forces typically mask the first portion of the loading sensor signal for an amount of time as oscillations in the load recorded at the beginning of the time window. The amount of time the inertial forces mask the signal is a function of the rate of loading, the characteristic acoustic impedance of the tup and the specimen: where Z_o=$C_D \cdot \rho$ is the characteristic acoustic impedance of the material, C_D is the dilation sound speed, and ρ is the material density, and the geometry of the specimen [22]. The characteristic acoustic impedance is a material property which defines the velocity at which waves will travel through a medium. The inertial load is at a maximum at the moment of impact and then rapidly decreases as the specimen velocity and projectile equalize [22]. The effects of inertia in interpreting experimental data in some intermediate strain rate tests have been neglected, however as the strain rate increases the effects of inertia can no longer be disregarded [23] [19] [5]. Unfortunately, there is no hard and fast separation of loading at which the inertial forces become significant, and so the experimenter must evaluate the importance of inertial forces in the individual test method [23].

As the strain rates in an experiment increase above $10^2 s^{-1}$, not only must inertial forces be considered but the propagation of the stress throughout the body as waves becomes more important [36]. Wave propagation complicates the measurement of the specimen response and special test geometries have been developed to control the propagation of waves in a manner such that accurate data may be recorded as waves propagate throughout the specimen. The SHPB test is an excellent example of a test geometry which relies on wave propagation in response to wave effects [38].

At intermediate strain rates, wave propagation can typically be neglected although again there is no hard and fast boundary at which the effects of wave propagation will not be significantly affect the measurement of the material response. In the slotted beam tests, the rate of loading and the geometry of the specimen allow for the neglect of wave propagation at the ligament and will not be taken into account in the analysis of the experimental data collected from the tests [36] [5]. However, stress wave propagation does play an important role in the deformation of the rest of the beam specimen, as flexural waves travel throughout the beam when the slotted beam is transversely impacted. It is therefore important to note that the measurement of the material response at other locations on the beam at high rates of loading would require a consideration of these flexural waves [3] [4]. Stress wave propagation is just one characteristic of high velocity impact, which differentiates it from low velocity impact and quasi-static loading. As previously discussed, low velocity impact results in the global deformation of a specimen, but will also include lower frequency modal responses, millisecond-second response times, strains up to 10%, strain rates between 10^{-2} and 10^{1} s^{-1}, pressures on the order of the yield stress, and plastic deformation as the principal deformation mode [36]. In high velocity impact the specimen response is characterized by local deformation, higher frequency modal responses, sub-millisecond response times, strains up to 60 percent, strain rates up to $10^{3}s^{-1}$, pressures as high as 100 times the yield stress, and material separation as the principal deformation mode [36]. The slotted beam experiments exhibit many of the characteristics of low velocity impact, and therefore inertial forces are regarded as important but stress wave propagation is not a significant factor in measuring the material response.

2.1.2 Dynamic Mechanical Response of Ductile Metals. In Chapter 1 the importance of determining the mechanical properties under dynamic loading conditions was introduced. To understand how the mechanical properties of materials are affected by dynamic loading, it is important to discuss the concepts of elasticity, plasticity, and strain rate dependency when attempting to predict the dynamic response

of materials, specifically structural metals. Mechanical properties are quantified by examining a material's response to specific loading conditions. Loading may come in the form of tension, compression, torsion, or combinations of these forms of loading and will create a one, two, or three-dimensional state of stress depending on the type of loading and the geometry of the loading and the specimen. Depending on the magnitude of the loading, the material's response to the loading may result in elastic deformation or the loading condition may be significant enough to result in yielding of the material and permanent or inelastic deformation. Depending on the geometry of the loading and the magnitude of loading, the material's response may be in the form of rigid body translation, rigid body rotation, dilatation, or distortion [49]. Classification of these responses is important when examining the behavior of the slotted beam after impact. The mechanical properties of materials are typically quantified through the use of a stress-strain curve and on this curve the material's elastic and inelastic behavior can be illustrated. Figure 2.2 shows the elastic, yielding, and inelastic portions for 1020 steel tested at various rates of loading in a state of uniaxial tension [38]. It is clear from Figure 2.2 that the mechanical properties of AISI 1020 Steel exhibit strain rate dependent material behavior as the elastic or linear portion of the curve is extended and the yield point or transition to inelastic, nonlinear behavior is raised at higher rates of strain [19]. In addition, the characteristic yield drop of steel is also illustrated in Figure 2.2.

For many metals, the elastic portion of the material behavior is also linear and can be described through the constitutive relationship developed by Robert Hooke in the 17th century. Also known as Hooke's Law, it is used to predict a material's elastic response to a particular state of stress. Assuming an isotropic material, Hooke's law can be used to define a material's elastic response to a three dimensional state of stress in tensor form as

$$\sigma_{ij} = 2\mu\varepsilon_{ij} + \lambda\delta_{ij}\varepsilon_{nn} \tag{2.1}$$

where σ_{ij} is stress, ε_{ij} is strain, δ_{ij} is the Kronecker delta, and μ and λ are Lame's constants [46]. In engineering terminology, the constants E, and ν, replace Lame's constants and the linear strains resulting from a uniaxial state of stress where only σ_{11} exists can be defined as [46],

$$\varepsilon_{11} = \frac{\sigma_{11}}{E} \tag{2.2}$$

$$\varepsilon_{22} = -\frac{\nu}{E}\sigma_{11} \tag{2.3}$$

$$\varepsilon_{33} = -\frac{\nu}{E}\sigma_{11} \tag{2.4}$$

Equations (2.2) - (2.4) make it clear that the uniaxial state of stress is much less complex than the three dimensional state of stress illustrated in Equation 2.1, and its simplicity makes it an excellent candidate for determining the mechanical properties in the elastic region which in this case would be E and ν. Unfortunately, Hooke's Law is only valid for the elastic response of linear materials before the elastic and proportional limit of the material is reached and the material yields. Beyond this point, Hooke's Law is invalid due to the nonlinear material response in the inelastic or plastic region, and a more complex law must be developed to predict the material response in this region.

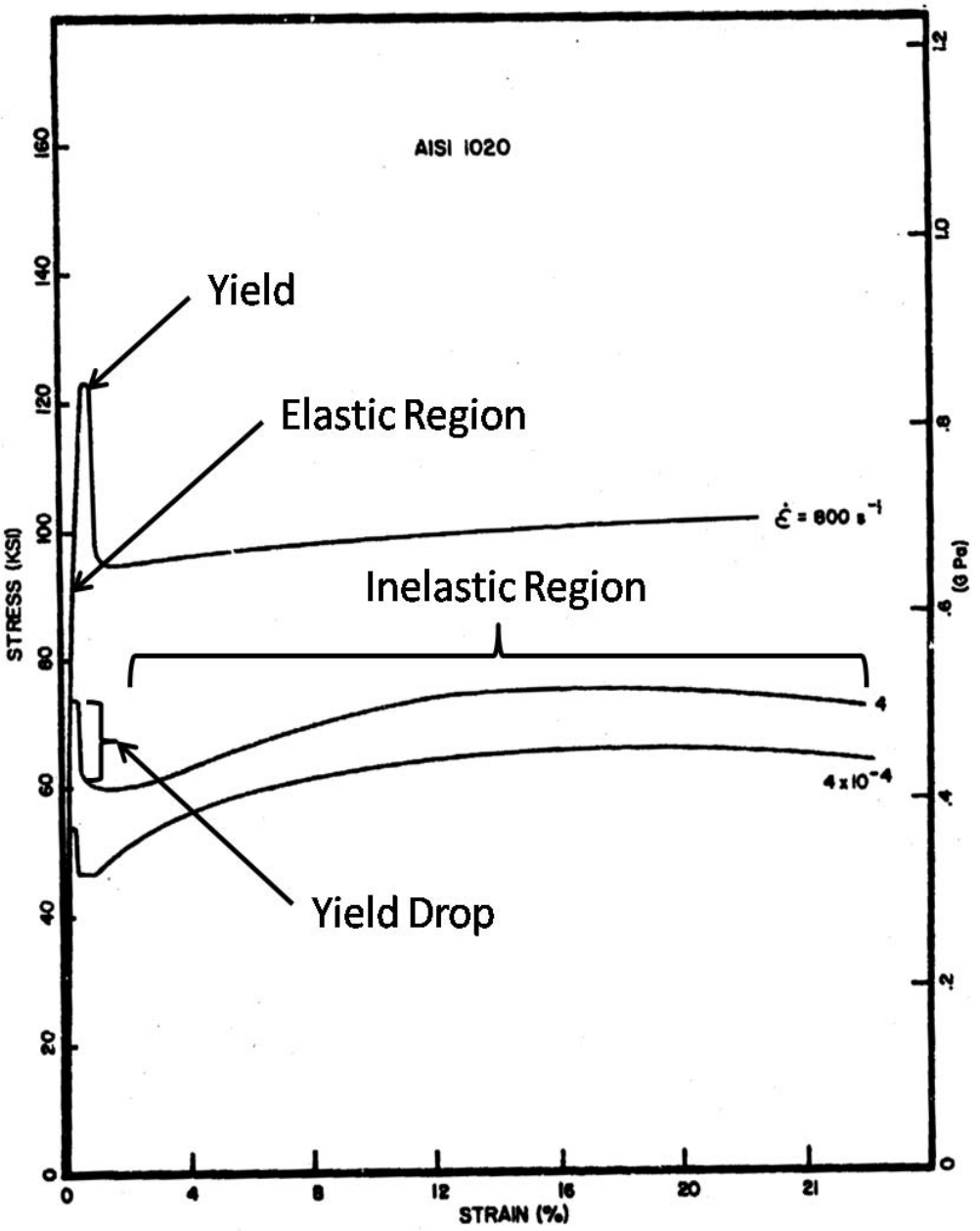

Figure 2.2: Stress strain curve for AISI 1020 Steel at Various Strain Rates [38].

Plastic laws attempt to predict the material's response after yielding has occurred. Plasticity can be treated as either rate-independent, also referred to as classical plasticity, or rate-dependent plasticity which is more appropriate in predicting the material response of metals at higher rates of strain [49] [10]. Another feature of plasticity is strain hardening, which is the phenomenon that upon loading beyond yield, unloading, and the subsequent reloading of a material, a higher yield point will occur making strain a history dependent function of the stress [49]. Strain hardening may take two forms; isotropic hardening which is the simple expansion of the yield surface, or kinematic hardening which is the translation of the yield surface [33]. These behaviors increase the difficulty of predicting the material response in the plastic region and require additional material constants beyond the elastic constants discussed previously to predict the plastic material response.

A number of rate independent and rate dependent models are now considered in a one dimensional state of tensile stress to examine the capabilities of each model. One rate-independent plasticity model is the linear elastic, perfectly plastic model which is be defined as [49]

$$\varepsilon = \varepsilon_p + \frac{\sigma}{E} \quad where \quad \varepsilon_p = 0 \begin{cases} if \;\; \sigma < Y or \\ if \;\; \sigma = Y \;\; and \;\; \dot{\sigma} < 0 \end{cases} \tag{2.5}$$

where ε is the total strain, ε_p is the plastic strain, and Y is the yield stress. This model does not take into account the nonlinear effects of plasticity and is therefore not applicable for most engineering materials. Another rate-independent plasticity model is the linear elastic, plastic model with power-law strain hardening defined as [49]

$$\varepsilon = \frac{\sigma}{E} \quad if \quad \sigma < Y \tag{2.6}$$

$$\varepsilon = \frac{\sigma}{E} + \left(\frac{\sigma - Y}{\mu_p} \right)^n, \; n \geq 1 \;\; for \;\; \sigma \geq Y \tag{2.7}$$

where both μ_p and n are plastic material constants. Figure 2.3 shows the stress-strain curves developed by both of these models. The power law hardening model does provides a nonlinear curve for the plastic region and one can see that if n is set equal to 1 in equation (2.7) a bilinear model is obtained where the constant μ_p is the plastic modulus in the bilinear stress-strain curve also shown in Figure 2.3. This model provides a better approximation of the plastic response of most engineering materials. A generalized relationship which exhibits the relationship between the plastic strain rate, $\dot{\varepsilon_p}$ as a function of the excess stress above the static yield condition, or overstress is [49]

Table 2.1: General Yield Criterion in a Three Dimensional State of Stress

Postulate	**Function**
1. General Yield Function, F(σ_{ij}) exists	Defines the limit of elasticity such that the material behavior is elastic if F(σ_{ij}) < 0 or if F(σ_{ij}) $= 0$ and F($\dot{\sigma}_{ij}$) <0 and the material behavior is plastic if F(σ_{ij}) $= 0$ and F($\dot{\sigma}_{ij}$) ≥ 0
2. Material is Isotropic	Ensures the function F has the same form no matter how the body is oriented making the function a symmetric function of the principal stresses such that F = F(σ_1,σ_2,σ_3)
3. Yielding is independent of Hydrostatic Stress	Makes the function F dependent only on the deviatoric principal stresses s_1,s_2, and s_3 and using the deviatoric stress invariants, J_1, J_2, and J_3. F becomes F = F(J_2,J_3) since by definition $J_1 = 0$
4. Identical Tensile and Compressive Behaviors	Requires that F(σ_{ij}) = F($-\sigma_{ij}$) and since J_2 is always positive by definition this requires F to be an even function of J_3

$$\dot{\varepsilon_p} = \frac{\sigma}{E} + A[F(\sigma) - \varepsilon], \quad where \quad F(\sigma) \geq \varepsilon \tag{2.8}$$

where A is a material constant with dimensions s^{-1}, and $F(\sigma)$ is a yield function representing the static stress strain curve. Using this generalized law, more specific constitutive relationships can be developed to predict the dynamic material response of engineering materials. Before discussing more complex models, it is appropriate to discuss the requirements for developing a yield function, which is the center of many classical plasticity theories. This discussion is also important in extending the classical plasticity models discussed previously from a one dimensional state where only the yield stress, σ_0 is considered to a general three dimensional state of stress. Any yield function should satisfy four postulates in the three dimensions. These postulates are presented in Table 2.1 along with each postulates function [49].

While there are no theoretical formulations which exactly give the state of stress for the yield condition in the general three dimensional state, two empirical yield criterion that satisfy postulates 1 through 4 and have shown good agreement in the experimental testing of ductile metals are the Tresca and Mises yield criterion [49]. The Tresca yield criterion can be defined as

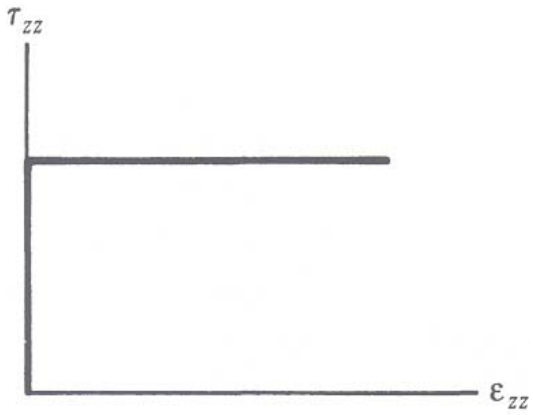

(a) Rigid, perfectly plastic

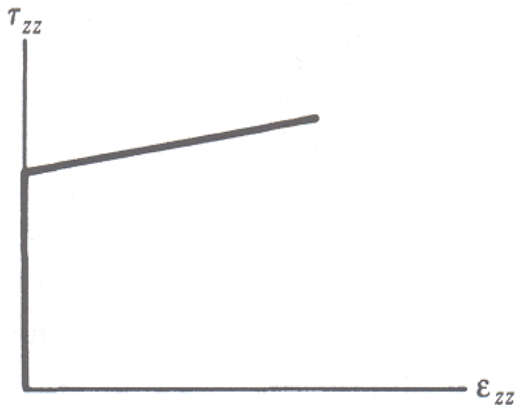

(b) Rigid, plastic with linear strain hardening

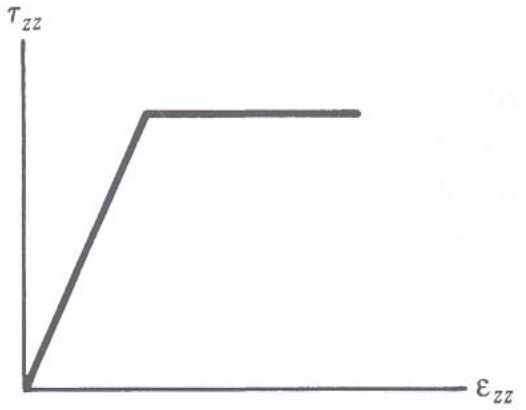

(c) Linear elastic, perfectly plastic

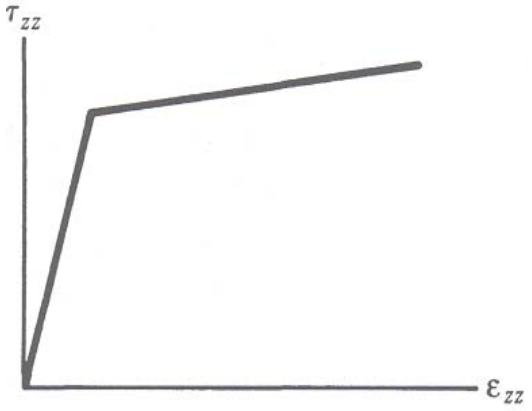

(d) Linear elastic, plastic with linear strain hardening

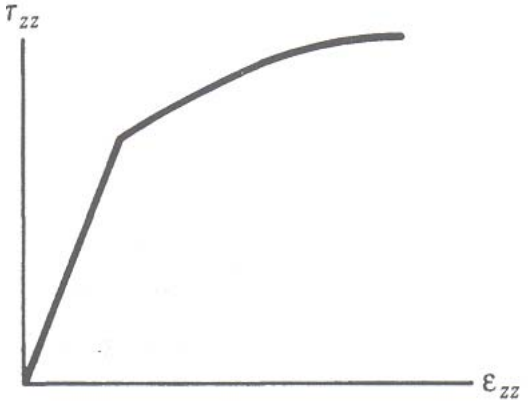

(e) Linear elastic, plastic with nonlinear strain hardening

Figure 2.3: Stress-Strain Curves from Various Rate-Independent Plasticity Models [49]

$$\frac{1}{2}(\sigma_{max} - \sigma_{min}) = k = \frac{Y}{2} \tag{2.9}$$

where σ_{max} and σ_{min} are the algebraic maximum and minimum values of the principal stresses, k is a critical value of the material, and Y is the yield stress in the prescribed loading condition. The Mises yield criterion is given by

$$J_2 = k^2 = \frac{Y^2}{3} \tag{2.10}$$

where J_2 is the second invariant of the stress deviator tensor, k is a value dependent on the material, and Y is the yield stress in the prescribed loading condition. Neither one of these yield criteria is satisfied precisely in real materials such that the yield criteria is stress-state dependent. The Mises yield criterion does however have the mathematical advantage of being a continuous function, while the Tresca criterion is a piecewise linear function [10].

Continuing an examination of classical plasticity on a macroscopic level, many metals and their alloys can be treated as rate-independent at moderate strain rates which Campbell defines as $10^{-1}s^{-1}$ to $10^{2}s^{-1}$. This allows for the usage of the flow laws of classical plasticity, which again state that no plastic flow occurs until the yield criterion

$$F(\sigma_{ij}) = k \tag{2.11}$$

is satisfied, where k is a material constant. The plastic deformation is then governed by the flow rule and the plastic strain rate is given as

$$\dot{\varepsilon}^p_{ij} = \dot{\lambda}\frac{\partial f}{\partial \sigma_{ij}} \tag{2.12}$$

where λ is a scalar factor of proportionality. Considering rigid, perfectly plastic materials such that the strain rate is assumed to consist of only plastic deformation a constitutive relationship is defined by the *Lévy-Mises* equations as

$$\dot{\varepsilon}_{ij} = \dot{\lambda} s_{ij} \tag{2.13}$$

where ε_{ij} is the total strain and s_{ij} is the deviatoric stress tensor defined as

$$s_{ij} = \sigma_{ij} - \frac{1}{3}\sigma_{kk}\delta_{ij} \tag{2.14}$$

To consider linear, elastic perfectly plastic materials, the *Prandtl-Reuss* equations were arrived at as a modification to equation (2.13) so that the plastic strains are proportional to deviatoric stress components such that

$$\dot{\varepsilon}^{p}_{ij} = \dot{\lambda}\, s_{ij} \tag{2.15}$$

Adding the elastic contribution of deformation, ε_e defined by equations (2.2) - (2.4) so that the total deformation, $\varepsilon_{ij} = \varepsilon^{e}_{ij} + \varepsilon^{p}_{ij}$ and separating the deviatoric, e_{ij} and bulk, ε_{kk} components of the elastic and plastic deformation, the constitutive equations for a linear elastic, perfectly plastic material are defined as [49]

$$\begin{aligned} \dot{e}_{ij} &= \dot{\lambda} s_{ij} + \frac{\dot{s}_{ij}}{2G}\sigma_{kk} \\ \varepsilon_{kk} &= \frac{\sigma_{kk}}{3K} \end{aligned}$$

where the plastic deformation is assumed to be incompressible and Lame's constants, G and K are used to define the material properties. Using the Mises yield criterion defined in equation (2.10), the flow rule for classical plasticity becomes,

$$f(\sigma_{ij}) = (\frac{1}{2}s_{ij}s_{ij})^{\frac{1}{2}} \tag{2.16}$$

where $(\frac{1}{2}s_{ij}s_{ij})$ is equivalent to J_2. The plastic strain rate using the Mises criterion is then given by

$$\dot{\varepsilon}_{ij}^{p} = \sqrt{3\lambda\frac{s_{ij}}{2\sigma_{eff}}} \tag{2.17}$$

where λ is a scalar factor of proportionality as defined in equation (2.13 and σ_{eff} is the effective stress, equal to $(\frac{3}{2}s_{ij}s_{ij})^{\frac{1}{2}}$. Assuming Drucker's normality and convexity postulates for the yield surface are satisfied, the flow rules described above can be used to define the constitutive relationships neglecting both strain hardening and strain-rate sensitivity.

To incorporate viscoplastic or rate-sensitive effects, it is necessary to modify classical plastic models such that the nonlinear region is not only a function of the yield point but also the strain rate [49]. Rate-sensitive behavior commonly occurs in soft materials or materials loaded at elevated temperatures, and many metals exhibit this rate-sensitive behavior [10]. For viscoplastic behavior the proportionality is no longer between the stress and the strain, but rather stress becomes a more complicated function of strain, strain rate, and temperature such that [33]

$$\sigma = f(\varepsilon, \dot{\varepsilon}, T) \tag{2.18}$$

Several empirical constitutive models which have been developed to include the effects of strain rate and temperature include the Johnson-Cook model, a shear stress/strain model used by Klopp, and a model for copper used successfully by Campbell and co-workers [33]. The Johnson-Cook model, Equation 1.2, was discussed in Chapter 1 and incorporates the effects of strain, strain rate, and temperature in an attempt to model elastic, visco-plastic response of materials. The model used by Klopp for shear stress and strain is given by [33],

$$\tau = \tau_0 \, \gamma^n \, T^{-\nu} \, \dot{\gamma}_p^m \tag{2.19}$$

where τ is shear stress, γ is shear strain, γ_p is the shear strain rate, ν is a temperature softening parameter, and n and m are work hardening and strain rate sensitivity parameters. The model developed by Campbell and co-workers is given by

$$\tau = A\gamma^n[1 + m \, ln(1 + \frac{\dot{\gamma}}{B})] \tag{2.20}$$

where τ_0, W, n, and m are experimentally determined parameters and τ, γ, and $\dot{\gamma}$ are shear stress, strain, and strain rate respectively. Both the models used by Klopp and Campbell showed good agreement in their respective research, but of all of these empirical models the Johnson-Cook equation has been the most widely used and its parameters are well known and have been published for a wide range of materials [33].

All of the models previously discussed adopt a macroscopic view of the material deformation and do not consider the micro-mechanical aspects of plasticity. While it is not necessary for a macroscopic constitutive model to explicitly incorporate the micro-mechanical aspects of plasticity, any macroscopic constitutive model should have a basis in the physical aspects of the material response, and should be in agreement with the micro-mechanical mechanisms of plasticity. For metals, a microscopic view of the mechanical behavior shows a dependence on the alterations in its crystalline structure or dislocation motion [19]. It has been well established that the predominant mechanism of plastic deformation in metals and alloys is slip caused by dislocation motion [10]. Dislocations are defects or irregularities within the crystalline structure in each type of metal. At these dislocations the energy required to break the bonds is much less and plasticity will result before the bonds of the perfect crystalline structure are broken [50]. The dislocation motion mechanism dominates plastic flow and has a strong influence on the ductility of a metal. The crystalline structure for most metals can be visualized as one of three lattice framework of atoms, the Body-centered cubic

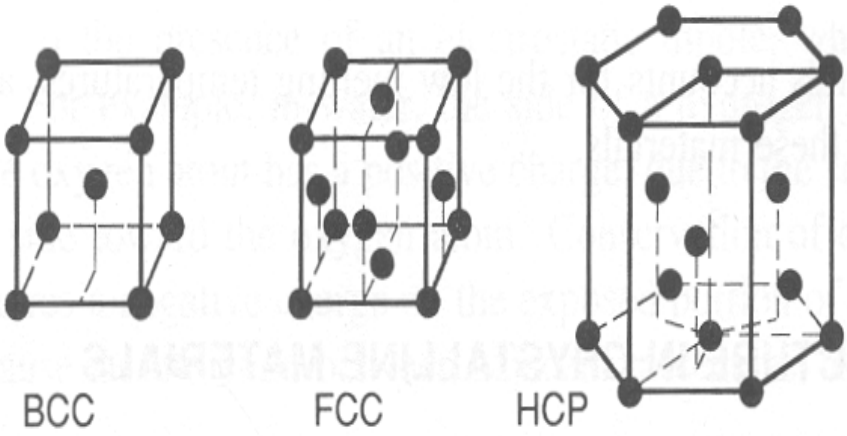

Figure 2.4: BCC, FCC, and HCP Crystalline Structures [15].

BCC crystal, the Face-centered cubic FCC crystal, or the Hexagonal close-packed HCP crystal as shown in Figure 2.4 [49].

Many metals including iron and low carbon steels are BCC, while other metals such as aluminum and its alloys are FCC, and metals such as titanium are HCP. As a metal is subjected to a tensile load, the spacing between the crystals increases and the metal specimen will elongate. If the tensile load increases beyond the yield strength of the metal some of the bonds within the crystalline structure break and crystal structures slip past one another resulting in permanent deformation. This slip occurs along planes known as slip planes, and the orientation of these planes is determined by the crystalline structure of the metal [49]. The number of slip systems within a crystalline structure is then defined as the product of the number of slip planes and the directions of slip most likely along these planes. Therefore, the crystalline structure determines the number of slip systems and has an important effect on the plastic behavior of a metal. It is clear that the crystalline structure will affect the mechanical properties of a metal, but continued research has also found that the crystalline structure will affect the rate-dependent behavior of the metal. Experimentation by Campbell [10] has shown that BCC metals usually show a greater

amount of rate sensitivity than FCC or HCP metals, while FCC metals have shown a small amount of rate dependence between strain rates of $10^{-3}s^{-1}$ to $10^{3}s^{-1}$. In addition, Campbell showed that the behavior of HCP metals are more complicated than both BCC and FCC metals due to a complex relationship between the dislocation mechanism and rate dependence at different slip systems [10]. Several relationships have been derived which attempt to take into account the grain size, and velocity and direction of dislocation motion in an attempt to describe the rate of plastic deformation. The variables within these relationships are complex and their values are sometimes difficult to ascertain [10]. However, through the use of several simplifying assumptions and neglecting strain-history effects, it is possible to develop stress-strain curves through the micro mechanical view. These equations have been applied in impact testing and are able to at least qualitatively describe the plastic response of poly-crystalline materials under a range of test conditions [10]. The number of dislocation mechanisms responsible for dynamic plasticity is quite large, making the possibility of developing constitutive laws based on the micro-mechanisms responsible for the plastic deformation small [10]. The important contribution of the microscopic aspect of dynamic plasticity is the that any constitutive relationship for the plastic behavior of a material should be consistent with micro-mechanisms which govern that type of behavior.

Clearly, many metals show a strain rate dependence on plastic flow within the material, also known as viscoplasticity and to model elastic, viscoplastic material behavior a more complex constitutive model is required [38]. The test of an appropriate constitutive model is its ability to explain observed physical phenomena over a wide range of test conditions and at the same time being mathematically manageable. However, the validity of a constitutive model is questionable when developed without regard to all phenomenon which may be occurring [23]. Any model should be able to predict the response of materials in both the loading condition in which it was developed, and other more complex loading conditions. The true test of the constitutive model constants determined with the slotted beam tests will be their ability to

predict the material response in more complicated states of stress than the uniaxial tension in which they were determined.

2.1.3 Transverse Impact of A Beam: The Rigid, Perfectly Plastic View.

Now that both the characteristics of low velocity impact and the elastic/plastic behavior of metals has been discussed, it is appropriate to examine the phenomenological characteristics of the transverse impact on a beam. Even under low velocity impact conditions a beam will deform plastically as has been shown by Menkes and Opat [24] while investigating the behavior of fully clamped beams subjected to uniform velocities over the entire span. This investigation showed three failure modes for the beam which were dependent on the velocity. These failure modes were large inelastic deformations of the entire beam, tensile failure of the beam material at the supports, and transverse shear failure of the beam material at the supports as shown in Figure 2.5 [24].

Theoretically, there have been several methods used to analyze the dynamic plastic bending of beams including the extension of an elastic flexural solution due to Boussinesq, rigid-perfectly plastic analysis, superposition of elastic and plastic harmonics of beam vibration, and wave propagation description [19]. While each method of analysis has its limitations [19], the rigid-perfectly plastic analysis provides a relatively simple technique which can be used successfully to model the dynamic plastic bending behavior of beams when large plastic strains are present [19]. Therefore, a brief theoretical discussion of the the transverse impact of a beam assuming the rigid-perfectly plastic is appropriate in understanding the behavior of the slotted beam at impact. The intent of this discussion is not to theoretically determine the behavior of the slotted beam when impacted, but only to discuss the characteristics of beams when impacted transversely.

Assuming a rigid-perfectly plastic material, as shown in Figure 2.3, which neglects both elastic behavior and strain hardening, the resultant motion of a fully clamped, constant cross section rectangular beam with respect to its length from the impact of a mass at the mid span can be described in two phases [24]. The first phase of motion is characterized by the development of a plastic hinge at the point of impact and the creation of plastic hinges on either side. As time elapses, the plastic hinges on either side propagate away from the point of the impact until they reach the clamped supports at each end of the beam. The second phase of motion involves the continued motion of the plastic hinge in the center of the beam in the direction of the initial impact. The plastic hinges at each end of the beam remain at the clamped supports as the center of the beam continues to deflect and plastic flow continues as each half of the beam remains straight but continues to elongate. This phase of motion is characterized by continued rotation of the plastic hinges at the beam's clamped supports until the beam and striker come to rest, at which time all of the initial kinetic energy of the striking mass is dissipated [24]. The magnitude of each phase of motion is dependent on the amount of energy in the impactor as the plastic deformation in the beam dissipates the energy of the impact. Figure 2.6 illustrates the two phases of

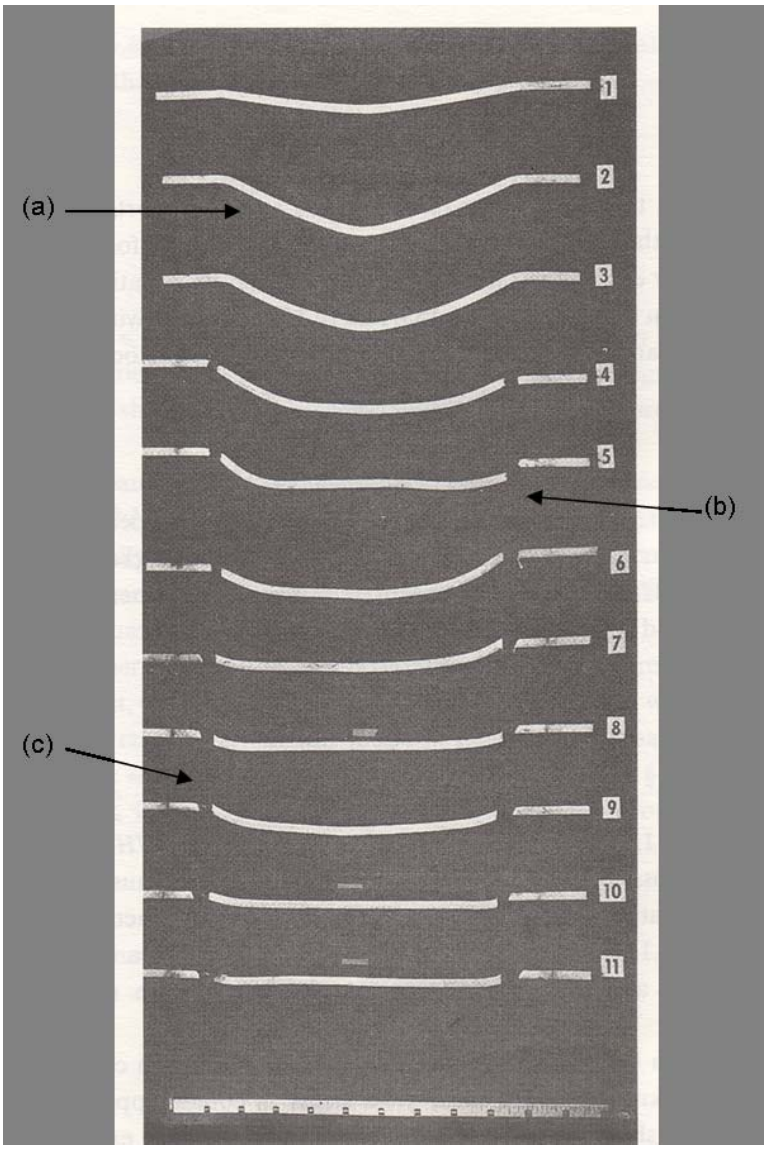

Figure 2.5: Failure Modes of Fully Clamped Beams Subjected to Impulsive Velocities; (a) large inelastic deformations, (b) tensile failure at the supports, and (c) transverse failure at the supports [24]

motion for the plastic deformation as the result of the transverse impact of a mass M with velocity V_0 of a fully clamped beam with length 2L, where $\dot{W}$ is the transverse velocity at the center of the beam, $\dot{w}$ is the transverse velocity of the beam at some point between the center and the support, and $\dot{\xi}$ is the velocity of the traveling plastic hinge [24].

As previously mentioned in Chapter 1, energy is a function of both mass and velocity and therefore the mass of the striker will influence the transverse motion of the beam. Approaching the impact event from an energy perspective, it can be shown for heavy strikers, which may be defined as $M \gg \frac{m}{L}$ where M is the mass of the striker, m is the mass per unit length of the beam, and L is the half-length of the beam, that the energy to be dissipated during the second phase of motion is approximately $\frac{1}{2}MV_0^2$ where V_0 is the initial velocity of the striking mass. The consequence of a heavy striker is the relative unimportance of the first phase of motion in dissipating the kinetic energy of the striking mass, such that the kinetic energy must be dissipated during the second phase of motion. For light strikers, which may be defined as $M \ll \frac{m}{L}$, the opposite is true and the kinetic energy of the mass and beam equals zero at the end of the first phase of motion and no plastic deformation occurs after the plastic hinges are developed at the supports [24]. It has been shown by Parkes [24] experimentally that beams impacted by heavy strikers behave in good agreement with the theoretical rigid-perfectly plastic development with the two halves of the beam elongating, as plastic hinges form at the supports and the impact point. However, tests using light strikers did not result in two halves which remained straight, and to achieve good agreement between the theoretical predictions of the maximum transverse displacement and experimental results it was necessary to consider the influence of material strain rate [24].

The rigid plastic analysis simplifies the theoretical analysis of the transverse motion of the fully clamped beam due to the omission of elastic response of the material, the affects of transverse shear, and geometry changes. In regards to the elastic response of the material it can be shown that this response is not important when the kinetic energy of the striker is significantly larger than S_e, the internal strain energy of the beam which may be absorbed in an elastic manner defined as,

$$S_e = \frac{\sigma_0^2 v}{2E} \tag{2.21}$$

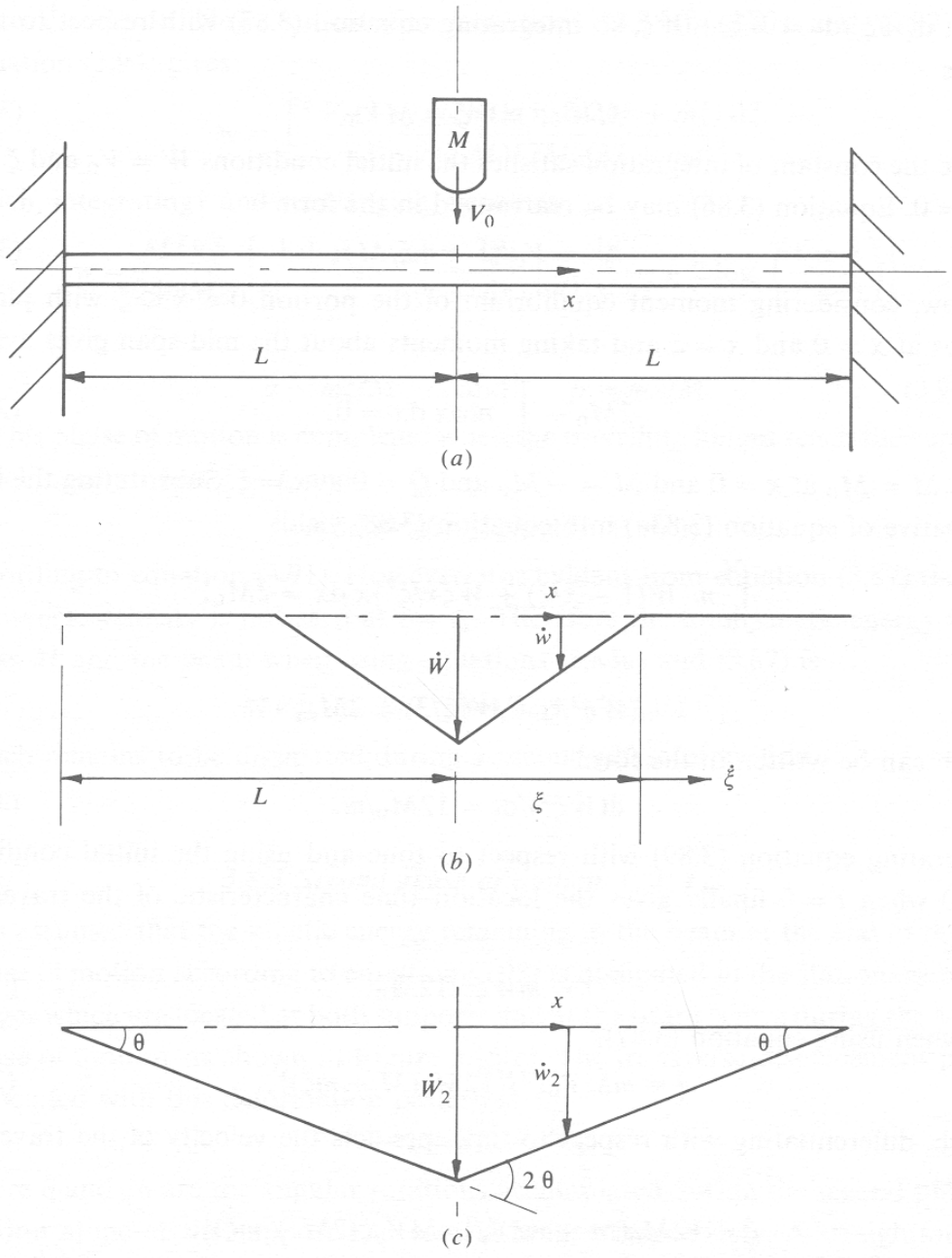

Figure 2.6: Diagram of Transversely Impacted Fully Clamped Beam (a) and the Resulting Phases of Motion (b) and (c) [24]

Table 2.2: Preliminary Calculations for Striker and Energy Ratio in Slotted Beam Experiments

	Striker			**Energy Ratio**		
	M (g)	$\frac{m}{L}$ (g)	$M \gg \frac{m}{L}$?	S_e (J)	K_E (J)	E_r
Steel	132.5	3.33	Yes	8.31	243.1	29.3
Aluminum	132.5	1.14	Yes	30.9	243.1	7.9
Titanium	132.5	1.91	Yes	27.6	243.1	8.8

where σ_0 is the yield stress, v is the volume of the beam, and E is the Young's modulus such that an energy ratio, E_r, is defined as

$$E_r = \frac{K_E}{S_e} \tag{2.22}$$

where K_E is the kinetic energy of the impactor and S_e is the internal strain energy as defined in equation 2.21. The energy ratio must be sufficiently large to ensure that a theoretical analysis using a rigid, perfectly plastic material will give reasonable predictions. S_e is an overestimate of the maximum amount of energy which can be absorbed in an elastic manner due to the omission of the effect of local plastic deformations. However, it has been shown by Symonds [24] that in conditions where the energy ratio, E_r is greater than 10, the theoretical predictions of the rigid perfectly plastic model overestimate the transverse displacement by less than 10 percent [24]. Preliminary calculations, shown in Table 2.2, using the proposed dimensions for the slotted beam specimen without the slot showed that the tup could be considered a heavy striker and that the E_r did approach 10 for most experiments suggesting that the rigid, perfectly plastic assumption may be a good approximation for describing specimen motion in the slotted beam experiments.

At the same time the rigid, perfectly plastic model does neglect several phenomenon which are important depending on the loading condition and material strength of the beam. These phenomenon are transverse shear and finite displacements. Typically each one of these phenomenon do not have a large influence on the static plastic

behavior of the transversely loaded beam, but dynamic loading can change the relative importance of these affects and therefore they should be briefly mentioned. Transverse shear is primarily important in the region underneath the impact in a beam. If the transverse shear strength of the impacted material is low, then shear slides will develop on either side of the impact site and result in material failure through transverse shear. If the the transverse shear strength of the material is large then the effects of transverse shear may be neglected and the beam will assume the behavior previously discussed. For materials in between, the effects of transverse shear will result in large deflections of the region directly beneath the impact site until the rest of the beam material attains the transverse velocity of the center section. The beam will then assume the plastic hinge motion previously described. Finite displacements also play an important role in the deformation of the beam if the energy ratio, E_r, is sufficiently large. This is due to the fact that the importance of the bending moment and transverse shear begin to diminish and the axial membrane force becomes dominant in the yielding of the beam therefore requiring its inclusion in the yield criteria [24]. The transverse shear strength of all the materials tested in the slotted beam experiments and the geometry of the slotted beam make the effects of transverse shear at the ligament negligible. The assumptions of rigid, perfectly plastic behavior including the omission of elastic behavior and a constant cross section beam are not consistent with the slotted beam experiments, however this model does provide insight into the dynamic behavior of the slotted beam at impact. However, the omission of elastic loading and unloading processes may introduce significant errors when small permanent deformations are present, and only works well for large plastic strains which are expected in the slotted beam experiments [24].

The deformation of the slotted beam specimen at impact can be described by the rigid, perfectly plastic model, except in the region where the beam is impacted. The slot prevents the development of a plastic hinge through the entire depth of the beam so that hinges develop on either side of the slotted area stretching the ligament underneath the slot. Therefore, the rigid, perfectly plastic assumption is not appro-

priate for the slotted beam specimens and is only presented in an attempt to describe the motion of a transversely impacted slotted beam. Fortunately, a three-dimensional FEM model can be used to analyze the slotted beam specimen's response to a transverse impact and determine the slot dimensions, which will produce a state of uniaxial tensile stress in the specimen ligament as the beam deflects. A study of the slot dimensions required to produce a state of tensile stress in Titanium was conducted by Larson and Deroche using an ABAQUS FEM and is detailed in Appendix 1 [44]. This study confirmed that the dimensions of the slot created a state of stress in the ligament which was predominately uniaxial along the length of the beam. However, these slot dimensions were determined using the material properties of CP Titanium and the slot dimensions for another material would be different. The creation of unixaial tensile stress is important to the development of a constitutive relationship for the materials tested since it is a less complex state of stress than multi-dimensional states of stress, and is therefore commonly used for determining the mechanical properties of materials. This highlights the importance of loading the ligament in uniaxial tension and developing a method of measuring the material response at this location, which leads into the next topic of discussion, experimental methods and devices for measuring the response under dynamic loading conditions.

2.1.4 Impact Testing Methods. Impact testing has not received a great deal of attention in material testing, not until interest developed in the rate dependence of materials during World War II was there a significant amount of work accomplished in the area of impact testing [38] [10]. After World War II, the desire to quantify the rate sensitive behavior of materials including structural metals increased, but the lack of reliable instrumented impact testing methods remained a significant barrier in this field of research [38]. Some of the first impact tests performed to investigate rate sensitivity include the work of Duwez and Clark, who measured the permanent strain in copper wires impacted by falling weights [23]. Since then, the need for the dynamic properties of materials and the investigation of strain rate dependence has

led to the development of many different tests to gather experimental data under impact loading. Some of the most popular impact tests include the SHPB Test, the Charpy Impact Test, and various other rapid loading tests. Each of these tests has its strengths and weaknesses in the characterization of materials under dynamic loading.

2.1.4.1 Split Hopkinson Pressure Bar Test. The SHPB test has been a major breakthrough in the effort to collect the mechanical properties of materials at high strain rates [38]. It was first performed as a high strain rate compression test by sandwiching a small cylindrical specimen between two long bars [38]. A compressive pulse is generated into one of the long bars either by the impact of a third bar or explosion. This pulse travels through the specimen and into the second long bar. During the transmission of the pulse the long bars remain elastic while the test specimen is deformed plastically due to the impedance mismatch. Both of the long bars are instrumented with strain gages. The strain gage signals are measured and analyzed with the equations of one-dimensional longitudinal wave propagation, which allow the determination of the time history of both force and displacement at the ends of the long rods contacting the specimen. From these calculations, stress strain curves in compression can be determined for strain rates up to 10^3 s^{-1} [38] The first tensile SHPB tests were attempted by Wood, Harding, and Campbell [38]. The specimen was loaded in tension again with a compressive pulse but only in an outer tube surrounding by an inner rod. The outer tube and inner rod were connected by a mechanical joint. At the mechanical joint, which acts as a free end, the reflection of the compressive pulse reflects back as a tensile pulse through the inner rod. The tensile specimen is threaded into the inner rod to create a mechanical connection for the transfer of the tensile pulse through the specimen and into another rod. The test achieved tensile strain rates of over 1000 s^{-1} while loading eccentricity of the apparatus was minimized to achieve stress accuracies within five percent [38]. While the mechanical joint provided the capability of loading a specimen in tension, it also acted as the primary drawback of this method by preventing the generation of tensile

waves with very short rise times due to wave dispersion in the joint. Another type of tensile SHPB test was developed by Lindholm and Yeakley, which used two pressure bars, one solid and the other hollow. Using a complex hat-type specimen design, a tensile pulse was achieved with the only limitation being the considerable machining required for the specimen [38]. Albertini and Montagnani were able to generate tensile pulses in a SHPB bar setup using an explosive device and the fracture of a prestressed clamp. They reported rise times of 25 μs in the impact pulses with the only negative aspect being the generation of impact pulses with explosives [38].

An additional method of tensile SHPB test was developed by Nicholas through the use of a collar around the tensile specimen sandwich between the two pressure bars. The collar is made of the same material and diameter as the pressure bars, and is manufactured so as to fit over the tensile specimen with a minimum amount of area. Machining the tensile specimen to the dimensions recommended by Nicholas creates a connection between the two pressure bars consisting of both the collar and the tensile specimen. The collar is not mechanically fastened to either of the pressure bars and remains in place due to friction. When the striker bar impacts the first pressure bar, the compressive pulse travels through the long rod and into both the collar and the tensile specimen. The area of the collar in contact with the pressure bar is much larger than the area of the tensile specimen in contact with the pressure bar. This results in the transfer of the compressive pulse to the second rod without the tensile specimen reaching its elastic limit. The compressive pulse continues traveling through the second pressure bar until it reflects off the free end of the bar as a tensile pulse. The tensile pulse then moves through the second bar into the tensile specimen and first pressure bar with the only difference being that the entire tensile pulse is transmitted through the tensile specimen instead of being shared by the tensile specimen and the collar. This is due to the fact that the collar cannot support any tensile loading since it is not mechanically connected to the two pressure bars or the tensile specimen. This mechanism is of primary importance to this type of tensile SHPB test and Figure 2.7 illustrates the test setup for a tensile SHPB test [38].

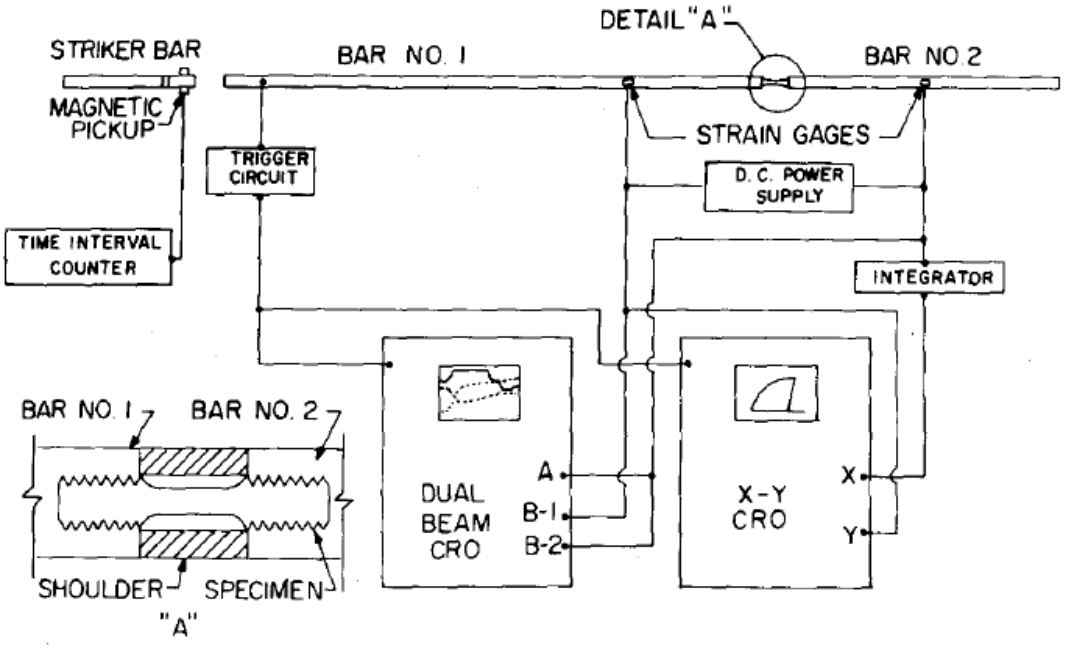

Figure 2.7: Schematic of Split Hopkinson Bar Tensile Test [38]

The primary limitation of the SHPB test is its use in determining material properties in the elastic region due to the rapidly changing strain rate during the first 25 μsec of the test [38]. For the test data to be valid some degree of stress and strain rate uniformity are required. In this amount of time the specimen has already been strained 1 percent and the use of this data will result in the calculation of a Modulus of Elasticity much lower than what is already known experimentally. This may also be a significant limitation for the slotted beam experiments, making it difficult to determine elastic material properties from the data collected. This limitation however does not outweigh the significant advancements the SHPB test has made in determining and documenting the dynamic material properties of many different types of materials. The SHPB test remains an excellent testing method for researchers with access to the equipment necessary to perform these tests [19].

2.1.4.2 The Charpy Impact Test. The Charpy Impact test is another popular impact test but lies on the opposite end of the spectrum of impact testing from the SHPB test [19]. The Charpy test is a relatively simple test to perform and is used to screen materials, compare similar types of materials, quantify the toughness of materials, and determine the ductile to brittle transition temperature of BCC metals [23] [47]. Also known as the dynamic bend test, the Charpy Impact test relies on the three point bending of a notched specimen with both ends of the specimen being simply supported and an impact force at the center of the beam. In this type of test, the strain rates, strain, and stress of the specimen are unknown but a measure of the dynamic fracture toughness is determined through the measurement of the load history required to fracture the specimen [36]. After discovering an excellent correlation between the fracture toughness, or the resistance to brittle fracture in the presence of a crack, and the ballistic performance of armor, the U. S. Army supported the standardization of the Charpy Impact test [32] [15]. This standardization solved many problems with the data due to inconsistencies in experimentation techniques between different test organizations and ensured the continued use of this test in the evaluation of the dynamic fracture properties of steel [43] [32]. In the early 1970's the development of velocity and load measuring equipment increased the popularity of the Charpy test as a method for quantifying the energy required to fracture a specimen [22]. While the test has been a popular method of impact testing, it has little practical application in the determination of dynamic material properties. This is primarily due to the fact that only a load time history is collected and the specimen response is not typically recorded. Furthermore, the notched specimen used in the Charpy test creates a complicated state of stress in the specimen, making it difficult to relate the loading of the test with the specimen response [19].

The Charpy drop weight or pendulum test is performed with an impact weight connected to a pivot point hoisted to some height above an impact specimen. The potential energy of the impact weight is calculated knowing the release height above the specimen. After release, the weight either falls or swings down to impact the

specimen. If the impact weight fractures the specimen, the weight will swing back up to some height corresponding to a lower energy level which can be calculated. Taking the net amount of energy from the initial and ending energy levels results in a calculation of the energy required to break the specimen. Instrumented impactors have been developed to automatically calculate these energy levels by relating the position of the impactor to the pivot point as shown in Figure 2.8 [19].

The Charpy impact test is differentiated from other impact tests not only by the limited data it collects, but also by the design and geometry of the specimen. The notch in the specimen simulates the corner of a part or some other critical region were a stress concentration would be present. In the Charpy test, the specimen is always oriented so that the notched section will fail in tension. This notch presented several issues for impact testers before the standardization of the test, which slowed the widespread acceptance of the Charpy test [19]. Some of these issues included the following. First, the notch in these tests must be maintained at the same dimensions for all specimens. Next, the notch radius is critical to material failure at different energy levels and may give a inaccurate impression of the actual qualitative impact behavior due to a dramatic decrease in impact resistance. Finally, cutting the notch in the specimen often results in surface damage which may affect the test results. The dimensions of the Charpy specimen in addition to the dimensions of the Izod specimen, a test which only differs from the Charpy test in the orientation of the specimen are illustrated in Figure 2.8 [19].

Instrumented Charpy tests rely on a strain gage instrumented load cell to collect a load-history during impact. However, the same fundamental limitations due to wave-propagation and inertia effects are inherent in the instrumented Charpy test, as other instrumented impact tests, limiting the velocities at which tests can be conducted [40] [47]. At impact velocities above 1.5 m/s, inertia effects become important and flexural wave transit times across the specimen become large compared to the total duration of the test and distort the recorded load-time history [22]. Furthermore, as increased velocities are attempted the equivalence of load at the beam supports and at the center of the beam becomes a poor assumption [23]. While constrained to lower velocities, the instrumentation of the Charpy test has transformed it from an almost purely subjective impact survivability test to a simple and quick test to perform that provides some quantitative data on the dynamic fracture of a specimen. Unfortunately, while more quantitative data may be collected, the instrumented version of this test is still not well suited for determining the dynamic mechanical properties of

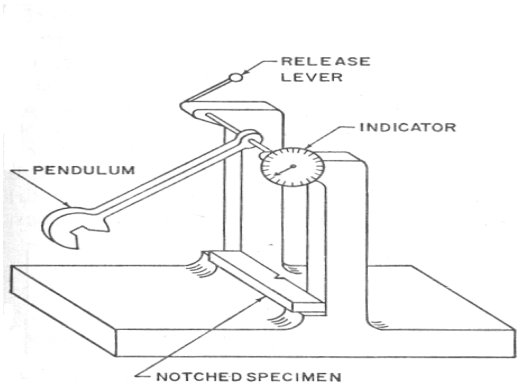

(a) Pendulum-type Impact Machine

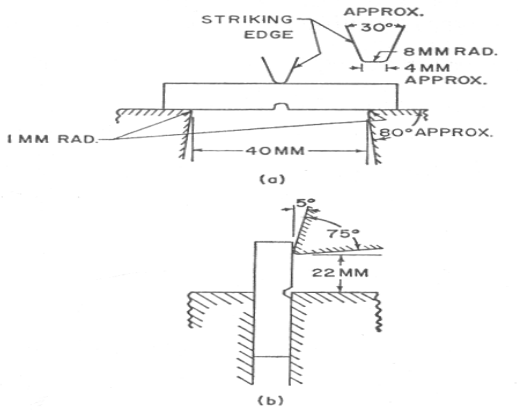

(b) ASTM Specifications for Notched-bar Tests (a) Charpy (b) Izod

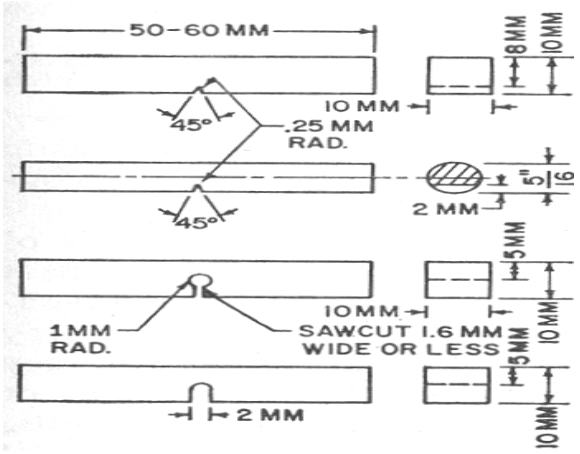

(c) Charpy Specimens

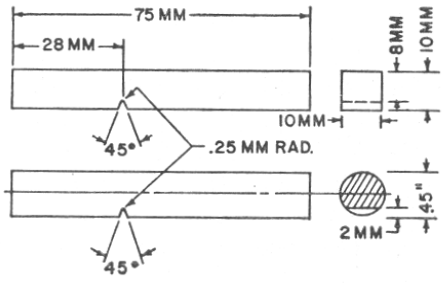

(d) Izod Specimens

Figure 2.8: Charpy Test Apparatus and Diagrams of Charpy and Izod Specimens [19]

metals. The only significant results these tests produce are the total energy required for fracture and the fracture appearance of the bar. The appearance of the fracture surface is important because it provides clues on whether the failure mode was due to brittle fracture or by ductile failure [19]. Therefore, the primary drawbacks to this type of testing are its subjective nature and its inability to develop constitutive relationships at dynamic loading conditions [23].

The Charpy test does not resemble other dynamic tests, whose purpose is to determine fundamental material properties, and clearly the Charpy test is not a satisfactory test method for characterizing the mechanical properties of ductile metals. However, the central impact of a beam specimen with a drop weight machine is a quick and simple method of impact testing which makes the Charpy test desirable for any impact testing method including the slotted beam tests [47]. Smooth bars have been used in the instrumented Charpy test setup, and beam theory has been applied to make approximate calculations about actual material response. One instrumented unnotched Charpy test conducted by Krinke and Barber [14] attempted to obtain meaningful load deflection from this test but found the measured deflection did not show good agreement with any analytical techniques for determining the deflection of the beam. Furthermore, they recommended the use of surface strain gages in future tests to measure the specimen response. These tests emphasize the importance of being able to accurately measure both the load and the subsequent mechanical response at a equivalent point on a specimen for the successful characterization of the mechanical properties of a material which must be addressed in the slotted beam tests.

2.1.4.3 Rapid Loading Tests. When attempting to determine the strain-rate sensitivity of material the simplest method is to increase the speed of the uniaxial test [19]. For the tensile test this simply means increasing the rate of loading and the capabilities of hydraulic and pneumatic machines have increased such that strain rates on the order of 10^2 s^{-1} are capable in both tension and compression [10]

[13]. The level of strain rates that can be achieved through these types of tests are primarily limited by the rate of loading at which the assumptions of uniform stresses and strains across the specimen are invalidated by wave-propagation considerations [36]. As the velocity of the impact increases, considerations must be made for the finite amount of time it takes for waves to propagate from the end of the specimen to the load recording device, the wave propagation through the load cell and attachment fixtures, and the inertia loads generated by the load cell and the fixtures [22]. High strain rates make the average value of stress/strain invalid and wave reflections and wave propagation must therefore be considered.

The tensile version of the rapid loading test is very similar to the standard uniaxial tensile test, and while the loading times are relatively short, they are still large compared to the transit time of a wave over the specimen length [19]. This is an important characteristic of the rapid loading test since it allows the assumption of a constant state of stress throughout the specimen, and permits the disregard for wave propagation effects. There are limitations to this assumption, and Goldsmith has stated that wave propagation effects cannot be neglected at strain rates of about 10 s^{-1} for a specimen with a gauge length of a few inches [19]. Campbell notes, "In rapid loading tests, it is often advantageous to use short specimens so that the wave effects can be neglected [10]". This is due to complicated interaction between wave propagation and the boundaries of a specimen. In a short specimen the transit time for the wave to propagate through the specimen is much smaller than the total duration of the test, and therefore the effects of the wave propagation may be neglected [10]. At higher strain rates, this becomes impossible because the specimen cannot be made small enough to increase the strain rates and neglect the wave propagation effects. In rapid loading tests using a pneumatic loading machine, Cooper was able to generate nearly constant strain rates up to 100 s^{-1} by decreasing the size of the specimen. The size of the specimen is an important consideration for the slotted beam as well, and while the beam dimensions are large compared to the wave transit times, the dimensions of the ligament are relatively small and allow for the assumption of a

constant state of stress. The affects of wave propagation in rapid loading tests have also been shown in drop weight tensile tests where drop weight machines have been used for tensile testing, but a non symmetrical loading pattern was created when one end of the specimen was held and the other end was impacted. The propagation of elastic and plastic waves in the specimen and the subsequent superposition of the faster elastic wave on the slower plastic wave caused a dramatic and sudden increase in the local stress at the top of the specimen and failure at this location [51].

Rapid loading tests are typically performed through pneumatic loading or by attaching the head of a specimen to a motor-driven screw [5]. Rapid loading tests have been performed by means of the modification of ordinary tensile testing machines modified to provide for faster motion of the driving head. Beyond the regime of low strain rates, it becomes necessary to store energy in a system to supply to the specimen because the instantaneous power requirement for a rapid rate of loading becomes quite large [10]. Some of the first energy storage systems employed included the use of the kinetic energy of a moving mass in the form of a pendulum, drop weight, or rotating flywheel. Later systems used the energy of compressed gases or liquids. A hydraulic testing machine which relies on pressure to move a crosshead at a rapid rate has generated nearly constant strain rates up to $10^2 s^{-1}$ [13]. Cooper was also able to show good axiality in his tests, which is needed to avoid the introduction of significant bending effects and is difficult to achieve in practice [13]. Other machines capable of generating intermediate strain rates include drop weight machines, the cam plastometer, and the rotary flywheel test machine and the reader is encouraged to consult Meyers [33] for more information on each of these test systems. Diagrams of these machines are included in Figure 2.9.

It is important to note that in the rapid loading tensile test the strain rate of the specimen cannot be determined from only a consideration of the specimen response [19] [13]. Instead the stiffness of the machine must also be accounted for in determining the strain rate of the specimen [19]. This is due to the fact that the strain rate is not equal to the rate of elongation of the system, but depends both upon the rigidity of the testing equipment and the applied stress rate such that the strain rate $\dot{\varepsilon}$ is given by [19]

$$\dot{\varepsilon} = \frac{v_0}{L_0} - \dot{\sigma}\frac{A_0}{kL_0} \tag{2.23}$$

where v_0 is the crosshead velocity, A_0 and L_0 are the original cross-sectional area and length of the specimen, respectively, and k is the stiffness of the test apparatus which is treated as a linear spring. Assuming a stress-strain relation given by

$$E\dot{\varepsilon} = \dot{\sigma} + g(\sigma, \varepsilon) \tag{2.24}$$

where $g(\sigma, \varepsilon)$ is a function dependent exponentially on the overstress, defined as the stress in excess of the yield stress, and E is the modulus of elasticity of the specimen. A mechanical equation of state such that σ is a function of ε is assumed, and Goldsmith shows that the strain rate for this type of test can be assumed to be [19]

$$\dot{\varepsilon} = \frac{\dfrac{v_0}{L_0}}{1 + \dfrac{d\sigma}{d\varepsilon}\dfrac{A_0}{kL_0}} \tag{2.25}$$

Since the spring constants of most testing machines range from $20,000$ to $500,000$ lb/in, the k in the denominator of the equation cannot be ignored, and reporting stress-strain data at various constant strain rates cannot be accomplished so that for many rapid loading tests the loading curve is reported as a function of the crosshead velocity, v_0 [19].

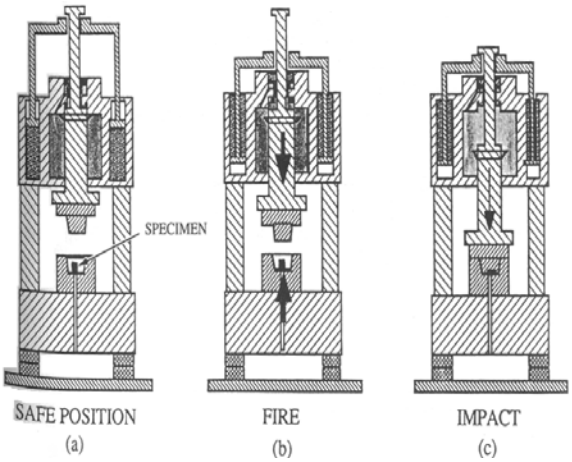

(a) Compressed Gas Drop Weight Machine

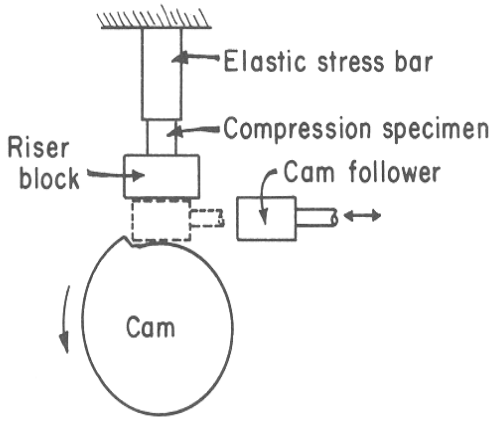

(b) Schematic of Cam Plastometer

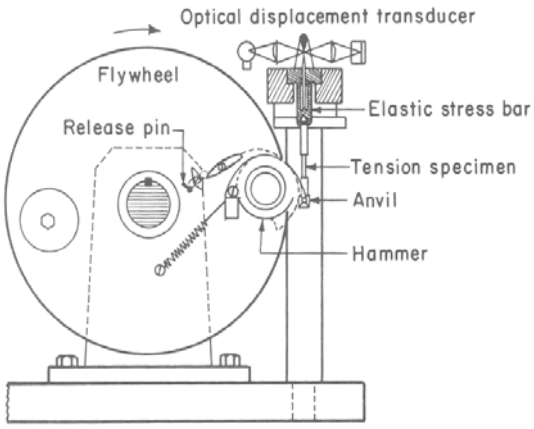

(c) Rotary Flywheel Tensile Machine

Figure 2.9: Various Rapid Loading Machines Capable of Generating Intermediate Strain Rates [33]

While rapid loading tests provide a capability for testing at intermediate rates of strain, the testing apparatus requires many considerations to achieve constant strain rates. Furthermore, these tests have strain rate limitations around $10^2 s^{-1}$ where inertial and wave propagations become too significant and the assumption of a constant state of stress in the specimen is no longer valid. The test apparatus for all of these types of tests are large, relatively expensive, and complex, contributing to the reasons that a great deal of testing has not been accomplished in the intermediate strain rate range [5]. The design of the slotted beam experiments aims to take these considerations into account and at the same time create an experimental method which is relatively simple and more direct to accomplish than past and present rapid loading tests.

2.1.5 Test Equipment for Dynamic Loading. The measurement equipment used in all dynamic tests plays an important role in providing the data required for the characterization of the dynamic response of materials [33]. Measurement equipment may prove to be the most significant limitation in an impact test [37]. To prevent this, the capabilities of all test equipment must be considered carefully before employment in any test. Not only does the test equipment need to have sufficient response time to measure a signal over the short time duration characteristic of an impact event [37], it must also be able to endure the impact conditions to continue to measure the response of the specimen for as long as possible. The impact of a specimen can be a very violent testing environment and either rugged test equipment which can survive this environment or measurement equipment which can sense the response of the specimen without being in contact with the specimen must be selected [9]. Even impact in the intermediate strain rate range may be significant enough to render test equipment useless and therefore it is appropriate to discuss the capabilities and operation of test equipment in an effort to successfully develop the slotted beam experiments. A discussion of the test equipment which can be used as part of a complete measurement system from the detection of a physical variable to the digitization and storage of that

signal will follow and is broken out into three different categories which include; arrival time indicators, particle displacement versus time, loading versus time. Finally, a brief discussion of the 'back end' of a measurement system is appropriate to provide a description of the signal conditioning and storage of the signal required to collect useful experimental data.

2.1.5.1 Arrival time indicators. The rapid initiation and short duration of the impact event, in addition to the necessity to capture the entire impact event make it impossible to trigger the data collection for impact tests manually. It is then necessary to sense the arrival of the impactor and in an attempt to correctly trigger the start of data collection. Typically, data collection is triggered by a signal generated by a piece of equipment related to the time of impact. These components in a test and measurement system are termed arrival time indicators. They may be an external component of the test system whose sole purpose is to detect the arrival of the impactor, or they may be part of an existing component in the test apparatus such that a signal already being generated during the test is used to trigger the data collection [33]. An excellent example of an integrated arrival time indicator is the generation of an electrical signal when an oil pressure valve opens to initiate a tensile test in the hydraulic test machine developed by Cooper [13]. Another instance of an integrated arrival time indicator is the triggering of an oscilloscope to collect after the threshold voltage in a strain gage is exceeded in a SHPB test conducted by Nicholas [38]. A variety of arrival time indicators can be used in impact testing and during selection it is important to consider the path and size of the impactor, the location of the impact, the velocity of the impactor, the magnitude of the electrical signals in the test environment, and the duration of the impact. Whichever type of arrival time indicator is used, it is important to ensure that the indicator produces a relatively large signal which will not be obscured by environmental noise. In addition, the indicator must trigger at an appropriate time in relation to the impact time with a

sufficiently fast response time as to trigger the data collection when the impact event initiates. Two types of arrival time indicators will be described in detail at this time.

The first type of arrival time indicator is the optical switch. An optical switch is a commonly used component for generating an external trigger signal using a photoelectric device operating opposite from one another [22]. The emitter and sensor create a gate across the path of the impactor. When the amount of light sensed by the photo-electric sensor is large, meaning the emitter/sensor combination is unobstructed, an arbitrary output voltage can be measured. The output voltage depends on the circuit used in conjunction with the emitter/sensor combination, but is typically a large positive voltage. When the amount of light sensed by the emitter/sensor combination is low, meaning the path between the emitter/sensor combination is obstructed, the output voltage will change. This change in voltage can be sensed and used as a trigger for data collection if the emitter/sensor combination is placed in close proximity to the impact event. Several different types of emitter/sensor combinations can be used to create an optical switch including light emitting diodes, lasers, and plastic fiber optics [18] but the basic operation of the switch is the same no matter which type of equipment is used. When selecting an emitter/sensor combination, several factors should be considered including the distance to be traversed by the light barrier, the magnitude of the voltage output necessary to overcome environmental noise, the environment in which the emitter/sensor will be used, and the required response time of emitter/sensor combination. The distance to be traversed by the light barrier will determine the size of both the emitter/sensor combination and the required power supply. The power supply requirement will also be a function of the voltage output necessary to overcome environmental noise since the two are typically related. The environment in which the emitter/sensor will be used is also important and if the emitter/sensor combination will be in contact with structures which will be impacted it is prudent to use an optical switch system which does not require electrical equipment in close proximity to the impact event. A fiber optic emitter/sensor combination which transmits and senses light through plastic fibers

and converts the amount of light into a voltage output through an amplifier circuit and can be located remotely away from the impact is a good option in this situation. Finally, a sufficiently fast response time, or the amount of time between a change in the physical measurement and the time required for a change in the voltage signal, is required for the successful sensing of an impactor. The velocity of an impactor may be fast enough in relation to the position of the emitter/sensor and the impact point that a slow response time will jeopardize the collection of the entire impact event. Many emitter/sensor combinations including the plastic fiber optic combination have response times on the order of 500 μs, but some may be as greater than 1 ms and therefore it is important to consider the response time of the optical switch when developing a test method [18].

As previously mentioned, other arrival time indicators may already be an existing component of the test apparatus and the signal already generated from these components is used to trigger data collection. The strain gage, which will be discussed in more detail further in this section, is one component that can be used as an arrival time indicator [42]. Used in conjunction with an external power supply and a Wheatstone bridge, a voltage output proportional to deformation in the strain gage can be measured. A strain gage in close proximity to the point of impact will be deformed shortly after impact and in turn a change in voltage output can be measured shortly after impact. Many oscilloscopes, which are typically used to record strain gage data, have the capability to trigger after some threshold voltage change occurs, and therefore can be used with a strain gage to trigger data collection and detect the arrival of the impactor. Several important considerations need to be made when using strain gages as an arrival time indicator and the rapid rise time of strain gages make them a good candidate to serve in this function. The 90% rise time of a bonded resistance strain gauge in μs can be approximated as [39]

$$t_{90} \approx 0.8(L/a) + 0.5 \tag{2.26}$$

where L is the gage length of the strain gage and a is the speed of sound in the material on which the gage is mounted. The typical response time for strain gauges on steel specimens have been found to be on the order of 1 μs [45]. While strain gages do have an excellent response time, the magnitude of the voltage output from a strain gage is typically low, which can be a problem in an environment where other electrical signals from the test apparatus or other extraneous equipment are large. In this case if the threshold value to trigger the data collection is set too low then the data collection will be inadvertently triggered due to extraneous signals. If the threshold value is set too high then valuable data at lower voltage levels will be lost. The strain gage signal may be amplified, but if the signals attributed to noise are not filtered then they will be amplified as well. This is an important consideration when using a strain gage as an arrival time indicator. If the strain gage is used as an arrival time indicator, it is also important to consider the geometry of the impact and the specimen to determine that both; a significant amount of deformation will occur to trigger the data collection and the stress waves will travel through the specimen in a manner to deform the "trigger" gage before the specimen has significantly deformed at other locations.

On that note, a brief discussion of wave propagation is appropriate in an effort to properly trigger the data collection. There are several different types of waves which travel through an elastic body subjected to impact, and depending on the magnitude of the impact either elastic or elastic and plastic waves are propagated through the specimen [23]. The elastic wave travels at a higher velocity than the plastic wave in the intermediate strain rate regime, and will be the wave which initially deforms the strain gage and therefore will be the only type of wave considered here [23]. Elastic waves can be classified as dilitational, distortional, surface waves, and flexural waves [23] [29]. Dilitational or longitudinal waves are characterized by particle motion normal to the wave front and can be either tensile or compressive. Distortional or shear waves are characterized by particle motion perpendicular to the wave front. Surface waves can be divided into two types of waves; Rayleigh and Love. Another

Table 2.3: Longitudinal and Shear Wave Velocities

Extended Media	**Bounded Media**
$c_L = \sqrt{\frac{E\,(1-\nu)}{\rho\,(1+\nu)\,(1-2\nu)}}$	$c_L = \sqrt{\frac{E}{\rho}}$
$c_S = \sqrt{\frac{E}{2\rho\,(1+\nu)}}$	$c_S = \sqrt{\frac{G}{\rho}}$

group of waves is flexural waves, which are propagated through beams, plates, and shells as the result of a transverse impact, and are of particular importance in the slotted beam experimentation. The velocities of the first three types of waves in a continuum have been characterized in much of the literature while the velocities of flexural waves are mathematically complex and are not easily characterized [33]. A consideration of the velocities of the first three types provides an indication of how fast the waves will propagate through the specimen and reach the "trigger" gage. Expressions for the velocity of longitudinal and shear waves in both extended and bounded media are given by Zukas and are defined in Table 2.3 [23], where ν and E are material constants previously defined, ρ is the material density, and G is the shear modulus of the material.

All of these relationships show the wave velocity dependence on the material properties. From the equations in Table 2.3 it is evident the longitudinal and shear wave velocities are dependent on both the Young's modulus and the shear modulus. Since $E > G$, the longitudinal waves will travel at a much greater velocity than the shear waves through a material [33]. The velocity of surface waves is dependent on the Poisson's ratio, which can be estimated from the calculated shear wave velocity and is typically 87.4% to 95.5% of the shear wave velocity [29]. While determining the actual motion of the waves propagating through a specimen like the slotted beam is extremely complex making a correct 3-dimensional (FEM) necessary to analyze the motion of the slotted beam, a calculation of the wave velocities is useful in estimating

the time in which disturbances should travel through the specimen and helpful for estimating the appropriate location for a 'trigger' gage [8].

2.1.6 Test Measurement Theory. Figure 1.2 illustrated the basic components of a general measurement system and it is now appropriate to discuss these components as they apply to impact testing. Sensors, which measure a physical variable, and transducers, which transform the physical variable into a measurable signal, form the foundation of any measurement system [45]. The remainder of the measurement system will be developed in an attempt to accommodate the sensor and transducer to conditions and record the signal which has been output. In low velocity impact testing, a number of sensors, several of which will be discussed later, can be used to measure physical variables such as displacement, velocity, and force. Sensors can be invasive, which are sensors that require connection or bonding to the test specimen or noninvasive depending on their location when sensing the physical variable. This may be important depending on the limitations of the test environment. Additionally, sensors and transducers may be active or passive depending on whether they require an externally based power supply; meaning a passive sensor and transducer does not require an external power supply to generate an electrical output while an active sensor and transducer does [17]. These environmental factors have a large influence on the sensor and transducer combination used in a test and in turn the entire measurement system. It is therefore important to consider the physical variable to be measured, the environment in which it will be measured, and the signal which will represent the physical variable in the selection of test measurement components. In impact testing, the material response to a loading condition is of interest, and measuring these physical variables is the primary objective of any impact test and measurement system.

2.1.6.1 Displacement and Velocity versus Time. Displacement, strain, position, velocity, and acceleration provide material response under impact conditions and can be measured with many different types of sensors and transducers [17]. The

two primary methods for measuring displacement and velocity are through either mechanical or optical methods. Mechanical methods are useful in test setups where space is limited. One of the primary drawbacks of the mechanical method is it only gives the material response at one point on the specimen while the optical method can typically characterize the entire material response. Impact events are of such a short duration that observations with the naked eye are of little use and therefore nothing is known about the entire material response unless an optical method is used to record the entire response of a specimen to impact [33]. Furthermore, optical methods may provide the only alternative to measuring the physical response of a specimen. In test environments were the mass and velocity of an impactor is large enough to create significant inertial loads, mechanical devices may not 'survive' the impact and optical methods provide the only method for quantifying the physical response of the specimen. Both methods have their advantages and disadvantages and combinations of both methods can be used in the same test setup in an effort to capture as much data as possible about the specimen response. A discussion of specific types of equipment will illustrate both methods in application.

Strain gages and accelerometers are both devices for measuring mechanical physical variables. Both of these devices rely on physical laws to transform physical variables into measurable signals. First, the strain gage, a common sensor transducer combination, relies on the phenomenon that the electrical resistance of some materials will change due to an applied mechanical stress and subsequent strain, also known as the piezoresistive effect such that [17] [12]

$$R = \frac{\rho l}{A} \tag{2.27}$$

where R is resistance, l is length of the grid material, A is cross-sectional area of the grid material, and ρ is resistivity. Some piezoresistive materials commonly used in strain gages for impact testing are listed in Table 2.4 include constantan, a copper-nickel alloy, and manganin, a copper-manganese-nickel alloy [41]. In the strain gage,

Table 2.4: Piezoresistive Materials used in Strain Gages [12] [58]

Material	**Composition**	**Typical Strain Sensitivity**	**Feature**
Constantan	60%Cu 40%Ni	2.1	High strain sensitivity which is constant over a wide range of strains and temperatures [41]
Annealed Constantan	60%Cu 40%Ni	2.1	Very ductile form of constantan capable of elongations >20%
Isoelastic alloy	36%Ni 8%Cr 55.5%Fe .5%Mb	3.5	High strain sensitivity which improves the signal to noise ratio in dynamic testing but nonlinear after 5000 μstrain
Manganin	86%Cu 12%Mn 2%Ni	.6	Low strain sensitivity but high hydrostatic pressure sensitivity [58]

the piezoresistive material can be configured in either the plane wire configuration, where the gage grid material consists of a thin wire wrapped around the grid, or the foil grid configuration, where the piezoresistive material is pressed into a thin foil to create the grid configuration shown in Figure 2.10.

The strain sensitivity, which is also referred to as the gage factor, is a dimensionless relationship expressed as [12]

$$GF = \frac{\Delta R}{R}\frac{\Delta l}{l} \tag{2.28}$$

where GF is the gage factor, ΔR is the change in the resistance, R is the initial resistance, Δl is the change in length, and l is the initial length. A suitable gage material has a high strain sensitivity over a wide range of strains and temperatures, meaning the resistance change can be measured even with a small amount of material. Equation (2.28) defines how the strain sensitivity is affected by the dimensional changes of the gage material and Poisson's effect also affects the resistance of the strain gage so that strain sensitivity "is a combination of the effects of geometric changes plus a resistivity change due to changing internal stresses [12]." This is an important con-

clusion since beyond the elastic limit of a gage material the change in internal stresses approaches zero and the Poisson's ratio approaches 0.5 [12]. The change on the gage factor due to Poisson's effect is defined as [12].

$$GF = 1 + 2\nu \tag{2.29}$$

and when the gage material is strained beyond its elastic limit the resistance will approach 2.0. If the strain sensitivity of a material is appreciably different than 2.0 in its elastic range then it will approach 2.0 beyond its elastic limit and exhibit nonlinear behavior over a range of strains. Therefore a material with a strain sensitivity of approximately 2.0 in its elastic range is highly desirable for maintaining linearity of the strain sensitivity over a wide range of strains. The small variation in the gage factor for constantan over a large strain range, makes constantan alloy one of the most linear of all strain gage materials over a large strain range and makes constantan a good choice for these experiments [55]

Piezoelectric materials, or materials which generate an electric potential when stressed have also been used to build strain gages, and some piezoelectric materials include quartz and lithium niobate [33]. While piezoresistive gages require a power supply, piezoelectric gages do not and this can be a significant advantage depending on the testing application. This is due to the fact that the piezoelectric gage can be made very thin, and without the requirement for a power supply can be placed inside a specimen. The PVDF gage developed by Bauer is only 25 μm and is embedded within the specimen and acts as a material gage [33].

For strain gages placed on the surface of the specimen, the matrix backing material serves as an interface with the specimen transferring the deformation of the specimen to the grid material. The backing material provides a mechanical couple between the strain in the specimen and the strain in the gage material and ensures an accurate transfer of the strain in the test specimen to the applied strain of the gage material [12]. Furthermore, an appropriate backing material ensures a bond

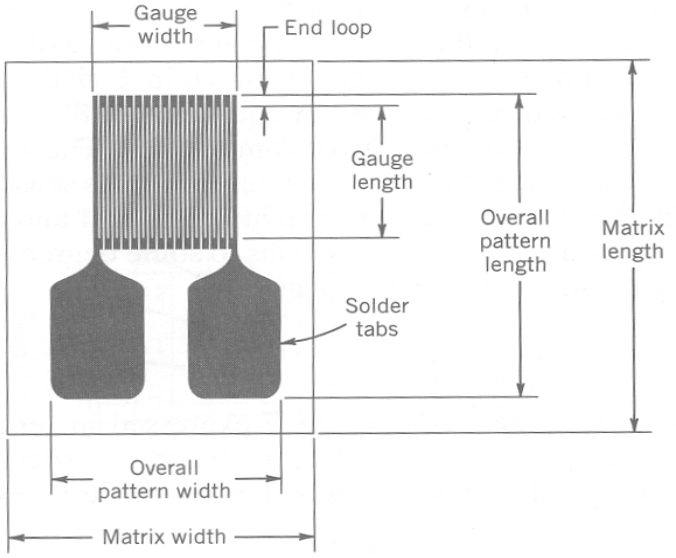

Figure 2.10: Strain Gage Schematic [45]

which electrically isolates the gage material from the test specimen. This allows the complete electrical signal generated during the straining of the gage material to be transmitted to the data collector. A diagram of a strain gage including the grid and matrix material is included in Figure 2.10.

The strain gage can be used in several different arrangements to create transducers to transform changes in resistance to measure displacement and deformation. It is important to note that several factors other than strain in the direction of interest may cause a change in the resistance of the strain gauge. These factors include temperature changes and the transverse sensitivity of the strain gauge. Changes in temperature may occur in increased temperature environments including high temperature rooms, intense lighting directed on the strain gage, or current flow through the strain gage for an extended period of time [42]. The slotted beam tests will be conducted in a controlled environment at room temperature, and the duration of the tests is so brief that heating of the strain gauge due to current flow will make changes in the resistance of the gages negligible [45]. In test environments where this is not the case, temperature compensation can be achieved by placing two identical gages

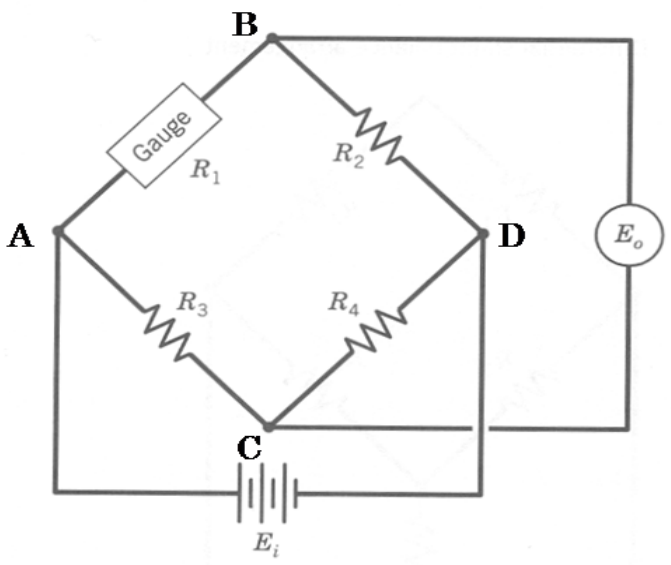

Figure 2.11: Basic Strain Gage Wheatstone Bridge Circuit [45]

experiencing an identical thermal environment in adjacent arms of a Wheatstone bridge.

The Wheatstone bridge is a common resistive bridge circuit which provides a means for accurately measuring resistance and and also detecting small changes is resistance [45]. Figure 2.11 shows a basic strain gage Wheatstone bridge circuit where R_1, R_2, R_3, and R_4 are individual resistors arranged in a parallel circuit between nodes A and D. E_i, a DC voltage, is input between these nodes and a voltage output, E_o, is then measured across nodes B and C. This particular bridge circuit configuration is a quarter bridge arrangement, where the designation indicates the number of active strain gages in the bridge circuit. Half and full bridge circuits are also possible and typically used depending on the the measurement application [45]. When E_o across nodes B and C is zero, the bridge is considered to be balanced and a relationship for the bridge output for the circuit in Figure 2.11 is

$$E_o + \delta E_o = E_i \frac{(R_1 + \delta R)R_4 - R_3 R_2}{(R_1 + \delta R + R_2)(R_3 + R_4)} \tag{2.30}$$

where δE_o is the bridge deflection and δR is the strain gage resistance change. If all of the resistances of the resistors and the strain gage in the bridge circuit are equal such that, $R = R_1 = R_2 = R_3 = R_4$ and the bridge is balanced such that $E_o = 0$, then equation (2.30) simplifies such that

$$\delta E_o \approx E_i \frac{\left(\frac{\delta R}{R}\right)}{4} \tag{2.31}$$

and using the relationship defined in equation (2.28) an expression relating the strain of the strain gage and the change in output voltage can be defined as

$$\delta E_o \approx E_i \frac{GF\varepsilon}{4} \tag{2.32}$$

where GF and ε are previously defined in equation (2.28). The simplicity of this relationship and the ability to balance the circuit such that a change in the output voltage can be related directly to the strain in the gage have contributed to the extensive use of the Wheatstone bridge in measurements with electrical resistance strain gages [45].

As part of the Wheatstone bridge, any change in the resistance of the strain gage will be measured through a change in voltage. Therefore when attempting to measure only the strain along the length of the strain gage, changes in gage resistance due to transverse sensitivity must be accounted for in measurement readings. The transverse sensitivity of a strain gage is due to the Poisson effect, and is magnified depending on the construction of the gauge, the difference between the Poisson ratio of the material being tested and the strain gage, and the orientation of the strain gage in regards to the direction of the strain of interest [56]. In a plane wire strain gauge the effects of strain in the perpendicular direction on the grid is insignificant due to the small diameter of the wire and the end loops of the wire which account for much of the transverse sensitivity these gauges [56]. However, in a foil gage the effect of strain in the perpendicular direction can be much larger due to end loop effects

and grid lines with a much larger width to thickness ratio than wires [56]. Another factor affecting the gage resistance due to the transverse sensitivity, is a difference in the Poisson ratio of the specimen material and the material used to calibrate the strain gage, which is commonly Steel. The strain gage calibration process accounts for the Poisson effect during the determination of the gage factor by testing the gage on steel with a Poisson ratio of 0.285 in a uniaxial stress field. Therefore, if the test conditions are not in a uniaxial stress field on steel with a poisson ratio of 0.285 then the Poisson effect must be accounted for. The Poisson effect may be accounted for in several ways. The first is a biaxial strain gauge arrangement with two strain gauges perpendicular to each other. This arrangement measures the strain in the direction of the principal strain and the strain in the transverse direction. If these two strain gauges are made active and placed into a Wheatstone bridge arrangement they will effectively negate the strain in the transverse direction. The measured voltage can then be converted into a strain, which is purely a measure of the strain in the direction of the principal strain. This method is not practical for the slotted beam tests due to limitations of the data acquisition device and the limited amount of area on the sliver of the beam. Another method of compensating for the transverse sensitivity of the strain gauges is through error relations for materials with different Poisson ratios than the material on which the strain gauge was calculated [56]. The error due to the transverse sensitivity in any strain field on any material is derived to be [56]

$$n_\varepsilon = \frac{K_t \left(\frac{\varepsilon_t}{\varepsilon_a} + \nu_0 \right)}{1 - \nu_0 K_t} * 100 \tag{2.33}$$

where n_ε is the error as a percentage of the actual strain along the gage axis, K_t is the transverse sensitivity as published by the manufacturer, ν_0 is the Poisson's ratio of the material on which the manufacturer's gage factor was measured, 0.285 in the case of most strain gage tests, and ε_a, ε_t are the actual strains parallel to and perpendicular to the primary sensing axis of the strain gauge respectively. This equation can be used when the Poisson ratio of the material is known and the specimen is subjected to an

axial strain field. In the case of the slotted tests, the Poisson ratios of both Aluminum and Titanium are known and therefore the error due to transverse sensitivity in an axial strain field can be calculated [15]. Finally, the transverse sensitivity of the strain gage can be controlled by taking care to place the gage length parallel to the direction of interest, which in these experiments is the length of the beam [52]. If not parallel, then the transverse strain effect will be falsely magnified. The error due to the transverse sensitivity of the strain gages should be small if care is taken to correctly place the strain gages, and the error due to the difference in Poisson's effect is accounted for through error calculations [52].

An accelerometer is another sensor/transducer used to measure the acceleration, velocity, or displacement of a test specimen. Accelerometers are commonly used to measure shock and vibration [9]. The accelerometer may be strain gage based or piezoelectric based. Strain gages can be used to detect acceleration can be constructed in an unbonded arrangement as shown in Figure 2.12 [27]. In the unbonded strain gage accelerometer, four strain gages (6, 7, 8, and 9) are combined with a mass(1) suspended at the center of the accelerometer by four springs (2, 3, 4 and 5) contained in a case(10) [27]. When the mass moves due to an acceleration, each of the strain gages will be deformed by an amount proportional to the acceleration experienced by the mass.

A piezoelectric accelerometer uses a quartz crystal to generate a voltage when deformed. Quartz has a modulus of elasticity of 85 GPa which can create load cells with static sensitivities of 0.05 to 10 mV/N and frequency responses of up to $15,000$ Hz making it an excellent piezoelectric material [45]. Figure 2.13 [45] shows a piezoelectric accelerometer configured such that a mass is threaded onto a post above a piezoelectric element. A nut threaded on the post above the mass is tightened to a manufacturer's specifications to pre-load the specimen. Positive or negative accelerations will result in a change in compressive forces on the mass and a corresponding output signal from the piezoelectric element [45]. While both types of accelerometers can be used to measure accelerations, the piezoelectric accelerometer is better suited

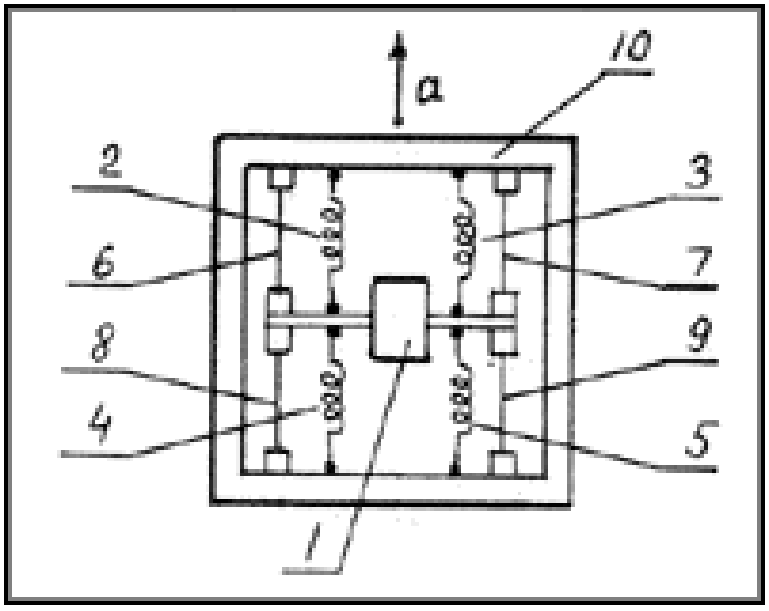

Figure 2.12: Unbonded Strain Gage Accelerometer [27]

to measure large accelerations and the strain gage based accelerometer is more appropriate for measuring steady acceleration oscillation events. This is due to the fact the piezoelectric accelerometers have the highest frequency response and acceleration ranges, while strain gage accelerometers have a much lower frequency response and acceleration range [45] [27]. Whether strain gage based or piezoelectric based, it is important to remember that all accelerometers rely on a mass accelerating within the transducer to generate an electrical signal from the piezoelectric material proportional to the acceleration. Knowing the sensitivity of the piezoelectric material, the acceleration can be determined from the voltage measured during a test event.

Not only can an accelerometer be used to measure the acceleration of a test specimen, but the output signal can be used to determine the velocity and displacement of that specimen at a point. This is accomplished through the numerical integration of acceleration, once for velocity data and twice for displacement data such that [45]

$$v(t) = \sum_i a_i \delta t \tag{2.34}$$

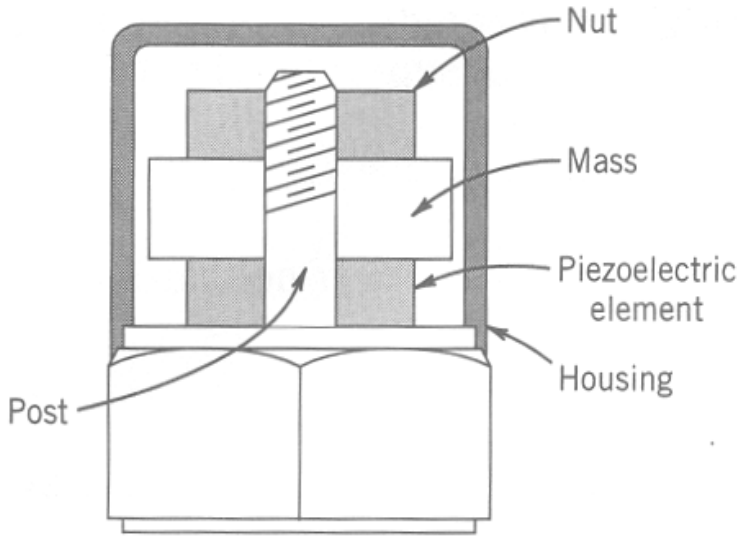

Figure 2.13: Piezoelectric Accelerometer [45]

$$d(t) = \sum_i v_i \delta t \tag{2.35}$$

where $v(t)$ and $d(t)$ are the velocity and displacement at some time t respectively and a_i and v_i are the velocity and displacement at some sample i respectively. Accelerometers offer an excellent method for measuring acceleration, velocity, and displacement of a specimen at a point, however their usage in impact testing is quite limited due to the large accelerations experienced by the impactor and the specimen. Large accelerations outside the accelerometers g-range will permanently damage an accelerometer, and therefore an accelerometer capable of handling the large decelerations at impact must be used. Unfortunately accelerometers capable of handling these decelerations are expensive and other mechanical methods provide a better option for measuring this type of data.

Optical methods for sensing the displacement, velocity, and acceleration of a test specimen include velocity photo-detectors, high speed photography, and flash radiography. A velocity photo-detector, shown in Figure 2.14, is a relatively simple sensor/transducer for measuring the velocity of the impactor of a drop weight test

machine. This type of velocity measurement device is used in the slotted beam tests on the Dynatup machine. The photo-detector is composed of several components, which include the photo-detector itself, the photo-detector bracket, and the flag. The photo-detector, which contains an infrared beam traveling across the center of it, is mounted in the photo-detector bracket. This bracket is located next to the guide rails of the Dynatup. The flag is mounted on the crosshead and when the crosshead is released, both the crosshead and the flag travel down the guide rails. The photo detector is very similar to the optical switch arrival time indicator previously discussed. Immediately before impact, the flag mounted on the crosshead travels through the center of the photo-detector and breaks the infrared beam until the length of the flag has passed through it. The amount of time the beam is interrupted is used to calculate a velocity by the Dynatup computer [21]. The velocity of the flag and the crosshead are the same and knowing the length of the flag, velocity is calculated by

$$V = l/t \tag{2.36}$$

where V is the velocity of the crosshead, l is the length of the flag, and t is the amount of time the infrared beam is broken. This is a relatively simple optical method for measuring the velocity of the impactor shortly before impact, and provides important data in characterizing the velocity and energy of the impact.

High speed photography provides an excellent noninvasive optical method to measure acceleration, velocity, and deformation of the specimen if the test setup is developed to accommodate this optical measurement method [33]. Several considerations for high speed photography should be mentioned. First, the exposure time necessary to create an image rate of the frame of the camera so a sufficient number of images of the impact event are captured. Second, the contrast of the specimen with the test setup at impact to include proper lighting so the material response may be accurately determined. Finally, an integrated trigger to start recording at the appropriate time so none of the impact event is omitted. In the past, frame rates

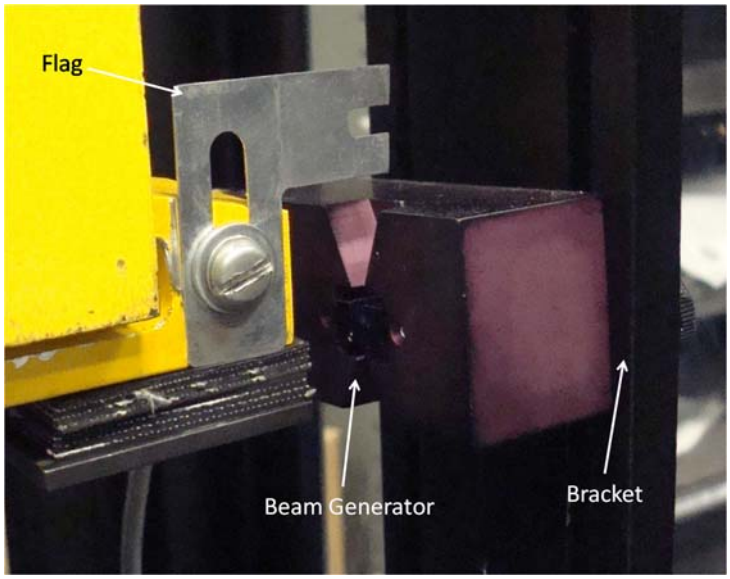

Figure 2.14: Flag and Dynatup Velocity Photodetector

and exposure times have limited the speed of cameras, but the development of both image converters and digital cameras have greatly increased these speeds such that some high speed image converter cameras can take images at least every μs [33]. In all tests where cameras are used, it is important to develop a test setup which provides an unobstructed view of the test specimen and impact [42]. This may dictate the geometry of the impact event in an effort to obtain the best image. Through the use of a grid with known dimensions and the frame rate of the camera, the velocity of the specimen can be calculated by dividing the distance traveled by the specimen in sequential frames by the interval between each frame. These calculations can only be performed if the specimen and the grid can be seen clearly and therefore the lighting and contrast of the specimen with the grid are important to these types of measurements [42].

Another optical method frequently used to measure the deformation of a specimen is flash radiography. In this optical method, an x-ray is used in penetration mode to develop an image of the impact event through a thick structure. However, typical x-rays are low power and require an amount of time which would be of no use in high speed impact tests. Therefore, the power of the x-ray is increased such that much

shorter flash times are possible. It has been demonstrated on high powered flash x-ray systems that flash times of 10^{-7} s can be obtained which allows for the measuring of extremely high velocities [33]. This method is not practical for intermediate strain rate tests, but can be particularly useful in impact experiments where explosives are used and the detonation may obscure the image recorded by optical cameras [33].

2.1.6.2 Force versus Time. A sensor/transducer which can measure the physical variable of force is a load cell. In intermediate strain rate tests, the load cell is usually the primary method for measuring load [22]. A load cell generates a voltage signal when subjected to an applied force. Like other sensors/transducers a load cell can use a change in capacitance, resistance, or the piezoelectric effect to create an output signal for an input of an applied force. [45] Therefore, three types of load cells are commonly used when attempting to measure an applied force. They include the strain gauge based load cell, the piezoelectric load cell, and the proving ring load cell. A load cell typically consists of two parts; an elastic member which deforms under the applied load, and a deflection sensor which measures the deformation. The shape of the load cell is usually constrained by its ability to measure the force in a particular direction. Load cells usually fall in to three categories: beam-type load cells, columnar-type load cells, and proving rings. [45]

Beam-type load cells are typically strain gage based load cells with a linearly elastic member manufactured out of metal. Two considerations must be made for this elastic member. First, is the shape of the member which allows the measurement of forces over a desired range of loading. Second, is the shape of the member which provides high sensitivity to loads in the direction of interest and a low sensitivity to loads in other directions. There are two types of beam-type load cells, the bending beam and the shear beam. The bending beam load cell functions as a cantilevered beam with strain gages placed at the top and bottom surfaces of the beam. These strain gages measure the bending strains, which are proportional to the applied load in the linearly elastic range of the load cell, such that

$$\sigma = \frac{My}{I} \tag{2.37}$$

where M is the bending moment also equal to the applied load times the moment arm, y is the distance from the neutral axis, and I is the moment of inertia. Hooke's Law, defined in equations (2.2) - (2.4), provides the relationship between stress and strain. Outside of the linear range of the load cell, these relationships are no longer valid and the load cell will not provide an accurate measurement. The shear beam load cell has the cross section of an I-beam with a strain gauge placed on the web. On the web of an I-beam, the shear stress due to an applied load at the top of the I-beam is nearly constant. This allows for the measurement of shear stress with reasonable accuracy with a strain gauge anywhere on the web and an output proportional to the applied load. The advantage of the bending beam load cell is lower cost, but the shear beam load cell provides lower creep and faster response times [45].

The piezoelectric load cell functions through the law behind the piezoelectric effect which says a charge is displaced across a crystal when it is strained. [17] In this type of load cell, the piezoelectric material, usually in the form a quartz crystal, creates a charge when the load bearing surface is deformed by the applied load. This charge is proportional to the deformation of the load bearing surface and is measured through a charge pickup and is output as a voltage through an impedance converter. The frequency response of a piezoelectric load cell is very high due to the size and material properties of the quartz crystal within the load cell. This type of load cell is typically a columnar type load cell due to the orientation of the applied force, the load bearing surface, and the piezoelectric crystal.

The proving ring load cell is a ring type load cell which is often used in the calibration of other material testing machines. This type of load cell relies on measuring the amount of deflection in the direction of an applied force of the ring. Approximating the proving ring as a right cylinder, the relationship between deflection of a right cylinder and the applied force defined as [45]

$$\delta y = (\frac{\pi}{2} - \frac{4}{\pi})\frac{F_n D^3}{16EI} \tag{2.38}$$

where δy is the deflection in the direction of the applied force, F_n is the applied force, D is the diameter, E is the modulus of elasticity, and I is the moment of inertia. Strain gages or deflection transducers are used to measure the deflection created by the applied force. Schematics of bending beam, piezoelectric, and proving ring load cells are included in Figure 2.15.

The Dynatup apparatus can use either semi-conductor strain gauge (piezoresitive) based or piezoelectric based load cells depending on the application. [1] Due to the direction of the applied load and a drop weight impact machine a columnar-type load cell is most appropriate to measure impact load. A piezoelectric load cell is used on the Dynatup because of its favorable qualities under impact conditions. Any load cell which is used for impact testing must be dynamically calibrated [22]. The most commonly used load sensor is the strain gage based load cell [22] The affects of inertial loading on the signal collected by the load cell must be considered.

2.1.7 Signal Conditioners and Oscilloscopes. The next step in the process of measuring a physical variable is commonly the amplifier. An amplifier takes some input analog signal, $E_i(t)$, and outputs an analog signal, $E_o(t)$. The relationship between $E_i(t)$ and $E_o(t)$ will vary depending on whether the amplifier is linear or logarithmic such that [17],

$$E_o(t) = GE_i(t) \quad or \quad E_o(t) = Glog_x E_i(t) \tag{2.39}$$

where G is the gain defined as the amplifier's output/input magnitude ratio. Amplifiers are commonly used to condition the input signal in an attempt to take advantage of the full scale of the data acquisition or DAQ board. An important characteristic of an amplifier is its common-mode rejection ratio (CMRR). This characteristic is a measure of an amplifiers ability to reject noise common to all of the inputs of an amplifier and is defined as [17]

$$CMMR = 20\,log_{10}\frac{G_d}{G_c} \tag{2.40}$$

where G_d is the gain when different voltages are applied across the amplifier's positive and negative input terminals and G_c is the gain when the same voltages are applied across these inputs. When using a sensor/transducer to measure a physical variable,

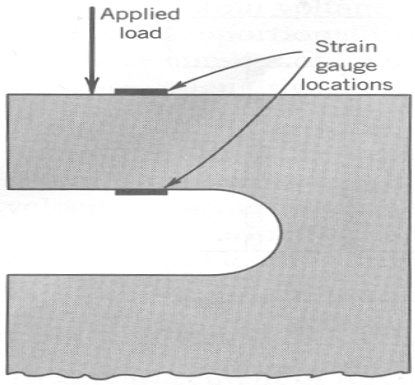

(a) Bending Beam Load Cell

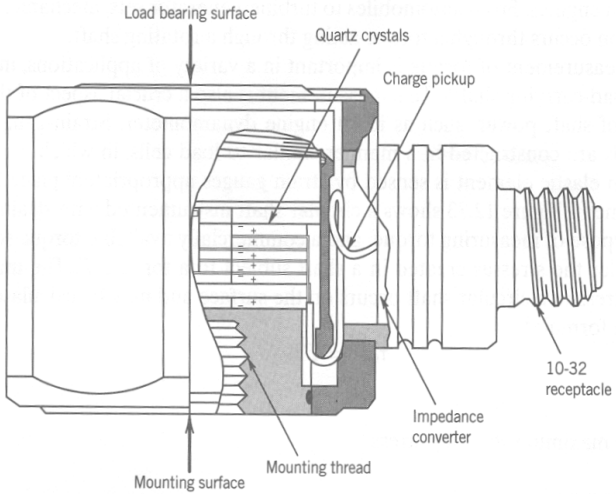

(b) Piezoelectric Load Cell

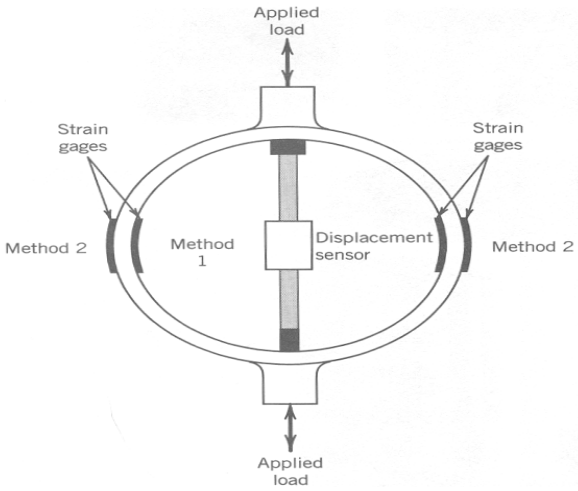

(c) Proving Ring Load Cell

Figure 2.15: Various Load Cells for Measuring Force [33]

detecting the voltage difference is the main goal and therefore ideally the gain output of any similar voltage between the two inputs should be zero. In reality G_c is not zero, but is instead some finite value and the lower this finite value the better. A CMRR measured in positive dB or decibels above 100 is considered desirable for most applications [17].

The most common type of amplifier used in measurement systems is the operational amplifier [17]. An operational amplifier's major attributes are a very high input impedance, defined as the measure of a circuit's opposition to the flow of current, of typically $> 10^7\Omega$, a very low output impedance $< 100\Omega$, and a high internal open loop gain $\sim 10^5$ to 10^6. A high input impedance is important since it results in very little current drawn from the input circuits, while a low output impedance implies that the voltage output will be independent of the output current. While the ideal operational amplifier is run in open loop configuration, most real world amplifiers are not run in this manner due to poor control during the manufacturing process. This can lead to operational amplifier saturation unless the voltage difference being amplified is very small. To correct for this problem an operational amplifier is typically run in a closed loop configuration. The closed loop configuration relies on negative feedback, or the output connected to the input through a resistor so that a feedback loop is established between the output and input terminals. This relationship between the voltage output E_o and the voltage input E_{i1} and E_{i2} is expressed as [17]

$$E_o = (E_{i2} - E_{i1}) \left[\frac{R_2}{R_1}\right] \tag{2.41}$$

where R_1 is the input resistance and R_2 is the output resistance.

Figure 2.16 shows the schematic for a common operational amplifier, the differential amplifier. The differential amplifier acts as a voltage comparator, which provides an output proportional to the difference between two input voltages [45]. In this configuration any difference in E_{i1} and E_{i2} will be amplified, which is well suited for transducers such as the strain gage and Wheatstone bridge circuit where

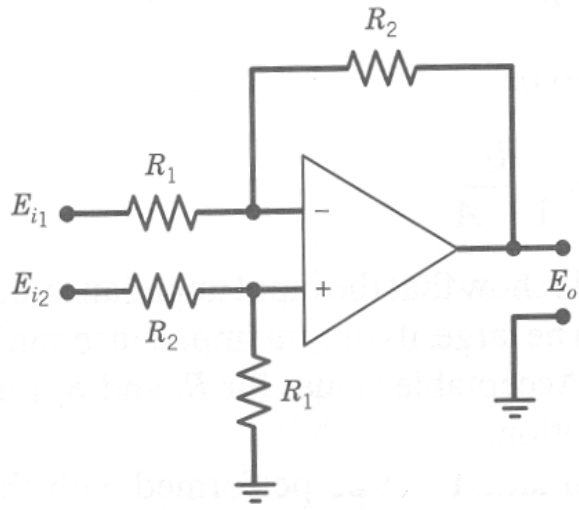

Figure 2.16: Differential Amplifier Circuit [45]

a voltage difference is directly related to the strain measured in the gage. A voltage supply is often commonly included as a separate component in the signal conditioning system. The voltage supply is responsible for providing the input voltage, E_i over the Wheatstone bridge in strain gage applications. Power can be supplied to the wheatstone bridge with Direct Current (DC) or Alternating Current (AC) and the advantages of each are illustrated in Table 2.5. Due to its numerous advantages, the DC voltage supply is more widely used in test equipment for general stress and strain analysis [48].

The signal conditioner may also provide another valuable function when used in conjunction with strain gages, which is shunt calibration. In most strain gage based test systems the signal conditioner provides the remaining passive resistors required to complete the Wheatstone bridge, and shunt calibration provides a means of electrically stimulating the gage to calibrate the entire system from strain gage to readout [48]. A shunt calibration circuit is shown in Figure 2.17 which illustrates calibration resistor, R_{cal}, being placed in parallel with one arm of the Wheatstone bridge to simulate a resistance change due to strain. The simulated strain can then be calculated by

Table 2.5: Advantages of DC and AC Voltage Supplies in Measurement Applications [48]

	DC Advantages	AC Advantages
1.	Simplest approach in terms of circuitry involved	Less sensitive to electromagnetic interference
2.	Wide frequency response	Does not measure thermocouple voltages
3.	Sensitivity of system i.e. the amplifier gain is more stable	Any amplifier zero drift does not affect system zero
4.	Better system linearity	
5.	No cable capacitive or inductive effects	
6.	Shunt calibration and bridge balance circuitry are simpler	

$$\varepsilon_{cal} = \frac{R_1}{GF(R_{cal} + R_1)} \tag{2.42}$$

where R_{cal} is the resistance of the shunt resistor and R_1 is the resistance of the resistor parallel to the shunt resistor. Shunt calibration provides a simple method of calibrating the strain gage test system but it is important to note that this method does not verify the stain gage or adhesive's mechanical performance.

From the signal conditioner, the amplified analog signal must be transformed to a digital signal by an A/D analog-to-digital converter or A/D converter for storage and analysis. This component is responsible for the digitization of an analog signal. This requires the translation of a continuous analog signal into a digital number representation of a specified number of bits. This conversion is necessary so the data acquisition device can record and represent the voltage signal from the strain gages. Two primary considerations, quantization error and aliasing of the signal, must be made when making the A/D conversion. Quantization error is due to the digital sampling process. When an analog signal is sampled it is converted to a digital number with a certain number of bits depending on the resolution of the sampling

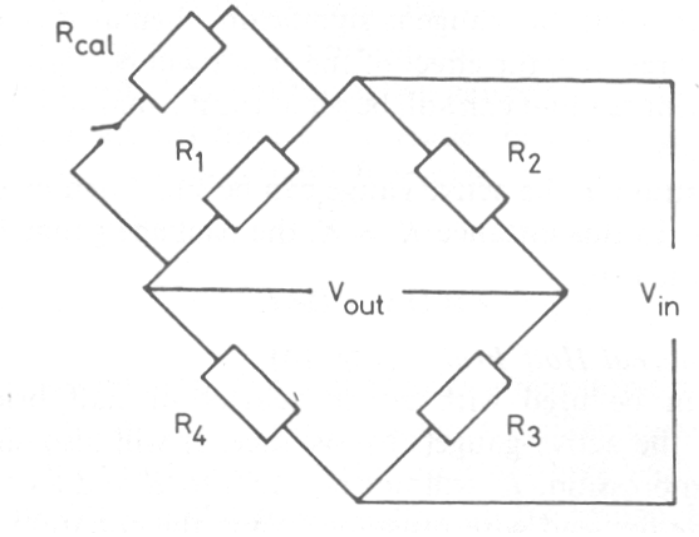

Figure 2.17: Shunt Calibration Circuit

device. When this occurs the actual value of the analog signal is lost as it is converted into the digital number associated with that magnitude analog signal. Therefore, at a low resolution the amount of quantization error is high and as the resolution of the A/D converter increases, quantization error will decrease. The quantization error can be determined by knowing the resolution of the system and the full scale range of the system. This is determined by calculating the resolution, Q defined as [17]

$$Q = E_{FSR}/2^M \tag{2.43}$$

where E_{FSR} is full scale range voltage and M is the number of bits.

Aliasing of the signal can also occur in the analog to digital conversion of the transducer signal. This phenomenon occurs when the digital sampling of the analog signal occurs at a rate slower than the frequency of the analog signal. To overcome the problem of aliasing, it is recommended that the sampling rate be twice the rate of the highest frequency to be measured [57]. In impact testing, all of the natural frequencies of the specimen are excited when the specimen is impacted, and therefore no one particular frequency is of interest. However, the short duration of the material

response at impact require a high sampling rate if the analog signal is going to be digitized so that none of the material response as it changes with time is lost during the digitization process. If data is not sampled at a large enough rate, then the fidelity of the measured material response may not be sufficient to analyze the actual material response.

After the effects of A/D conversion, are considered the digitized signal can be stored and displayed. The oscilloscope is the signal display component most commonly used for instrumented impact testing because it provides better signal resolution with respect to time [22]. In the past oscilloscopes were analog devices, which did not digitize the signal but rather displayed the signal continuously as it changed with time. Therefore, it did not encounter the problems of quantization error and aliasing. Increases in technology have resulted in the development of digital oscilloscopes, which can digitize the analog signal at a resolution and sample at a rate which results in a digital signal with the fidelity approximately of the analog signal. When using an oscilloscope in impact testing, the number of traces and triggering capabilities should be considered, in addition to the resolution sampling rate for reasons previously mentioned. The number of traces are the number of separate signals or waveforms which can be measured at the same time. The voltage signal produced from the deformation of a single strain gage is one waveform and many oscilloscopes can measure multiple waveforms at the same time. The waveform contains information about the magnitude of the voltage output from the strain gages and how the voltage signal changes in time [45]. Multiple trace capability can be important when used in conjunction with a triggering system. As previously discussed, the triggering of the data collection at the appropriate time is important for successful data collection during the impact test. Digital oscilloscopes with advanced triggering capabilities can measure changes in the waveform and the user can program the data collection to trigger if the waveform varies in a specific way.

There are several types of digital oscilloscopes including digital storage oscilloscopes (DSO) and digital phosphor oscilloscopes (DPO). The DPO is more suited

to capture transient events than other digital oscilloscopes since it has a dedicated processor for generating waveforms and is the only oscilloscope which will be discussed in detail. The dedicated processor enables the DPO to measure the waveform much like an analog oscilloscope [2]. The DPO's parallel processing architecture allows for the capture and storage of voltage data independent of the waveform image generation allowing for display creation and storage of the transducer data simultaneously. The DPO is commonly used in the electronic diagnostics community to find glitches and other transient signals which require fast responding capability to capture these signals [2]. This makes the DPO an excellent measurement tool in impact experiments [22].

Finally in any instrumented impact testing, it is important to understand the effects of limited frequency response on measurements during testing [22]. Frequency response is the measure of a system's response at output to a spectrum of frequencies at input and every electronic instrument has some limited frequency response which must be evaluated [22]. To evaluate the frequency response, the manufacturers published value for frequency response should be consulted. However, it must be kept in mind that this is not typically the actual frequency response value of the system but rather a frequency response value at which the signal amplitude has been attenuated by 30 percent [22]. For most instrumented impact tests, no more than 10 percent of the measured signal should be attenuated by the frequency response of the system [22]. Frequency response will dictate the range of frequencies output by the system, which is important in impact testing as a large frequency response will ensure higher or lower frequencies are not omitted from the system output. In impact testing, it is often more appropriate to consider the rise time of the system than it is to consider the frequency response of the individual components [22]. Rise time is defined as the time required for the signal to increase from 10 to 90 percent of its full amplitude, and a relationship between signal frequency f and rise time t_r for a sine wave, which can be used to characterize an impulse signal, is given by

$$t_r \simeq \frac{0.35}{f} \tag{2.44}$$

Like frequency response, all components have a limiting response time, and it is suggested that the rise time for the entire instrumented impact test system should be determined to set limits for dynamic signal analysis [22]. This is important since an insufficient rise time will result in the distortion of higher frequency signals [22]. By definition, the rise time t_r of a system can be found through the following relationship

$$t_r = t_{0.9} - t_{0.1} \tag{2.45}$$

where $t_{0.9}$ is the time value at 90 percent of the signal and $t_{0.1}$ is the time value at 10 percent of the signal. Figure 2.18 illustrates the effects of limited frequency response on various load time histories, where (a) is the load histories of an impact test at various impact velocities, v_u, v_c, and v_a and a maximum load P_a is reached each time and (b) shows the distortion of the signal due to the limited frequency response. Clearly as impact velocity increases the both the signal amplitude and apparent time to reach maximum load is affected and therefore considering the rise time of the entire data collection system is important in collecting accurate data for any impact test.

2.1.8 Need for Slotted Beam Technique. This chapter has provided a discussion of the various aspects of impact, including the response of a beam to transverse impact, constitutive modeling of materials at elevated strain rates, different methods of impact testing, a brief history of impact testing, and a description of the various test equipment which can be used in impact testing. It is now clear that impact conditions create several issues which make it more difficult to execute than quasi static loading. Furthermore, the response of metals at elevated strain rates can differ significantly than the response measured under quasi static loading conditions, and therefore impact testing is necessary to quantify the differences in these responses. Unfortunately, the field of impact testing is much less developed than the field of quasi

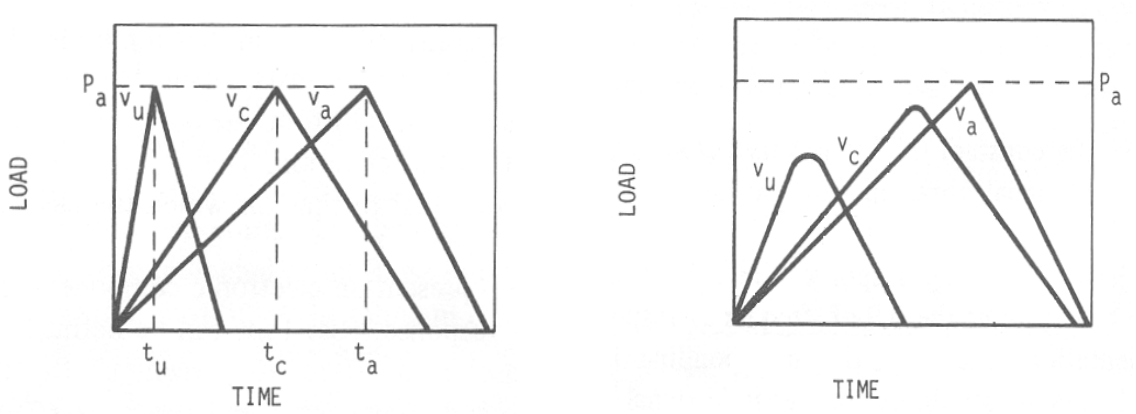

(a) Actual Load Time History (b) Recorded Load Time History

Figure 2.18: Effect of Limited Frequency Response on the Recorded Load Signal [22]

static testing, so the development of additional testing methods is appropriate. Impact testing creates additional demands on testing equipment which is not experienced in quasi static testing, and these demands must be considered if any impact testing method is to be successful. These issues demonstrate the need for additional impact testing methods and the development of the slotted beam tests. An understanding of all these issues is important in the achievement of a functioning slotted beam test which measures the response of ductile metals and provides for the modeling of the constitutive behavior of these metals at intermediate strain rates. The next chapter will detail the methods developed to accommodate the difficulties of measuring the specimen response at impact and modeling the constitutive behavior at strain rates above quasi static loading conditions.

III. Experimental Method

3.1 Development of the Slotted Beam Experimental Technique

The behavior of the slotted beam is expected to be similar to the rigid, perfectly plastic model of a transverse impact of the beam, except the material strain hardens such that the development of a plastic hinge at the center of the beam and deflection of the beam results in a primarily uniaxial state of tensile stress in the ligament underneath the slot. A significant amount of plastic deformation is expected in the ligament of the slotted beam at higher velocities, and the specimens are expected to exhibit some strain rate dependent behavior. To quantify this elastic viscoplastic behavior, it will be necessary to determine the response at the center of the ligament, and therefore an appropriate test and measurement system must be designed to accurately analyze the material response. The effects of inertia and stress wave propagation will have to be considered, and a method to determine the loading at the equivalent location on the ligament must be developed so that the constitutive behavior of each material may be modeled. As the slotted beam technique is explained, the motivation behind and the procedures to execute this experimental method will be discussed in addition to a detailed description of the test equipment used. To do this, special attention must be paid to the manufacturing of the test specimen, the instrumenting of the specimen, the development of the test apparatus, the selection of the test equipment, the test procedure, and the development of an accurate three dimensional FEM for constitutive modeling. This chapter will begin with details of the slotted beam specimen.

3.1.1 Slotted Beam.

3.1.1.1 Materials. The test specimens for these experiments consisted of 36 beams with the following dimensions: length - 15.24 cm, width - 2.54 cm, and height - 1.27 cm. The beam dimensions were selected due to their standard size and availability from most metal stock suppliers. The materials chosen for these experiments were 1018 Steel, 2024 Aluminum alloy, and commercially pure (CP)

Table 3.1: Mechanical Properties of 1018 Steel, 2024 Aluminum alloy, and CP Titanium [15]

Metal	**1018 Steel**	**2024-T3 Aluminum**	**CP Titanium**
Young's Modulus, E (GPa)	200	73.1	120
Yield Strength, σ_0 (MPa)	260	303	345
Poisson's Ratio, ν	.285	.33	.34
Density, ρ ($\frac{g}{cm^3}$)	7.87	2.70	4.51
Description	General purpose low carbon steel with good machinability	Widely used aircraft alloy with superior strength and good machinability	High strength to weight ratio when compared to Aluminum and good durability

Titanium, and the number of specimens of each material were evenly divided between the three materials so that twelve Steel, twelve Aluminum, and twelve Titanium specimens were tested. Table 3.1 contains the published mechanical properties and a brief description of each metal [15].

These three metals were selected for several reasons. First, there has been a large amount of previous impact testing accomplished with these metals and their alloys in an effort to quantify any rate dependent behavior [38] [10]. Secondly, these metals are readily availability and inexpensive when compared to more exotic alloys. All of the metal stock was procured from an industrial supplier, McMaster-Carr Supply Co., Elmhurst, IL, in 1.27 cm sheets and then cut into beams using a Computer Numerically Controlled (CNC) water jet machine. The tolerance for the beam dimensions during this cutting process was ± 0.16 cm from the center of the beam, ± 0.08 cm for the width of the beam, and ± 0.16 cm for the height of the beam. After cutting the beams and confirming the dimensions, the slots were placed in the beams. The slot dimensions were determined through an analysis using the finite element program, ABAQUS of the stresses developed in the ligament when struck at the top of the beam [44]. During the ABAQUS analysis, a design of experiments was used

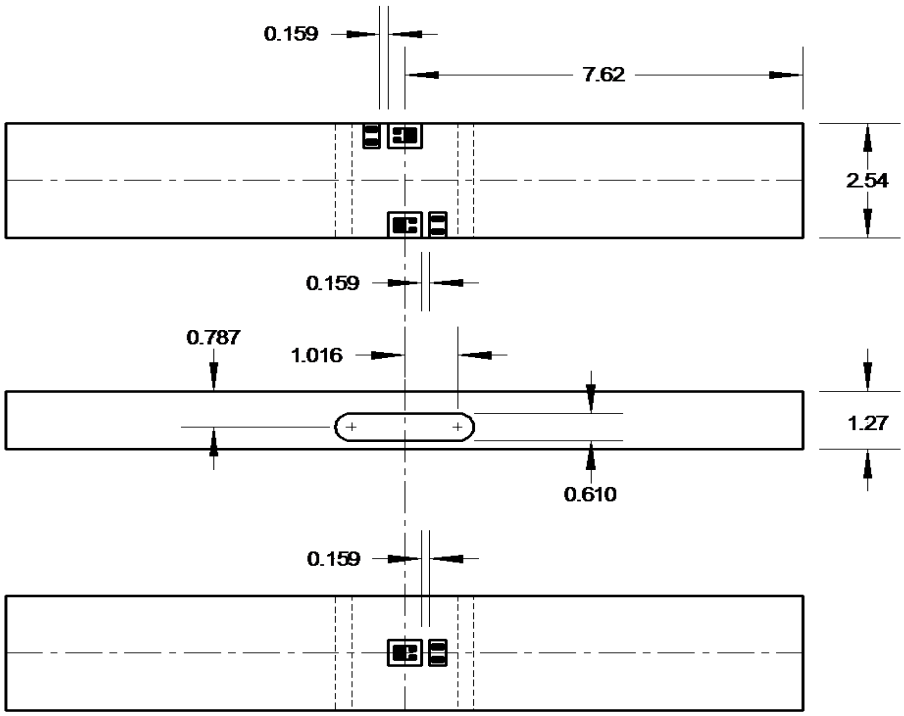

Figure 3.1: Slotted Beam Specimen Dimensions and Locations of Strain Gages in (cm) [28]

in an effort to determine the slot configuration, which minimized the difference between the Mises stress measured at the center node of the ligament and the stress in the principal direction parallel to the length of the beam. The dimensions of the slot are material dependent and this initial design was based on Titanium material properties. These slot dimensions were used for all of the specimens due to time constraints but further analysis may have to be performed to modify the slot dimensions for other materials such as Aluminum and Steel. Several constraints were placed on the dimensions of the slot so the dimensions could be easily manufactured, including a minimum thickness of the ligament in the slot. Both the final slot dimensions, the beam dimensions, and the locations of the strain gages are shown in Figure 3.1.

The slot dimensions selected were small and a precision cutting technique which did not damage the specimen during the machining process was desired. Electrical Discharge Machining (EDM) is a non-contact cutting method which offers these capa-

bilities. EDM is a machining technique which is capable of machining small complex shapes in hard materials. One of the benefits of EDM is that the tool never contacts the specimen surface so that the specimen is never subjected to any cutting forces. EDM functions by eroding very small parts of the work item by creating repetitive short duration sparks between an electrode and the work item. This requires the work specimen to be electrically conductive, which is the case for all specimens being machined with EDM. For erosion to occur, the gap between the electrode must be very small usually on the order of .025 to .05 mm. This gap is maintained by the cutting machine throughout the cutting process. The frequency of spark production is usually on the order of $10,000$ sparks per second which requires a direct current power supply. The region between the electrode and the work specimen where the current is discharged across the gap is turned to plasma and temperatures of $20,000$°C can be reached [20]. This melts a tiny portion of both the specimen and the electrode, which requires the electrode to be replenished throughout the machining process. When the current is turned off, the heated material is flushed away by the dielectric liquid and a small crater remains. This process is repeated until the area to be removed from the specimen has been eroded away. The typical volume of material removed is in the range of 10^6 - 10^4 mm^3. This results in a material removal rate of 2 - 400 mm^3/min depending on the particular system used [20]. While not quick, EDM does result in very precise material removal due to the small amount of material removed per discharge and the computer automation of the electrode. The EDM process allowed the placement of the slot in the same location for each specimen, which is important in the repeatability of a test method. After all specimens were machined with slots, the dimensions of each slot were confirmed to be within tolerance and any specimens with slots outside of the tolerance were rejected.

3.1.2 Instrumentation.

3.1.2.1 Strain Gage. After the machining process it was necessary to instrument the specimen to measure the slotted beam response to impact. Strain

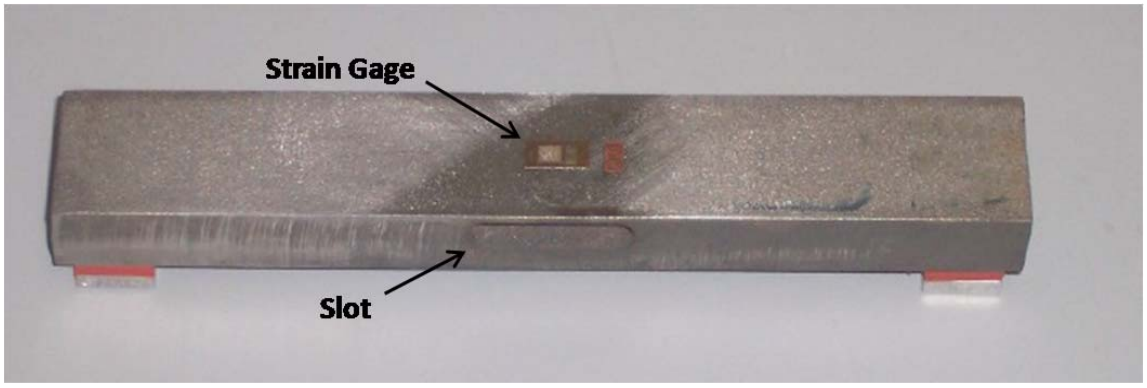

Figure 3.2: Strain Gage on Ligament of Slotted Beam

gages, accelerometers, and high speed photography were evaluated as methods to measure the specimen response. After a consideration of the clearances in the test apparatus, the cost of instrumentation, and the effort of installation, the strain gage was selected as the best transducer to measure the material response at the ligament when the slotted beam is impacted. The strain gages selected for the tests were EP-08-125AC-350 Vishay Micro-Measurements gages which have a resistance of 350Ω, gage factor of 2.1, and a transverse sensitivity of 0.8 %. These strain gages have grid dimensions of 0.318 cm by 0.318 cm and matrix dimensions of 1.02 cm by 0.56 cm. They are manufactured from an annnealed constantan foil grid and high-elongation polymide backing capable of sustaining elongations up to 20 percent. Polyimide is a type of plastic which is very durable and easy to machine and at the same time is also highly insulative and does not contaminate its surroundings. Finite element analysis of the slotted beam experiment strains up to 8 percent were sustained, and therefore a high elongation strain gage is required for these experiments. The location of the strain on the slotted beam specimen is shown in Figure 3.2.

In addition to a high elongation strain gage, bondable terminals and strain relief loops were used in effort to prevent the premature disbonding of the strain gage during the test. Inertial forces at impact also put significant demands on the solder joints of the strain gage and specific efforts, including small gauge wire and bondable terminals were selected to reduce the chance of failure during testing. Several actions can be

taken to help prevent the premature failure of the strain gage including proper surface preparation, use of bondable terminals and strain relief loops [58] [53]. The slotted beam tests will be unsuccessful if the strain gage prematurely fails, and therefore all of these actions are essential to the success of these tests. The following is a detailed description of the procedure for instrumenting the slotted beam with strain gages.

The most important step when instrumenting with strain gages is surface preparation. To accurately measure the material response, the strain gage must have a strong defect free bond with the material surface. This is accomplished through proper surface preparation and the use of an appropriate adhesive. The primary goal of surface preparation is to create a chemically clean surface with an alkalinity corresponding to a pH value of 7 so the adhesive will properly wet the surface and bond to it [34]. The traditional steps in surface preparation for strain gages include five steps: solvent degreasing, abrading, marking, conditioning, and neutralizing the specimen surface all listed in Table 3.2.

The significant demands on the strain gage bonds result in special requirements for the porous surface of Titanium, and an additional step is necessary for the Titanium samples. A porous surface makes it difficult to properly degrease the specimen surface, and therefore heat is required to drive off absorbed oils and deposited lubricants [34]. A heating cycle of 2-6 hours at 175°C is recommended before degreasing materials with porous surfaces, so all Titanium samples were heated for six hours in the AFIT lab, Rm 257 oven before the surfaces were prepared. Silicon carbide paper is preferred during the abrading process since the grit is securely fastened and reduces the likelihood of grit being deposited into the specimen surface. In addition, the mild phosphoric acid solution acts as an etchant to speed the cleaning process [34]. If the condition of the specimen surface is poor, then milling or grinding of the surface may be required to remove scale, machining marks, or surface indentations. In this experiment, the surface of all specimens was smooth enough that additional milling or grinding was not necessary. Typically a smoother surface is better for creating the thin glue lines required by most strain gage adhesives and the thinner the glue line

Table 3.2: Surface Preparation Steps for Strain Gage Application

Preparation Step	Purpose	Chemical/Tools Used
1. Degreasing	Remove any organic contamination, oils, or grease deposited on the specimen surface prior to surface preparation [34]	Isopropyl Alcohol
2. Abrading	Smooth the surface of the specimen in the area of the gauge application to provide a surface finish which promotes optimum bonding by the adhesive	400, 320, and 120 grit silicon carbide paper and mild phosphoric acid solution
3. Marking	Position the strain gauge for application and align the strain gauge so any errors caused by the transverse sensitivity of the strain gauge are minimized	Straight Edge and Pen
4. Conditioning	Clean the surface of any contamination caused by previous operations such as marking or abrading	Conditioner and Cotton Tipped Applicators
5. Neutralizing	Neutralize the surface so the pH of the surface is returned to 7 eliminating any remaining acidity on the specimen surface	Neutralizer and Cotton Tipped Applicators

required, the smoother the finish must be [34]. High elongation testing and dynamic events require a rougher surface for optimum bond strength, and the recommended surface finish is around 250 μinches (rms). This is achieved through an additional abrading step were the gage area is cross hatched with silicon carbide paper. All of the specimens in these tests were dry abraded, wet abraded, and then cross hatched to achieve the recommended surface finish for high elongation testing and dynamic events. To minimize the amount of strain measured in the transverse direction of the strain gage, the length of the gage must be aligned with the direction of the applied stress. For the slotted beam specimens, this means aligning the length of the strain gauges with the length of the beam. In practice a specimen is marked with a drafting pencil or ballpoint pen, however care must be taken to not score the surface which may cause surface damage and stress concentrations [34]. Conditioning and neutral-

izing play an important role in surface preparation since any residual acidity on the specimen surface would prevent the bonding of some adhesives [34]. After the surface preparation process, it is important to place and adhere the strain gauges on the specimen surface as soon as possible to prevent surface re-oxidation. Different materials oxidize at different rates, and strain gauge application should not be delayed for more than forty-five minutes in general steel, thirty minutes in aluminum, copper, and beryllium, and ten minutes in titanium. This was considered during the instrumentation of the slotted beams, and to ensure surface re-oxidation was prevented titanium specimens were prepared in fewer number so that no specimen surface was exposed to the environment for longer than 10 minutes before strain gage application.

3.1.2.2 Gage Preparation and Placement. As previously discussed, bondable terminals were used in conjunction with the strain gage. The bondable terminal allows the use of strain relief loops, which prevent premature failure of the solder connections in high elongation and also reduce the mass of the solder joint on the strain gage [56]. The CPF-75C Vishay Micro-Measurements bondable terminal was used in the slotted beam experiments, but each terminal was cut in half as recommended by Vishay Micro-Measurements to reduce the size of the terminal pad and again reduce the mass of the solder joint. Both the strain gage and the bondable terminal were set on a clean plexiglass surface and placed with a minimum distance of 10 mm between each other to prevent adhesive buildup between the gage and bondable terminal. Adhesive buildup between the gage and the bondable terminal can cause the premature failure of the gage in high elongation applications [52]. Adhesive tape is then used to pickup up the gage/terminal arrangement and placed on the specimen surface. This prevents damage from touching, bending, or scratching of the gage foil material from handling. As the gage is placed on the surface, the markings designate the center of the foil grid and are oriented with marks made during the marking step of surface preparation. This ensures the placement of the strain gage in the center of the ligament oriented along the length of the beam. Adhesive can then be applied

to the strain gage and terminal by picking up one side of the tape at a shallow angle until the bottom surfaces of the gage and the terminal pad are exposed.

3.1.2.3 Adhesive Application. An evaluation of adhesives revealed that an epoxy based adhesive would be necessary to prevent the strain gage from disbonding prematurely. The elongation capabilities and bonding strength of M-Bond 200 and M-Bond AE-10, a cyanoacrylate capable of handling 6 percent elongations and a two component 100 % solids epoxy capable of handling 6-10 percent elongations respectively did not make good adhesive candidates [58]. M-Bond GA-2 is a two component epoxy capable of handling 10-15 percent which was considered but later ruled out due to its complicated cure cycle. M-Bond AE-15 is a two part 100% solids epoxy capable of handling up to 15 percent elongation. This adhesive requires a relatively simply cure cycle of 2 hr at 150°F. It was selected for its ease of use and its large elongation capability. However, as with any two part epoxy, a consideration for the pot life, or amount of time the adhesive can be used and must be made when planning the application schedule. The pot life for M-Bond AE-15 is 1.5 hours, and once exceeded is no longer good for applying strain gages. The pot life along with the oxidation of the specimen surface made it important to properly coordinate and execute the adhesive mixing and strain gauge application process.

After mixing, the adhesive is applied in very small amounts to the back of gages, terminal pads, and the specimen surface. Applying a large amount of adhesive during this process will result in a buildup of adhesive during curing and should be avoided. To prevent adhesive buildup, a clamping pressure of 5-20 psi, provided by spring clamps and silicone gum pads, was applied to each strain gage location. The specimens were placed in an oven for 2 hours at 150° F to cure.

3.1.2.4 Considerations for Large Elongations. After curing for 2 hours the specimens were taken from the AFIT lab, Rm 257 oven and allowed to cool. Soldering lead wires and jumper wires was the next step in the specimen instrumentation. Micro-Measurements M-Bond solder and flux was used to attach 326-DTV

wire to the strain gages and terminal pads. 326-DTV wire consists of three 26-gauge twisted, copper wire which is recommended in low voltage high noise applications and is a size which is smaller than the 20 American Wire Gauge (AWG) limit by Micro-Measurements. [53] [54]. This will reduce the mass of the solder joints at the bondable terminals and the strain gage tabs. The twisting of the wire is important for reducing electromagnetic noise in the strain gage signal. These wires were used because they satisfied the requirements for these tests and were readily available in the AFIT lab. In soldering the strain gages, the lead wires were prepared by taking a single strain of wire from each and then twisting the remaining wires. The single strand of wire was used to create jumper wires, and the remaining wire was tinned and trimmed for soldering to the bondable terminal pads. After soldering to the terminal pads, the jumper wires were formed so that they connected at a 90 degree angle to the expected uniaxial stress as shown in Figure 3.3. After soldering the lead wires on each specimen, the integrity of solder joints were checked by a visual inspection and with a multi meter to ensure the resistance of the gage was 350Ω. If there was a bad connection in one of the solder joints, the multi meter would have read a much larger resistance than 350Ω or no resistance value at all.

3.1.2.5 Investigation of Other Stress States. In an effort to investigate other stress states on the slotted beams during the analysis of strain gage data, two specimens of each material were instrumented with two additional strain gages on the top of the slotted beam as shown in Figure 3.4.

These gages were placed at these locations because a preliminary analysis showed that at these points a state of bending in compression with significant plastic deformation was present. These gages were applied using the same application techniques previously described for the strain gages placed at the center of each beam ligament.

3.1.3 Test Procedure.

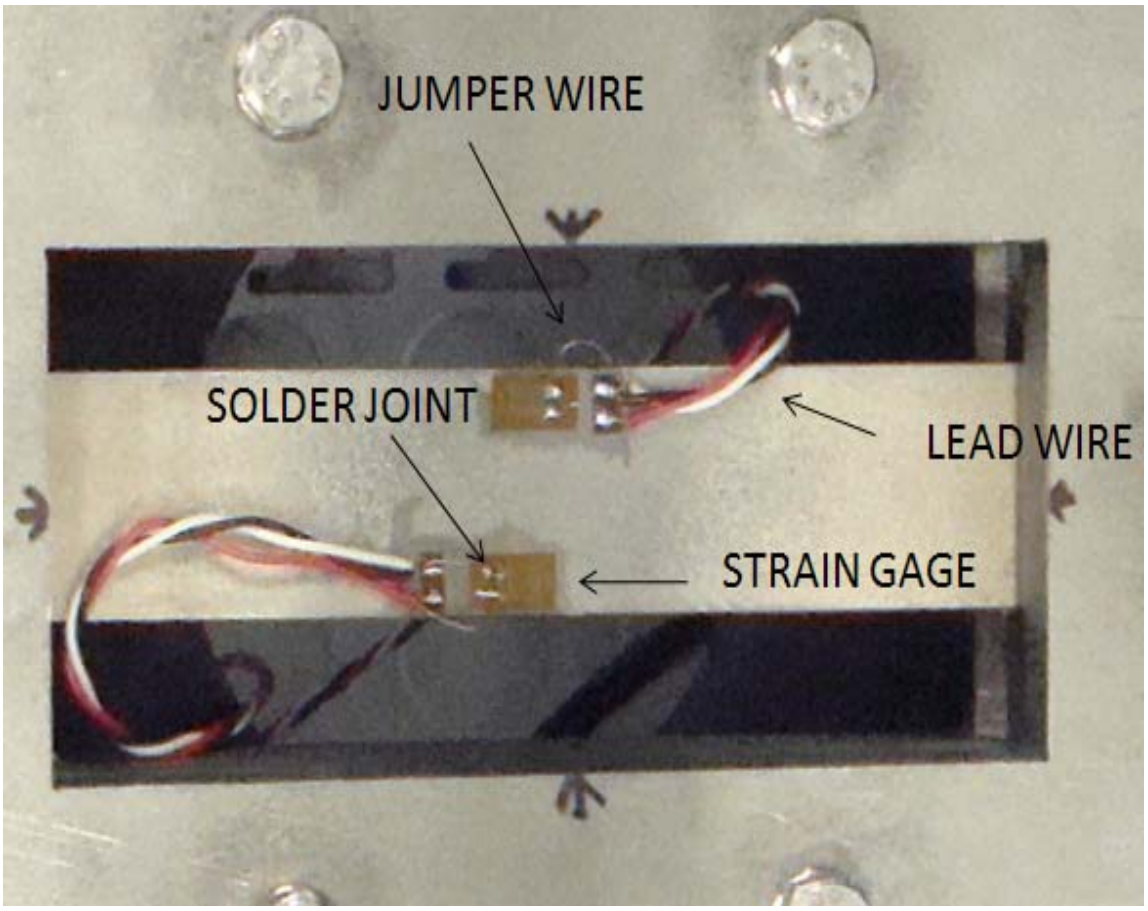

Figure 3.3: Lead Wires, Strain Relief Loops, and Solder Joints

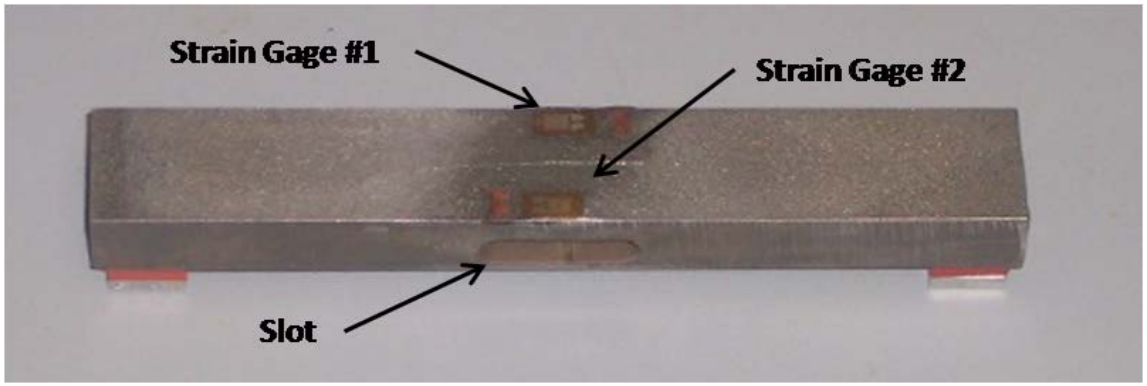

Figure 3.4: Additional Strain Gages on Slotted Beam Specimen

3.1.3.1 Dynatup. After all of the specimens were determined to be ready they were transported in a sealed container to Bldg 65, AFRL Structural Sci-

ence Center, the location of the drop weight test apparatus. This drop weight test apparatus, an Instron Dynatup 8250, is a small to medium weight impact machine capable of impact energy levels between 0.6 to 442J as shown in Figure 3.5.

The Dynatup is an instrumented drop weight impact machine with both; a piezoelectric load cell connected to a tup to measure impact load, and a velocity photodetector to measure impact velocity, shown in (a) and (b) respectively of Figure 3.6. The Dynatup has two modes, gravity driven and pneumatic assist. In the gravity driven mode the crosshead, shown in (c) of Figure 3.6, is raised or lowered along the guide rails to achieve a range of velocities from 3.66 to 0.61 m/s. The mass of the crosshead can be increased to a maximum of 45 kg from a minimum of 2.5 kg, creating an energy range of 0.6 J to 225 J in the gravity assist mode. Energy levels above 225 J are achieved in the Dynatup's pneumatic assist mode. In the pneumatic assist mode, two large springs, shown in (d) of Figure 3.6 are compressed against the crosshead, which is locked into place, with pressurized air from pneumatic cylinders, shown in (e) of Figure 3.6. Increasing the pressure to a maximum of 100 psi, the pneumatic mode is capable of accelerating the crosshead to a maximum velocity of 13.41 m/s. Shock absorbers are used to arrest the crosshead after initial impact in the pneumatic mode and rebound brakes are used to arrest the crosshead after initial impact in the gravity driven mode. An important note is that the crosshead mass at velocities above 4.42 m/s is limited to 5 kg due to limitations of the shock absorbers, and to reach the Dynatup's maximum energy of 442 J it is necessary to maximize the crosshead mass at 45 kg at a velocity of 4.42 m/s. The height of the photo-detector can be adjusted and may need to be raised or lowered depending on the length of the load cell/tup combination being used in the particular test. When adjusting the detector, it is necessary to ensure the entire flag will travel through the detector just prior to impact of the specimen. The Instron $20,000$ lbs piezoelectric load cell measures the load at impact, and the maximum load throughout the duration of the impact. Beyond the $20,000$ lbs load range, the load cell deformation is no longer proportional to the load experienced at the tup, and the load cell voltage signal is saturated such that loads above $20,000$ lbs can not be measured. The crosshead can be raised and lowered at the Dynatup contol panel, shown in (f) of Figure 3.6, when not armed and is triggered after arming the system at the same control panel. The load values

Figure 3.5: Instron Dynatup 8250

and the crosshead velocity for each impact event are stored by the Dynatup data acquisition system and saved for further analysis.

3.1.3.2 Test Fixture. A fixture will be anchored to the Dynatup and a test specimen will be clamped within the fixture. The test fixture is required as an interface between the specimen and the Dynatup and performs serval functions in these tests. The first function is to position the beam and plate specimens to the Dynatup such that the specimen is centered and the tup impacts the center of the top surface of the beam. This function is accomplished by marking both the center of the fixture and the center of each specimen, and placing the specimen within the fixture so that both set of markings are aligned as shown in Figure 3.7.

This is important since the development of uniaxial tension in the ligament relies on the symmetric deformation of both halves of the slotted beam resulting from the center impact of the tup. If the impact is not in the center of the beam then the deformation will not be symmetric and states of stress other than uniaxial tension will begin to develop in the ligament.

The second function of the fixtures is to create a fixed-fixed boundary condition for the beam specimens and anchor the specimens to the Dyantup. The fixed-fixed boundary condition is created by fastening a second and third plate to the bottom plate with ten $\frac{1}{4}$" bolts. In this configuration the top and bottom plates providing the clamping pressure while the middle plate protects the specimen from crushing. Analysis of these fixtures in ABAQUS showed an even pressure distribution at the boundaries of each specimen with the fixture bolts torqued to 20 N-m [28]. This torque specification will be evaluated during initial testing to ensure no specimens are coming loose and to verify no crushing of the boundaries of any specimens. When secured in the fixture, the specimen resultant length is 11.43 cm long. Another function of the fixture is to provide the interface between the specimen and the Dynatup, and securely anchor the specimen in the Dynatup. This is accomplished with four $\frac{3}{8}$" bolts torqued to 30 N-m. These mate with existing holes in the Dynatup base plate and anchor the fixtures during testing. The test fixture is machined from 304 Stainless Steel, which was chosen on strength, cost, machinability, and corrosion considerations. A CNC water jet cutter was used to cut the plates for the beam fixture. After initial

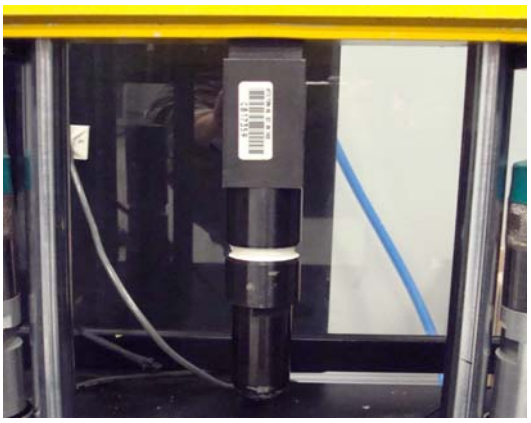

(a) Piezoelectric Load Cell

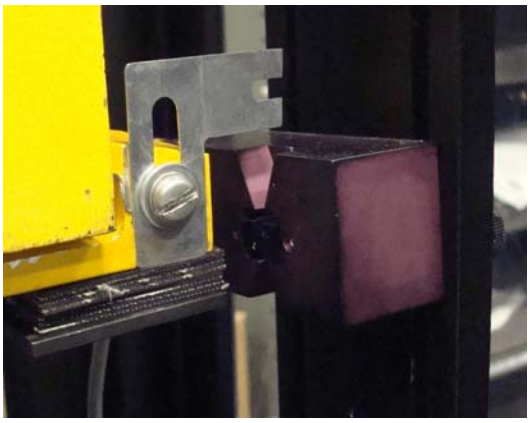

(b) Velocity Photo-detector

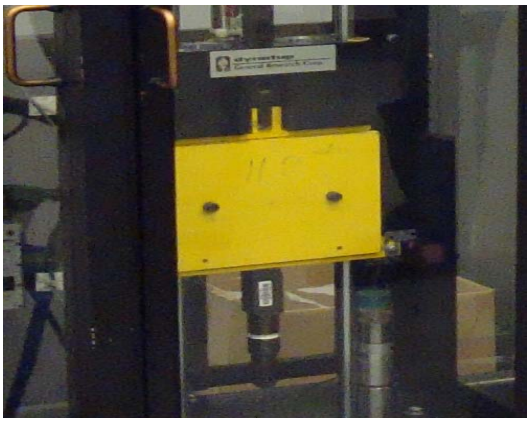

(c) Crosshead

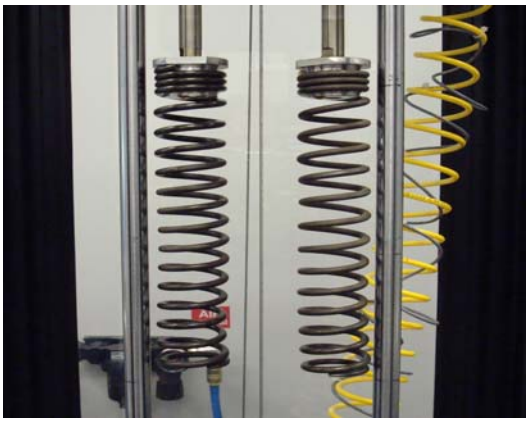

(d) Springs

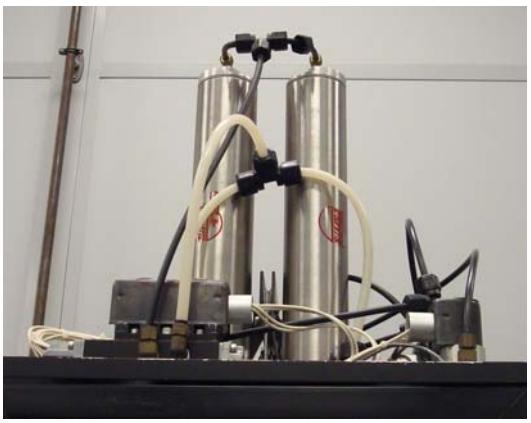

(e) Pneumatic Cylinders

(f) Dynatup Control Panel

Figure 3.6: Components of Instron Dynatup 8250

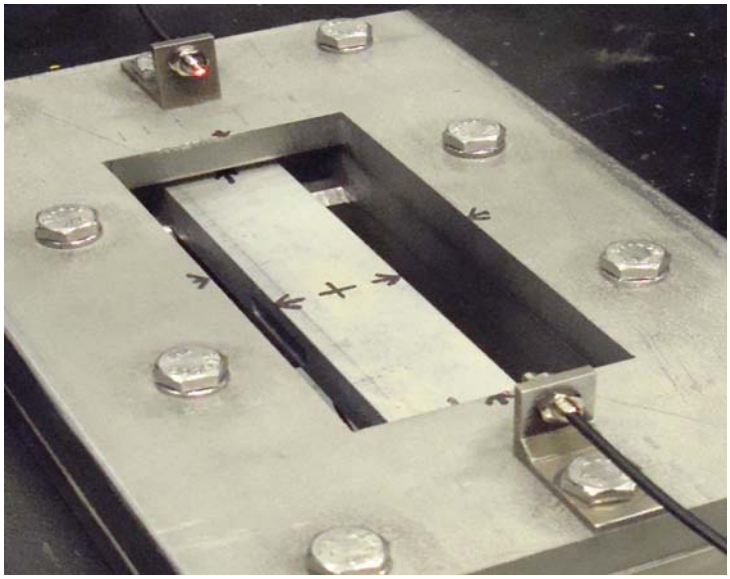

Figure 3.7: Slotted Beam Centered within Fixture

machining of all of the pieces, dimensions and tolerances were inspected to check for clearance problems which were corrected using a milling machine until the dimensions and tolerances were achieved. An exploded view of the beam fixture is shown in Figure 3.8 and Autosketch drawings of the three fixture plates are shown in Figures 3.9 through 3.11.

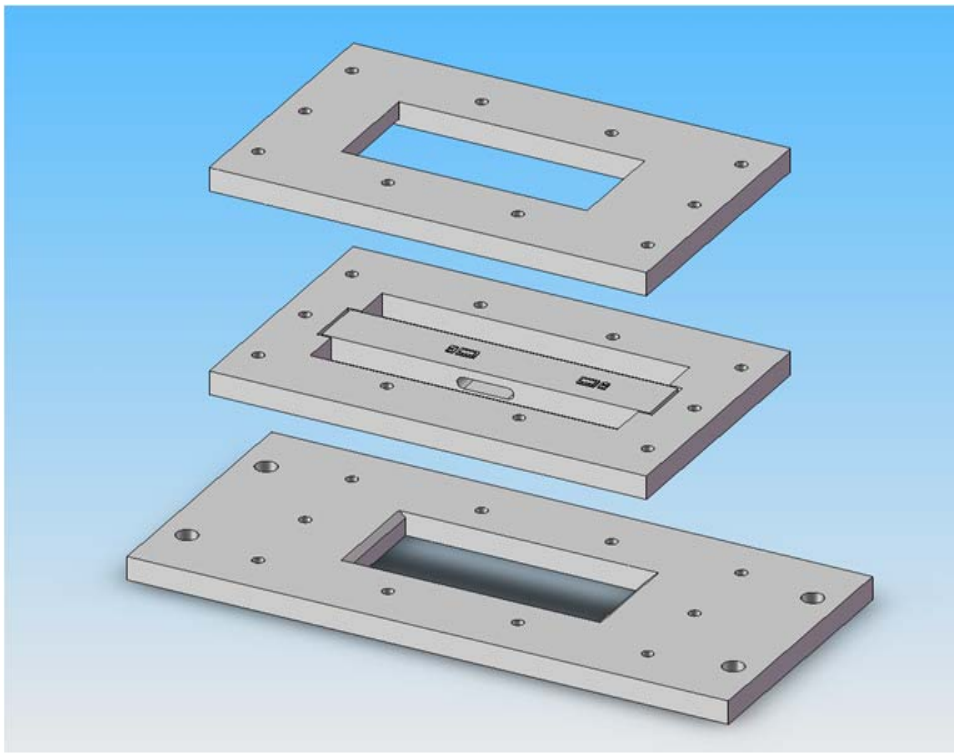

Figure 3.8: Exploded View of the Slotted Beam in Fixture

The fixture also provides a location for the fiber optic trigger used as an initial trigger for data collection in the slotted beam tests. The fiber optic trigger is anchored to the fixture through 304 Stainless Steel brackets and two of the ten $\frac{1}{4}$" bolts which clamp the specimen. The fiber optic trigger is a Banner Electronics fiber optic amplifier and plastic fiber optic cables, part # FI22FP and PIT46U respectively, operated in opposed mode. The fiber optic trigger, with a maximum range of 20.54 cm, functions as a optical switch which outputs approximately 10V when the light intensity is high and the path between the fiber optic emitter and sensor is unbroken. The output of the fiber optic trigger is controlled by the power supply which in these experiments was an Hewlett Packard 6023A DC Power Supply with a voltage range of $0 - 20$V. When the the path between the emitter and sensor is broken, the voltage output drops to approximately 30mV and the voltage drop is used as an initial trigger for data collection. It is important to note that the published response time of the fiber optic trigger is 500 μs, which is the amount of time required for the voltage out-

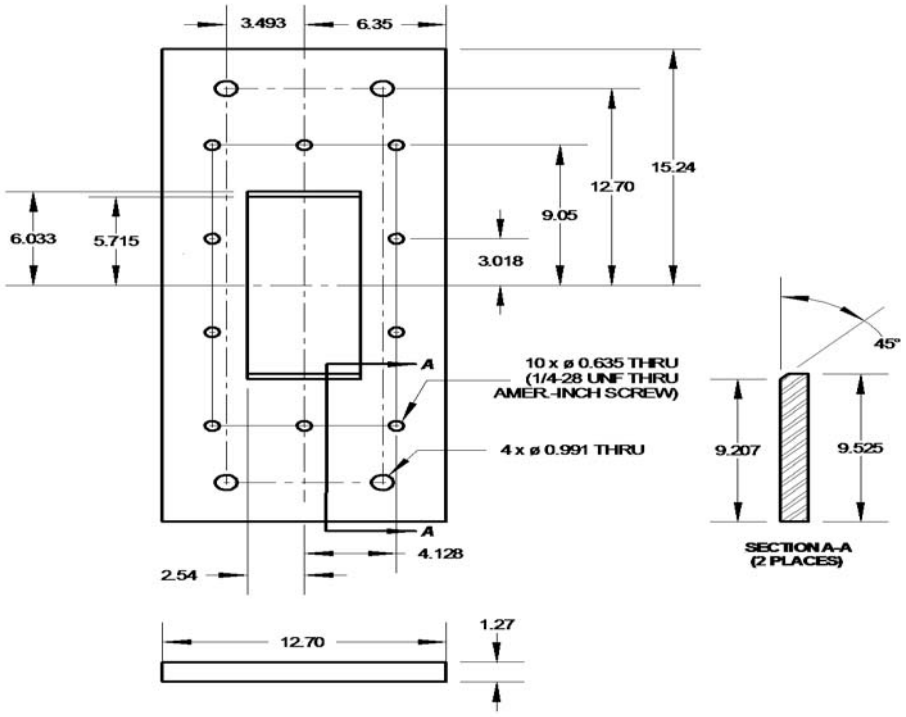

Figure 3.9: Autosketch Drawing of Beam Fixture Bottom Plate [28]

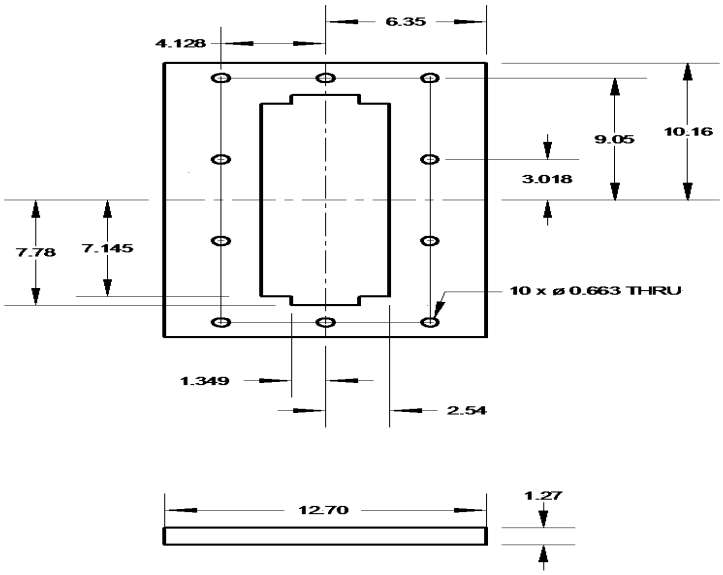

Figure 3.10: Autosketch Drawing of Beam Fixture Middle Plate [28]

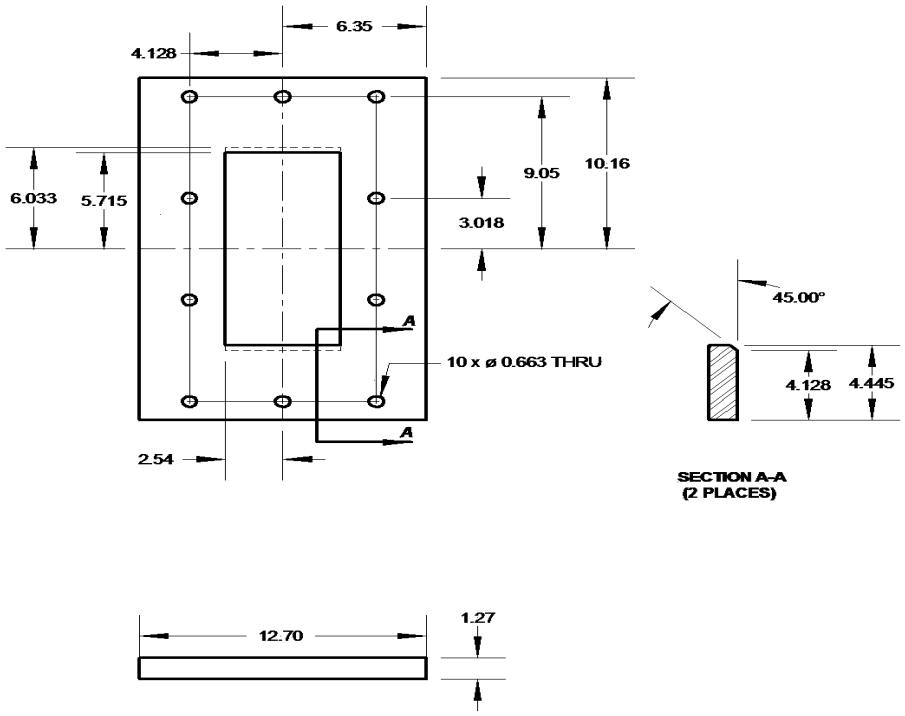

Figure 3.11: Autosketch Drawing of Beam Fixture Top Plate [28]

put to change after the path between the emitter and sensor is broken. It is therefore necessary to place the fiber optic trigger at a height above the specimen at which it takes longer for the tup to travel at its maximum velocity than the response time of the fiber optic trigger. The fiber optic trigger was placed 2.54 cm above the top surface of the specimen and secured using Steel brackets, a drawing of which is shown in Figure 3.12. At the Dynatup's maximum velocity of 13.41 m/s, this distance will be traveled in approximately 2 ms, which is significantly longer than the response time of the fiber optic trigger and therefore an appropriate location for the fiber optic trigger. The plastic fibers used in this trigger are also important due to the shock created by the impact on the specimen. This shock could damage electronic components anchored to the fixture, however the plastic fibers do not contain any electronic parts and rather only transmit light through the fibers. This is transformed into an electronic signal by the fiber optic amplifier located away from the Dynatup with the

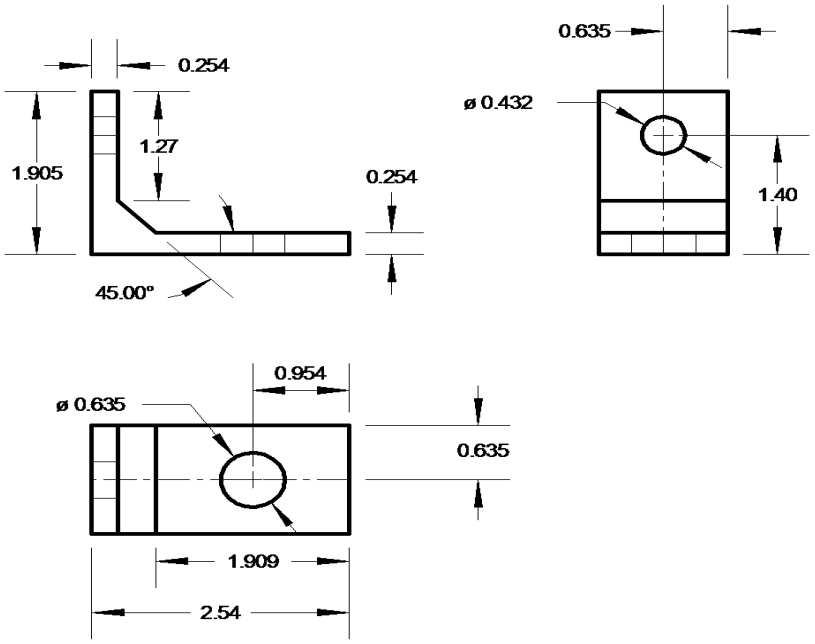

Figure 3.12: Drawing of Steel Bracket to Secure Fiber Optic Trigger (cm) [28]

(a) Banner Electronics FI22FP Fiber Optic Amplifier (view from above)

(b) Hewlett Packard 6023*A* DC Power Supply

Figure 3.13: Components of Fiber Optic Trigger System

rest of the test and measurement equipment. Figure 3.13 contains images of both the Banner Electronics FI22FP Fiber Optic Amplifier and the Hewlett Packard 6023*A* DC Power Supply. Several views of the fixture with a specimen and fiber optic trigger are shown in Figure 3.14.

3.1.3.3 Test Preparation. Once the fixture is securely fastened within the Dynatup and before a specimen is placed within the fixture, it is necessary to ensure none of the solder joints were damaged during transportation or installation of the specimen. This is accomplished with both a visual inspection and with the use of a multi meter to confirm the resistance of the strain gage remains 350Ω. After this is confirmed, the specimen is placed within the fixture and the lead wires are connected to an Ectron 562 DC Differential Amplifier. The Ectron unit, supplied by the University of Dayton Research Institute (UDRI), consisted of three 350Ω internal resistors to complete the Wheatstone bridge and a 49,000Ω resistor for the shunt calibration process. This meant that only a $\frac{1}{4}$ bridge arrangement and 350Ω strain gages could be used with this amplifier. In addition, the Ectron unit contained the power supply to create a 5V DC voltage across the Wheatstone bridge. The 5V excitation voltage provides a balance between a large voltage input, which is needed to measure the change in resistance of the strain gage, and the possibilities of errors due to gage heating [42] [41]. The Ectron unit also provides the capability to amplify the voltage signal from 1x to 1000x and an amplification of 20x was used for all tests. The published values of the Ectron amplifier's CMRR, as discussed in section 2.1.7, is 50 dB, indicating the magnitude of the common mode signal which will appear in the measured signal, and while this is less than optimum according to the literature it still provides significant capability in increasing the signal to noise ratio from the strain gage [42]. The lead wires are securely connected to the Ectron unit through a terminal strip to complete the Wheatstone bridge, and then the bridge was 'balanced' by zeroing the bridge output voltage as discussed in section 2.1.6.1. This is accomplished by adjusting a calibration screw with the amplifier in operational mode, such that the voltage measured by a multi-meter linked to that channel of the amplifier is zero. The calibration mode of the amplifier is then selected and the positive and negative voltages across the Wheatstone bridge created by the strain gage and shunt calibration resistor are measured by the multi-meter and recorded as V_{cal}. These voltages are used to the determine the relationship between voltage and

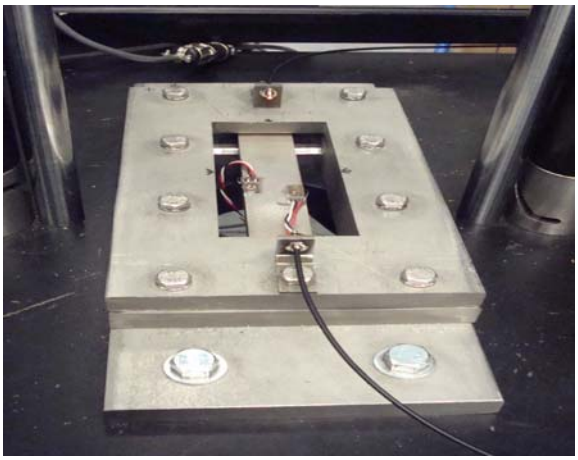

(a) Front View

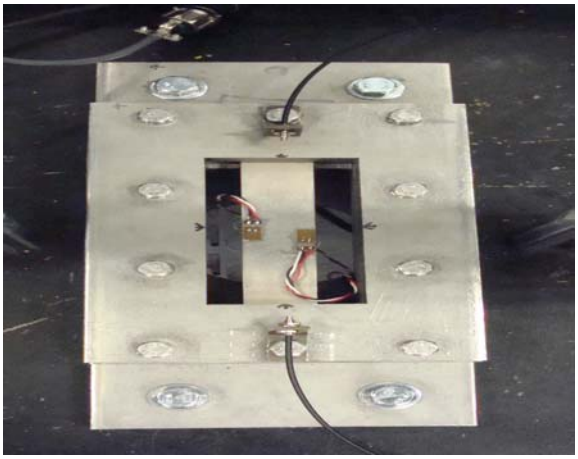

(b) Top View

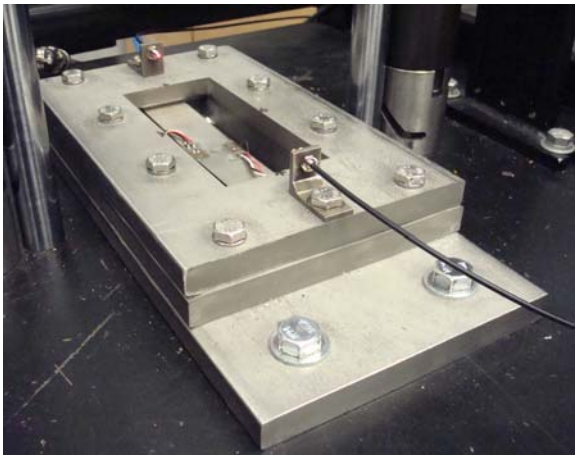

(c) Side View

Figure 3.14: Several Views of the Beam Fixture with Specimen and Fiber Optic Trigger

strain for the strain gage after each test, so that the strain measured at the strain gage can be calculated from the voltages recorded during the test. V_{cal} is typically on the order of 170 to 190 mV and values much higher or lower than this may be an indication that there is a poor connection or other problem with the strain gage and lead wires. Figure 3.15 shows the Ectron amplifier and the multi-meter used during the strain gage calibration process. The tape placed over the Ectron unit was due to the close proximity of the calibration screw and the RTI zero screw and while the calibration screw will be frequently adjusted during testing the RTI zero screw should not be adjusted after the initial calibration of the Ectron amplifier by UDRI.

After 'balancing' the strain gage, it is necessary to configure the Tektronix TDS 3034 Digital Phosphor Oscilloscope, shown in Figure 3.16, used to measure and store the voltage signal during the impact test. This particular oscilloscope has four channels with a bandwidth of DC to 300 MHz and a sample rate of 2.5 $\frac{GS}{s}$ [2]. The Tektronix DPO is capable of storing $10,000$ data points for each channel at a time. This storage capability in conjunction with the time window selected for the experiment which was 1 ms, translates into a sampling rate of 10MHz or 10 samples every μs. The TDS 3034 has a 9-bit resolution and a dual trigger capability. The dual trigger capability in these tests ensures the data collection will trigger due to the change in resistance of the strain gage mounted on the ligament underneath the slot, and not due to noise from the Dyantup electronic equipment. The initial trigger in the dual trigger configuration is the voltage output from the fiber optic trigger as measured on channel 1 of the DPO. This trigger is set for a voltage drop below 5V, which is characteristic of the drop in output voltage of the fiber optic amplifier when the path between the fiber optic emitter/sensor is broken. 5V is used due to the fact that it is higher than any voltage signal created by the Dynatup electrical equipment and at the same time not as large as the voltage output of the fiber optic amplifier when the light path is unbroken. The initial trigger prevents any signals from the Dynatup electronic equipment from inadvertently triggering the data collection system. The secondary trigger, which is responsible for triggering the actual data collection, is the

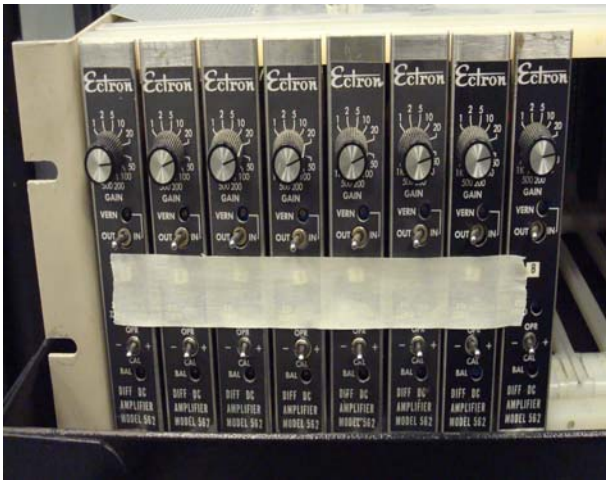

(a) Ectron 562 DC Differential Amplifier

(b) multi-meter

Figure 3.15: Ectron Amplifier and Multi-meter used for Shunt Calibration of Strain Gages

voltage output from the strain gage mounted on the ligament underneath the slot. Measured on channel 2, the settings for this trigger are 200 mV with a rising slope, which is characteristic of the voltage output over the Wheatstone bridge as the strain gage begins to deform in a uniaxial tensile stress field. A 2 ms delay between the initial and secondary trigger is used to provide sufficient time for the initial trigger to be satisfied before the secondary trigger can be met. The Tektronix DPO also has a pre-trigger capability, which allows the collection of data before the trigger thresholds are met. This is possible since the oscilloscope constantly samples 10000 data points from each channel in the data acquisition mode and the pre-trigger defined in percent selects the number of samples to be collected before the data collection is triggered. The pre-trigger setting for the slotted beam tests is 10 percent or 100 μs. After all of these settings are programmed into the Tektronix oscilloscope, the measurement system is ready to collect data for the slotted beam tests. 1V vertical voltage divisions were selected on the Tektronix unit which meant a maximum of a 5V positive or negative signal could be recorded before the voltage signal would be 'clipped'. The vertical voltage divisions were selected due to the the voltage outputs recorded during preliminary testing. After the oscilloscope is configured, the Single Sequence button is pressed and the system is armed for data collection.

At this point the fiber optic trigger is checked by breaking the path between the two sensors and checking to make sure the data collection triggered due to noise from the Dynatup. If this is confirmed then the oscilloscope is rearmed and the crosshead is raised to the top of the guide rails so that both springs are compressed and the air pressure is dialed to the appropriate setting. After the pressure in the pneumatic cylinders has equalized, the Dynatup is armed and the Dynatup data collection system is turned on. Once this system is turned on a thirty second window exists to perform the test before the Dynatup data collection system turns off. At this point the trigger signal from the fiber optic amplifier and the oscilloscope are both checked to confirm they are to still ready for data collection. If this is confirmed then the trigger button on the Dynatup control panel is pressed and the crosshead released. After each

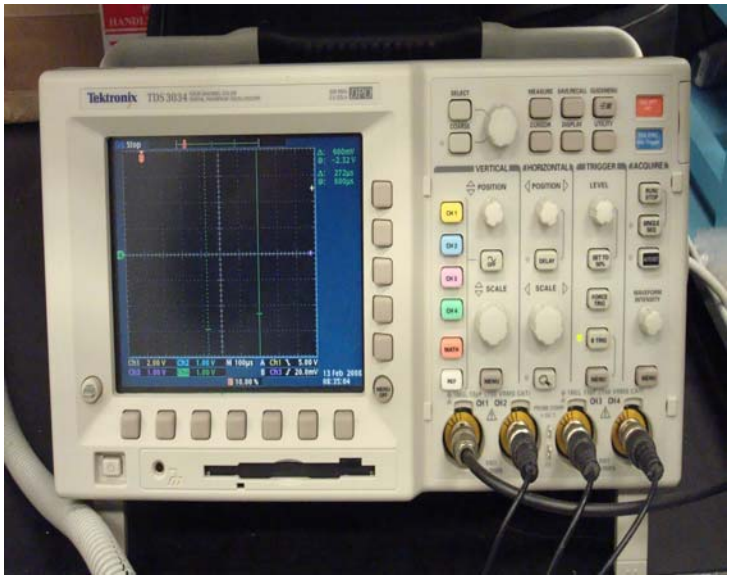

Figure 3.16: Tektronix TDS 3034 Digital Phosphor Oscilloscope

impact, the voltage signal is saved onto a 3.5" floppy disk for further processing at AFIT. Table 3.3 summarizes all of the test equipment and components selected in the slotted beam tests and the reason for their selection.

3.2 Test Parameters

The test procedure described above was used for all of the slotted beam tests and is summarized in List 3.1. Table 3.4 summarizes the number of tests to be run for each material, the pressures at which the tests will be run, the estimated velocity at impact for each test, and the estimated energy level of each test.

List 3.1. Slotted Beam Test Procedure

1. Surface Preparation
   (a) Heat Materials with Porous Surfaces
   (b) Degrease Entire Specimen
   (c) Sand Gage Application Area

Table 3.3: Slotted Beam Test Equipment

Test Equipment	Reason for Selection
Beam Fixture	Provides clamping pressure for fixed-fixed boundary condition, Anchors specimen to Dynatup, 304 Stainless Steel provides sufficient strength and stiffness for repeated impacts
Vishay Micro-Measurement EP08-125AC-350 Strain Gages	Large elongation capability >20% strain
Vishay Micro-Measurement 326-DTV Copper Wire	Twisted wire to reduce noise and small gauge to reduce mass of solder joints
Instron 8250 Dynatup	Instrumented drop weight machine capable of collecting load and velocity data, Pneumatic mode capable of generating velocities up to 13.4 m/s
Banner Fiber Optic Cable PIT46U	Plastic fiber optic cable not damaged by repeated impact
Banner Fiber Optic Amplifier FI22FP	Adjustable voltage output in 'light' and 'dark' conditions and 500 μs response time for use as initial trigger
Dynatup Velocity Photodetector	Infrared transducer system integrated into the Dynatup provides velocity for each impact
Ectron 562 DC Differential Amplifier	Differential amplifier circuit rejects signal noise and gain amplifies low voltage wheatstone bridge output
Tektronix TDS 3034 Oscilloscope	High sampling rate, dual trigger capability, and 4 channels allow the collection of multiple strain gage signals while isolating noise and taking multiple data samples every μs

(d) Mark Gage Location

(e) Condition Area with Mild Phosphoric Acid Solution

(f) Neutralize Area with M-Bond Neutralizer

(g) Crosshatch Gage Application Area

(h) Repeat Conditioning and Neutralizing Steps

2. Strain Gage Application

(a) Apply Strain Gage and M-Bond AE-15 Adhesive

(b) Clamp Application Area to Remove Excess Adhesive

(c) Cure Adhesive for 2 Hours at 75°C

(d) Prepare and Solder Lead and Jumper Wires to Specimen

(e) Confirm Strain Gage Resistance of 350Ω

(f) Apply Protective Coating

3. Specimen Installation

(a) Verify Strain Gage Resistance of 350Ω after Transport to Test Facility

(b) Install Specimen in Beam Fixture

(c) Torque Fixture to Fixture Bolts to 20 N-m

(d) Torque Fixture to Dynatup Bolts to 30 N-m

(e) Connect Lead Wires to Ectron Amplifier via Terminal Strip

4. Strain Gage Calibration

(a) Zero Wheatstone Voltage Output, E_o to ± 4 mV

(b) Place Ectron Amplifier in Shunt Calibration Mode

(c) Record ± Shunt Calibration Values

5. Set Oscilloscope

(a) Set Time Window to 1 ms

(b) Set Voltage Divisions to 1V/div

(c) Set Trigger 1 and Trigger 2

i. Ch 1 - 5V, falling slope

ii. Ch 2 - 200 mV, rising slope

iii. Delay - 2 ms (calculated from kinematic relationships for the highest Dynatup velocity)

(d) Lower Dynatup to Interrupt Light Path over Fixture and Verify Initial Trigger is Operating Properly

Table 3.4: Slotted Beam Test Parameters

Test Runs	Air Pressure	Estimated Velocity	Energy Level
1-3	30 psi	5 m/s	50 J
4-6	45 psi	6.5 m/s	90 J
7-9	60 psi	8.5 m/s	150 J
10-12	90 psi	12 m/s	300 J

6. Trigger Dynatup
   (a) Pressurize Dynatup
   (b) Arm Dynatup and Allow Pressure to Equalize
   (c) Arm Oscilloscope
   (d) Trigger Dynatup to Drop Crosshead
7. Save Test Data
   (a) Label and Save Voltage Traces
   (b) Record Impact Velocity
   (c) Photograph Specimen

The air pressures in Table 3.4 were selected in an attempt to generate a range of strain rates from 1 s^{-1} to greater than 100 s^{-1}. The actual velocity of the crosshead will be measured by the Dynatup's velocity photo-detector and varies slightly at each air pressure setting due to friction on the guide rails. Tests will be repeated three times at each air pressure in the case that there is a problem, such as strain gage disbonding or inadvertent triggering, with a test run at a particular test setting. Figure 3.17 shows a schematic of the entire test setup used to conduct the slotted beam tests.

3.3 Data Analysis

The voltage data from each test must be converted into strain data. This is accomplished with the published gage factor of the EP08-125AC-350 strain gage, the

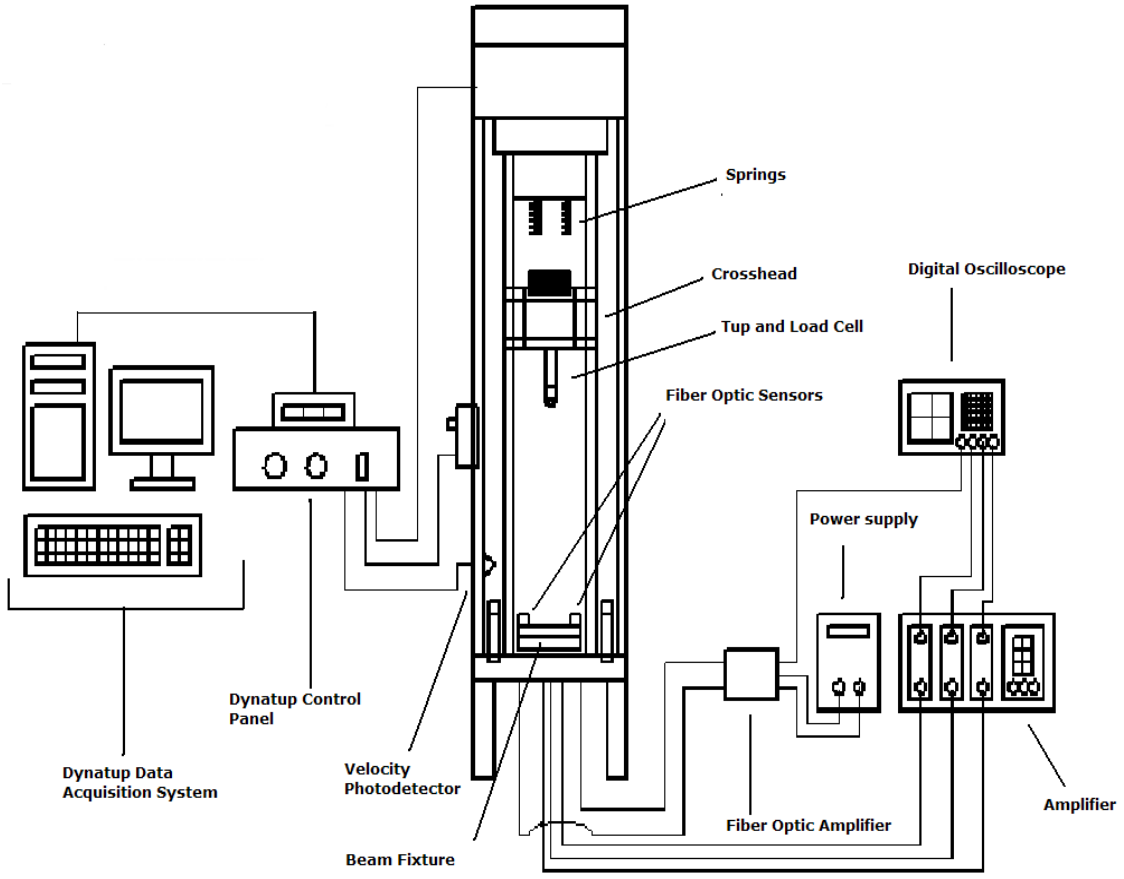

Figure 3.17: Slotted Beam Test Setup

voltages recorded during the calibration of the strain gage, and the resistance values of the strain gage and the Ectron shunt calibration resistor. To determine the strain value from the measured voltage, first a simulated strain, ε_s, over the shunt calibration resistor and the strain gage is calculated using the relationship between voltage and strain for a Wheatstone bridge such that [42]

$$\varepsilon_s = \frac{R_g}{GF(R_g + R_s)} \tag{3.1}$$

where R_g is the resistance of the strain gage, R_s is the resistance of the shunt calibration resistor, and GF is the gage factor of the strain gage. Equation (3.1) is of the same form as equation (2.42) described in section 2.1.7. A strain per volt, S_v, can

then be calculated by dividing ε_s by the voltage recorded during the shunt calibration process, V_{cal}, such that [42]

$$S_v = \frac{\varepsilon_s}{V_{cal}} \tag{3.2}$$

and S_v is then multiplied by the voltage signal measured during the tests to arrive at a strain value. For a large number of voltage traces and data points, this process can be accomplished efficiently through the use of a Matlab script to calculate the strain history from the voltage data. An example Matlab script used to convert voltage to strain in these tests is included in Appendix 3. The strain gages used in these experiments were calibrated on Steel specimens in a uniaxial stress field and the published gage factor, GF, reflects this fact. Therefore, the measured strain value for the steel specimens accurately reflects the strain in the longitudinal direction, however the measured strain values on the aluminum and titanium specimens do not account for the transverse sensitivity error due to the differences in Poisson's ratios as illustrated in Table 3.1. The error due to these differences should be calculated using equation (2.33) and either determined to be negligible or if not negligible then corrected for [56]. The calculation of the error in the Titanium specimen is shown in equation (3.3).

$$\begin{aligned} K_t &= .008 \\ \frac{\varepsilon_t}{\varepsilon_a} &= -.34 \\ \nu_0 &= .285 \\ n_\varepsilon &= \frac{K_t\left(\frac{\varepsilon_t}{\varepsilon_a} + \nu_0\right)}{1 - \nu_0 K_t} * 100 \\ .04\% &= \frac{.008 * -.34 + .285}{1 - .285 * .008} * 100 \end{aligned} \tag{3.3}$$

The error for both titanium and aluminum was calculated and found to be 0.04% and 0.03% respectively and therefore assumed to be negligible. The strain measured and calculated with equation (3.2) therefore represents the strain history of the ligament in the longitudinal direction at the center of the beam, and will be referred to as the experimental strain history from the remainder of this discussion.

3.3.1 Constitutive Modeling. After experimental strain histories have been collected for the steel, aluminum, and titanium specimens a method to relate the strains to the stress at this location is required if stress-strain curves are to be generated for each material. The Johnson-Cook equation, equation 1.2, has been identified as the constitutive relationship to be used to predict the material response in these experiments. This constitutive model requires the determination of four material dependent constants to accurately relate stress to strain and therefore the goal of this step of the data analysis will be to converge on those constants. However, without the collection of loading data at the ligament a traditional method of fitting the material constants cannot be used [26]. Therefore, a hybrid method to converge on these constants will be attempted and the constants that are converged upon will be input into a (FEM) of the impact event developed by Capt Reid Larson and compared to other states of stress in an attempt to verify the validity of the material constants [29].

The hybrid method of converging on the constants utilizes a graphical curve fitting method and the ABAQUS FEM of the slotted beam experiment [26]. In this method the components of the Johnson-Cook equation, which define the plastic response, the effects of strain hardening, and the effects of strain rate are separated and determined in a methodical process using both quasi-static elevated stress-strain data. Before determining any of the Johnson-Cook constants it is important to note that any engineering stress and strain data should be converted to true stress and strain values with the following relationships [26]

$$\varepsilon_{true} = ln(1 + \varepsilon_{nom}) \tag{3.4}$$

$$\sigma_{true} = \sigma_{nom}(1 + \varepsilon_{nom}) \tag{3.5}$$

where σ_{nom} and ε_{nom} are engineering stress and strain values. The first component of the Johnson-Cook equation, $(A + B\varepsilon_p^n)$, and its coefficients A, B, and n are fitted by analyzing the quasi-static stress strain curve. First, it must be recognized that A is the yield stress and defines the initiation of the plastic response of the material. When quasi-static stress strain data is available, A is typically found using the .2% offset method, which requires the creation of a line originating from .2% strain and drawn parallel to the linear region of the stress strain curve. The stress at the point at which the line intersects the stress strain curve is taken as the yield stress or A. Without quasi-static stress strain data, A must be gathered from published data and for the materials tested in this research, A can be obtained from Table 3.1 recognizing that the stress values must be converted from engineering stress-strain values to true stress-strain values. The coefficients B and n represent the effects of strain hardening, and can be determined by analyzing the plastic region of the quasi-static stress-strain curve. If an overstress is defined as $\sigma - \mathrm{f}(\varepsilon)$, where $\mathrm{f}(\varepsilon)$ is the stress at yield, the coefficients B and n are obtained by first calculating the effective stress difference (ESD) defined as, the total stress minus the yield stress, and the plastic strain taken as, the total strain minus the strain at yield. Next, the log base 10 of both the ESD and the plastic strain are taken and plotted. Applying a linear fit to this plot provides the equation of a line, $y = ax + b$, where a is equivalent to n and 10^b is equivalent to B. It is important to note that the process to determine these constants is relatively straight forward when the quasi-static data is available, however since quasi-static data was not available for these experiments, the published quasi-static data for each material will be used to determine the Johnson-Cook coefficients, A, B, and n [6] [59] [11]. Taking the stress strain values for each material, a Matlab script

will be written to execute the process described above and Matlab's curve fitting toolbox, *cftool*, will be used to collect the slopes and y-intercept values required to determine an initial estimate for the Johnson-Cook coefficients. While this process can be automated in Matlab, it is valuable for understanding the process to examine the curve fitting technique graphically. Subfigures (a) and (b) of Figure 3.18 show the graphical process employed by Kennan [26] to determine the coefficients A, B, and n for 1080 Steel and for more information on this process the reader is encouraged to consult this document. Next, it is necessary to fit the parameter C. This is typically accomplished by choosing an arbitrary strain value $\varepsilon(t)$ at various strain rates and taking the corresponding stress value at $\varepsilon(t)$. Making each of these stress values the Dynamic stress, and calculating the ratio of Dynamic Stress to Static Stress, values for this ratio can be obtained at each elevated strain rate. Plotting these values against the ln of their respective strain rate and fitting a line to these values with (0,1) as the origin of the line, the slope of this line the Johnson-Cook coefficient C. Unfortunately, the slotted beam test only provides strain data at elevated strain rates and C can not be determined in a traditional manner. To determine C, the ABAQUS FEM must be utilized by inputting the constants A, B, and n into the ABAQUS model and varying C until the ABAQUS strain output and the experimental strain histories are in agreement. The varying of C can be accomplished manually, but a more efficient process would be to use optimization techniques to minimize the difference between the ABAQUS and experimental outputs. Unfortunately, the development of a program to perform this process is beyond the scope of this work. Therefore C will be determined manually and considered to be determined when both outputs show the best agreement. This will result in all of the material constants for the Johnson-Cook equation being fitted. Regardless of the method used to derive the constitutive relationship of a material, any model should be able to predict the material response under a wide range of loading conditions. In this case, the derived Johnson-Cook model should not only predict the strain response at the ligament, but also predict the specimen response at the top of the specimen adjacent to the impact at a location

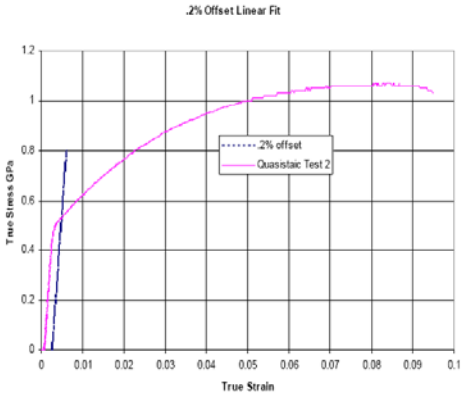

(a) Determining A using .2% offset method

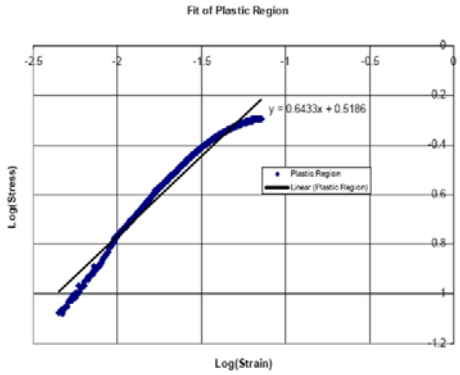

(b) Curve fit to Determine B and n

Figure 3.18: Determination of A, B, and n for 1080 Steel from Quasi-static Stress Strain Data

were significant compressive bending and plasticity should be experienced. Therefore after the Johnson-Cook coefficients have been determined, the FEM's ability to predict the response at the top of the slotted beam will be evaluated. If both the ABAQUS output and the strain gage signal show good agreement then the probability that the derived Johnson-Cook model is a unique solution with the ability to predict different states of stress is increased, and effective stress-strain curves will be generated for each material.

3.4 Slotted Beam Technique

An experimental method for impacting slotted beams and collecting a strain history at a ligament underneath the beam has been developed in this chapter. The selection of specific test equipment and the motivation for the selection of this equipment has also been discussed. The characteristics of impact testing including inertial forces, rapid loading, and short durations have all been considered in the selection for this test equipment in an effort to maximize the chance for success of this test. During the development of the experimental method, particular emphasis is placed on the development of a reliable method of testing and therefore a small rugged transducer was chosen to measure the specimen response and a dual trigger system was

developed to minimize the impact of extraneous noise. However this experimental method lacks the capability to measure the stress experimentally at the equivalent point where the strain response is measured. Therefore, a three dimensional FEM is necessary to determine the constitutive relationship for the materials tested. Two different methods of converging on the constitutive relationship have been developed and will both be evaluated as part of the analysis of the experimental strain history in an effort to generate stress-strain curves at the strain rates generated by the slotted beam tests.

IV. Experimental Results of Slotted Beam Tests

4.1 Test Results

This chapter provides the results for the titanium, steel, and aluminum slotted beam tests. The results include images of both the impact location and global behavior of each beam, plots of the strain histories calculated from the tests, a table of the strain rates achieved at each impact velocity, and an attempt to determine the Johnson-Cook coefficients for each material tested. Results from each impact velocity for each material are reported except for aluminum at 12 m/s due to an inability to collect data at this impact velocity. The challenges which prevented the collection of the aluminum response at this impact velocity will be discussed as part of the presentation of results.

4.1.1 General Comments about Slotted Beam Tests. Some general comments about the performance of the slotted beam tests that will be examined, include the surface preparation of the specimens, the Dynatup, the impact location, the performance of the fiber optic trigger, and the performance of the selected strain gages and terminal pads. In preliminary testing, both the Dynatup's load cell and velocity photo-detector recorded data which could provide the parameters for the impact condition in ABAQUS. However, at the time of testing only the velocity photo-detector was functioning correctly and due to time constraints the slotted beam tests were performed without collecting load cell data. This did not affect the results of the slotted beam experiments, and only affected the amount of information which could be used to model each slotted beam condition in the FEM. Therefore the velocity measurement became the loading parameter in ABAQUS to model each rate of loading. Of the 36 tests conducted, only 4 tests failed to produce an output which could be collected. The reasons for the inability to collect data were both, an improperly configured measurement system and a shorting phenomenon discussed in section 4.1.3. Of the 32 tests conducted successfully, several issues did introduce inconsistencies into the test results which will be discussed and were considered in the reporting of results.

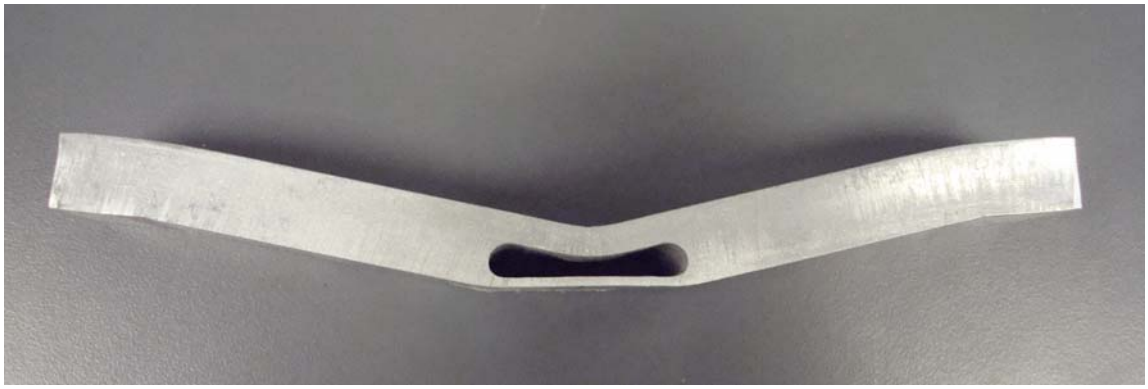

Figure 4.1: Global Deformation of Slotted Beam Specimen Resulting from Center Impact

First, the Dynatup proved difficult when attempting to impact each slotted beam specimen in the center of its top surface. This can be attributed to several factors. The first factor was that the tup was not always completely parallel with the guide rails due to deformation in the crosshead from previous impact experiments. In an attempt to alleviate this condition, the tup was shimmed to make it more parallel with the guide rails, however the need to use a 4" tup extension in these experiments exacerbated this problem. Furthermore, the design of the Dynatup crosshead is such that repeatability of the same impact location is inconsistent. This is due to slip in the transverse direction of the crosshead as it moves along the guide rails and is inherent in the Dynatup crosshead design. In spite of these limitations, there were many tests with impact locations either at the center of the specimen or very close to the center and no impact occurred more than 5mm in any direction from the center of the beam. A center impact in the slotted beam experiments is the primary mechanism in creating both symmetrical deformation of the slotted beam and a uniform state of stress in the instrumented section of the slotted beam. The resulting global deformation of both a slotted beam impacted at the center of the specimen and a slotted beam impacted away from the center of the specimen are shown in Figures 4.1 and 4.2. For all of the results reported, the distance from the center of the impact point to the center of the beam was measured both along the width and the length of the beam for use when modeling each individual impact condition with the FEM.

Figure 4.2: Global Deformation of Slotted Beam Specimen Resulting from Off-Center Impact

An issue in regards to data collection which was encountered was the 'clipping' of the strain history at higher velocities for the titanium and steel experiments. This was due to the voltage divisions on the DPO being set too low to capture the entire voltage output from the amplifier. The point at which the voltage signal was clipped was 5V, equivalent to 10% strain in these tests. While voltage data over the entire 1 ms was not collected when the signal was 'clipped', data was measured for more than 500 μs and enough data to allow for a comparison with the ABAQUS model was collected.

While there were several difficulties encountered during this experiment, some of the techniques used in the slotted beam proved themselves to be very robust and important to the success of these tests. The first technique, surface preparation, performed as discussed in section 3.1.2.1 resulted in many tests were data was collected over the entire 1 ms time window. This was contrary to preliminary tests were strain gage and terminal pad disbonding was an issue in collecting data over the duration of a 500 μs time window for the majority of the tests. The surface preparation steps for all of the slotted beams was followed exactly and many hours were spent on specimen preparation. This was done in an effort to create an optimum bond between the specimen and the strain gage. The importance of surface preparation can not be emphasized enough to the success of the slotted beam test. One component of the slotted beam test and measurement system which dramatically improved the

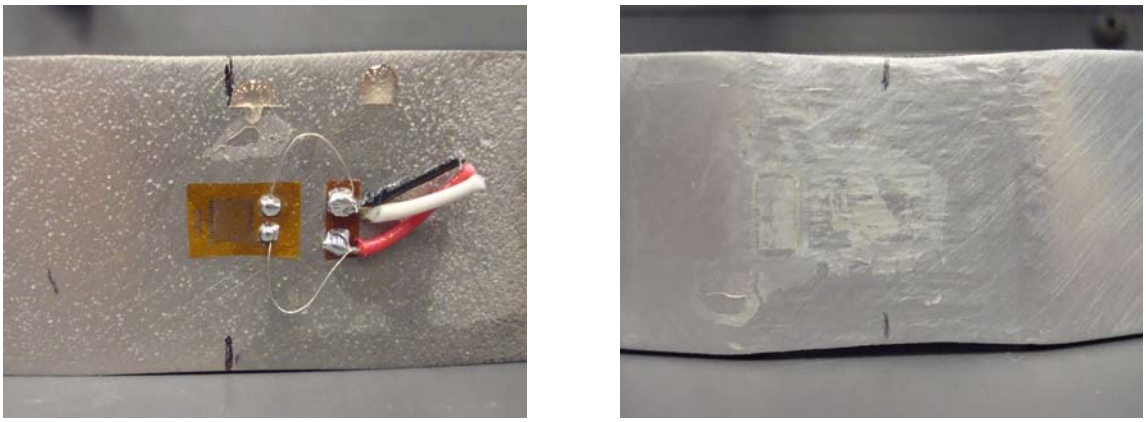

(a) (b)

Figure 4.3: Minor Disbonding (a) and Complete Delamination (b) of the Strain Gage and Terminal Pad

performance of the measurement system from the preliminary testing was the fiber optic trigger. In preliminary testing, noise from the Dynatup and other equipment inadvertently triggered data collection for many tests. The inadvertent triggering also prevented the threshold voltage level from being set at an appropriate level to capture the initiation of deformation at the ligament. The fiber optic trigger isolated any electrical noise and allowed the reduction of the threshold voltage from 500 mV to 200 mV for the slotted beam tests. When configured properly, the fiber optic trigger ensured the proper triggering for each test run and proved to be an essential component of the test system. Finally, the performance of the strain gage and terminal pad configuration was excellent for many tests. An examination of the ligament area for each specimen after testing revealed anything from minor strain gage disbonding to total delamination of the strain gage for most tests, as shown in Figure 4.3, however the results of the data collected from the oscilloscope showed no evidence of disbonding of the strain gage and terminal pads throughout the 1 ms time window for almost 70 percent of the successful tests and data up to $500\mu s$ for over 90 percent of the successful tests.

4.1.2 Phenomenological Behavior of the Slotted Beam. Measuring the response of the ligament with a strain gage was the primary objective of these tests,

Figure 4.4: Necking at the Ligament

however valuable information about the specimen behavior could be collected by examining the slotted beam after impact. This was due to the fact that several distinctive phenomenon were exhibited by the slotted beam specimens after impact. The first phenomenon was the necking of the ligament as illustrated in Figure 4.4.

Necking is common in tensile specimens stressed beyond yielding, and indicates that during the test plastic flow due to tensile stress occurred in the ligament [49]. In addition, the ligament in the aluminum and titanium specimens remained straight after impact while the steel specimen ligaments did not appear to remain perfectly straight especially at higher rates of loading. This indicates that some amount of bending stress occurred in the ligament during these tests. The slot dimensions are material dependent and were initially designed for a titanium specimen as described in Appendix 1, while at the same time the impacts were not concentric. These two factors make it unclear whether the deformation in the ligament in the steel specimens was the result of an off center impact or due to slot dimensions which may not have maximized the state of uniaxial tensile stress in the ligament. Further analysis using the ABAQUS FEM is appropriate to investigate the state of stress in the ligament.

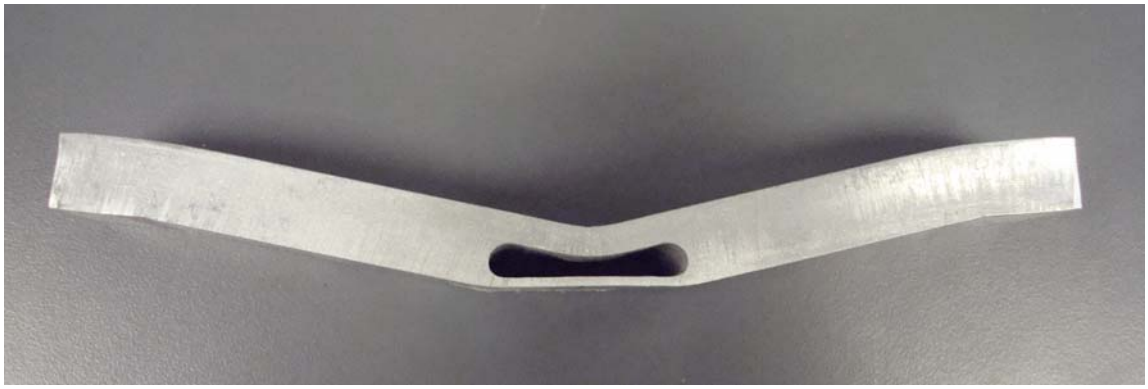

Figure 4.5: Development of Plastic Hinges at Center and Supports of Aluminum Specimen #7

Finally, plastic hinges were visible in the slotted beam specimens as predicted by the rigid, perfectly plastic model at the higher rates of loading in each material. Figure 4.5 shows the plastic hinges in center and at the supports of aluminum specimen #7 impacted at 11.63 m/s.

4.1.3 Strain Histories and Strain Rate Determination. Voltage data over a 1 ms window for the three different materials was collected at the four pressures and velocities listed in Table 3.4 except for an aluminum at the highest rate of loading. The fact that aluminum data at the highest velocity could not be collected was due to two reasons. The first reason was due to the strain gage disbonding as noted in section 4.1.1. The second reason was a shorting phenomenon encountered in some of the tests which appeared as interruptions in the voltage signal as shown in Figure 4.6.

This was determined to be a shorting phenomenon due to the almost instantaneous decrease in voltage registered on the oscilloscope. The voltage drop meant the resistance had become very small which is characteristic of a short. This is fundamentally different than the result of solder joint or jumper wire failure were the voltage quickly increases due to an almost instantaneous increase in the resistance. The increase in resistance is caused when the circuit is broken as appears as the voltage signal shown in Figure 4.7.

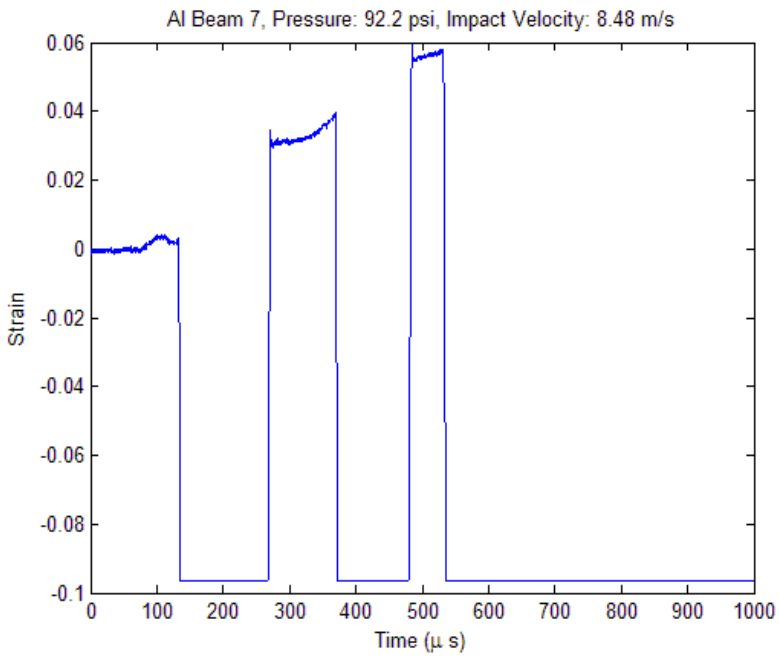

Figure 4.6: Shorting Phenomenon

The shorting phenomenon is believed to have been caused by the strain relief loops and solder joints contacting the beam specimen during the impact event and was not isolated until after the majority of the aluminum and titanium specimens had already been tested. This phenomenon was isolated during the slotted beam tests using an acetate coating, as recommended by the AFRL laboratory technician who assisted with the slotted beam experiments. To prevent the exposed metal of the strain gage solder joints and terminal pad from contacting in future tests, an M-Coat protective coating supplied by VMM should be used in testing. In some tests the shorting phenomenon was not severe enough to prevent collection of data for the entire test and only appeared to be brief spikes in the strain gage signal. Brief spikes were not removed or smoothed and appear in some of the strain histories reported. Any spikes which were not brief and resulted in the signal descending to a -.1 ε (m/m) were removed in the reported strain history to prevent the plot from being distorted. This 'corrected' voltage data appears as straight lines in the strain history.

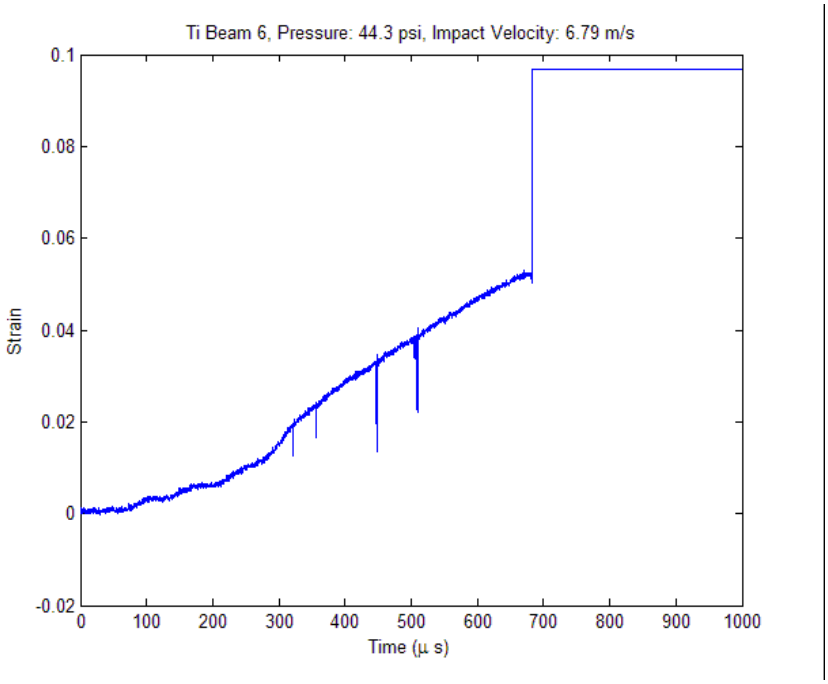

Figure 4.7: Results from Solder Joint of Jumper Wire Failure

To calculate the strain history from each voltage trace, a Matlab script was written to first calculate, S_v, as defined in equation (3.2) from the recorded shunt calibration data for each test. Next, the Matlab script applied the calculated S_v to the voltage data collected from each test, determining the strain measured over the duration of the test. It is important to note that the strain calculated in all of the test results is strain with units (m/m) and not μstrain, which is commonly reported in tests using strain gages due to the small strains measured. In these tests, noise was apparent in all of the measured signals and the Matlab moving average filter function, *smooth*, was used to filter some of the random noise in each voltage signal [31]. To create the plot of strain history, the strain in units (m/m) calculated by the Matlab script was plotted against time in units μs as shown in Figure 4.8. In the steel # 10 and titanium # 10 specimens the signal was 'clipped' as discussed in section 4.1.1 and the strain signals from these tests appear to end before the end of the 1 ms window due to disbonding or lead wire failure. However this is not the case in these particular

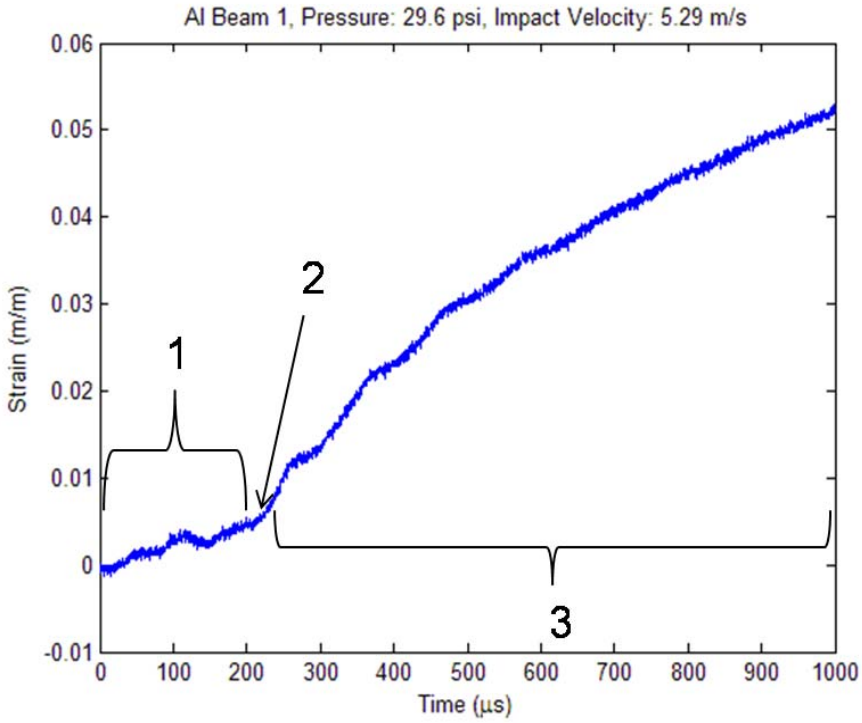

Figure 4.8: Typical Strain History from Slotted Beam Tests with Regions of Deformation

tests and the signal only terminates due to the fact that the voltage had exceeded the maximum voltage the oscilloscope could measure in its current configuration.

Strain histories for selected titanium, aluminum, and steel specimens are shown in Figures 4.9, 4.10, and 4.11. The strain histories from these particular tests were selected due to the appearance of the test data, which indicated that the strain gage remained bonded for as long as possible through the 1 ms test window. The distance between the impact and the center of the beam was also a consideration in selecting which tests were reported, with the impacts which were most concentric being selected over tests were the impacts were more eccentric. Images of the top surface of the beam were also analyzed to determine whether the dynatup impact was in close proximity with the center of the beam.

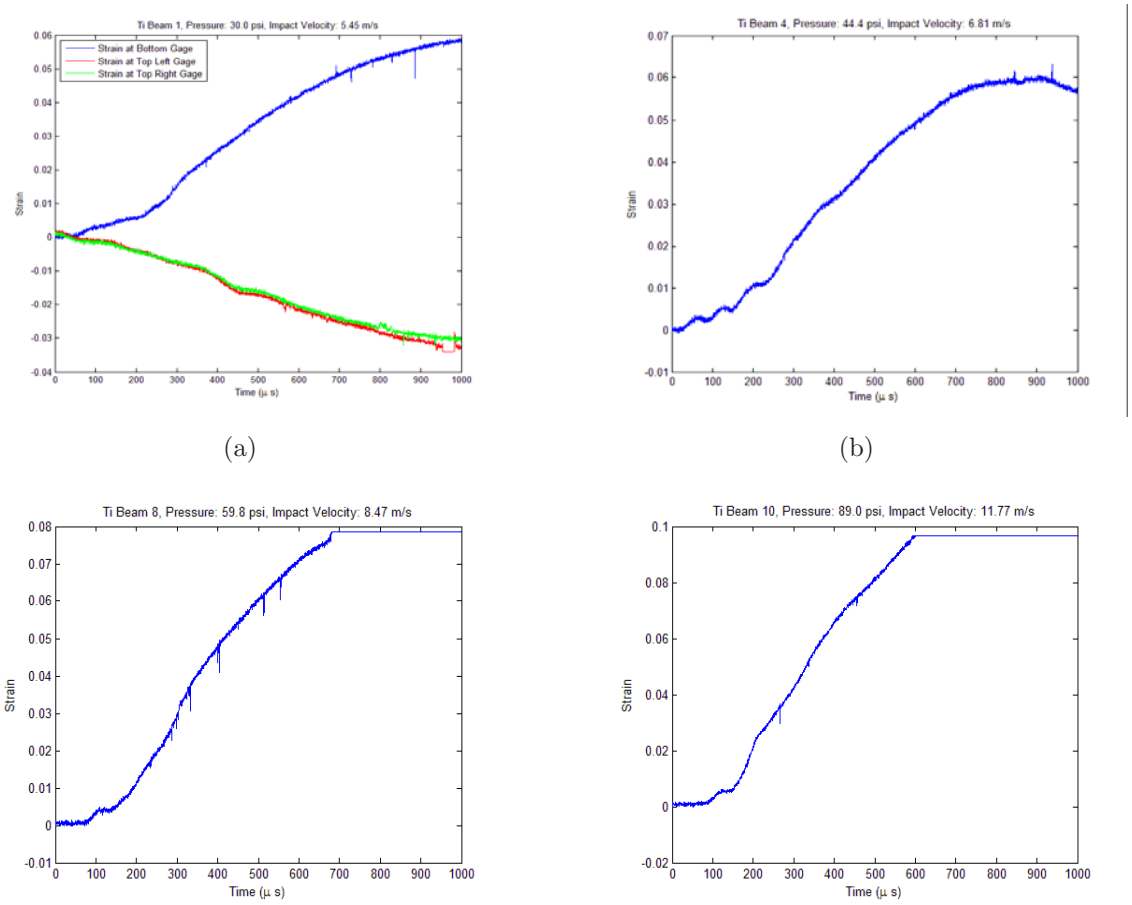

Figure 4.9: Strain Histories for Titanium Specimens #1, #4, #8, and #10

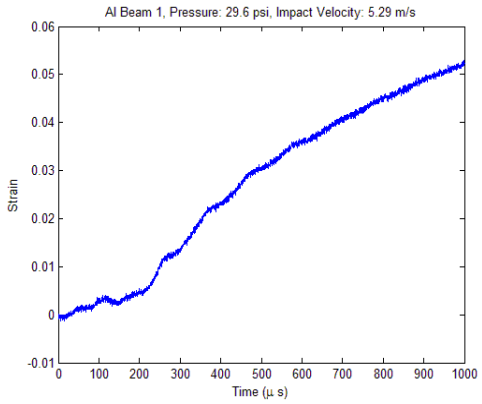

(a)

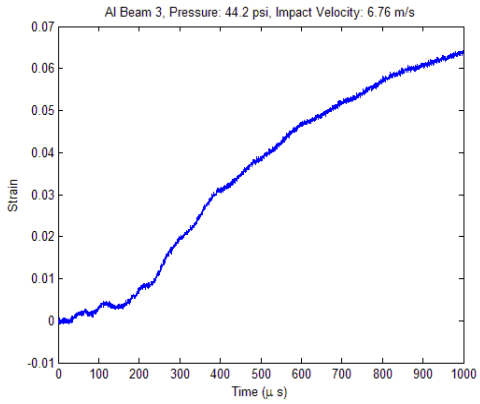

(b)

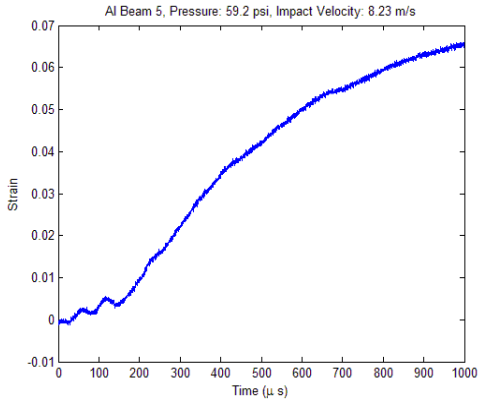

(c)

Figure 4.10: Strain Histories for Aluminum Specimens #1, #3, and #5

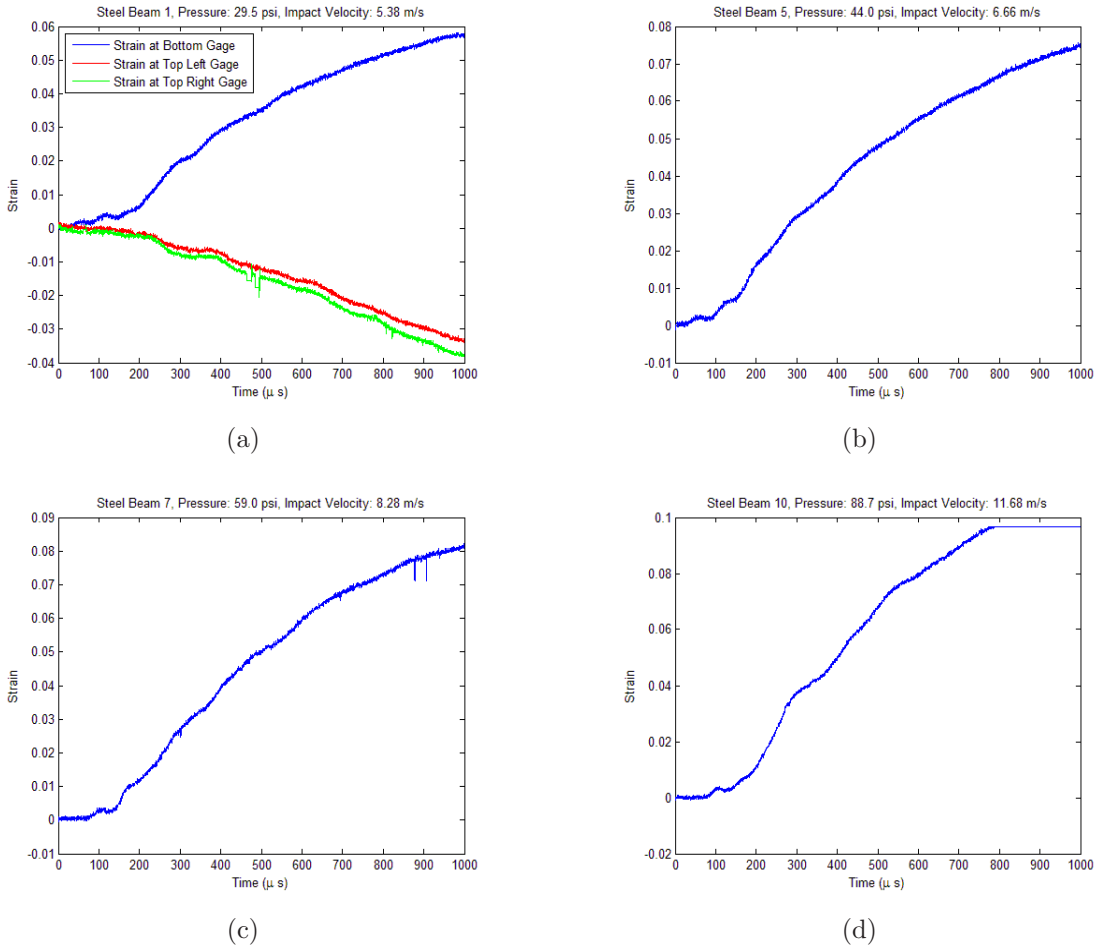

Figure 4.11: Strain Histories for Steel Specimens #1, #5, #7, and #10

Analyzing the individual strain histories for each test, it becomes clear that several regions of deformation are present within the strain data collected at the ligament. In all of the strain histories, an initial region of deformation is present which occurs from 0 to approximately 250 μs depending on the rate of loading and the material. This region is characterized by an initial slope which is more shallow than the rest of the strain history and is shown in region 1 of Figure 4.8. Furthermore, this region contains oscillations which are characteristic of stress waves as they propagate across the ligament. As an individual wave propagates across the ligament a sudden increase in the deformation is measured from the strain gage. As the wave propagates past the strain gage, the strain decreases but not to zero as some amount of elastic deformation remains in the ligament. Each of the materials tested displays at each one of these oscillations, while the magnitude and frequency of the oscillations varies depending on the material and rate of loading. This is consistent with the dependence of the elastic wave velocity on the material properties as discussed in section 2.1.5.1. To investigate the propagation of waves in the ligament, the test condition for aluminum specimen #1, which can be seen in Table 4.1, was run in ABAQUS and the strains in the E22 direction at 15 different nodes along the length and in the center of ligament were measured over 100 μs. Figure 4.12 shows the results of this ABAQUS run. From Figure 4.12, it can clearly be seen that the strains in the outward most nodes, 98 and 102, increase before the nodes in closer proximity to the center node, 128, as the 100 μs elapses. This indicates that the stress in the ligament is traveling from the ends of the ligament toward the center of the ligament in the form of waves.

At approximately 200 μs, a knee in the strain history defines the end of the elastic region and initiates the start of the plastic region of deformation in the ligament. The point at which this occurs is the yielding of the material and is shown as region 2 of Figure 4.8. Figures 4.13, 4.14, 4.15 contain an inset which show the region where the elastic to plastic transition occurs. This point appears to occur at approximately the same point in time between all the rates of loading for the three materials. This indicates that while the rate of loading is higher than a quasi-static

state of loading, the range of tup velocities used in these tests does not produce a range of loading rates, which will generate observable strain rate dependency effects between different tup velocities. Estimating where each of these points occur from the insets in Figures 4.13, 4.14, 4.15, the yield in these tests for CP Ti, 2024-T3 Al, and 1018 Steel occur at 0.005, 0.004, and 0.002 strain (m/m) respectively. The strain at yield in the quasi-static case for CP Ti, 2024-T3 Al, and 1018 Steel using the data provided in Table 3.1 turns out to be 0.0024, 0.004, 0.001 strain (m/m) respectively. These results indicate that some rate sensitivity may have been exhibited by both the titanium and steel samples while the aluminum samples do not appear to exhibit any strain rate effects. This is consistent with the results shown by both Nicholas and Campbell from intermediate strain rate tests accomplished on titanium, aluminum, and steel alloys. In these tests the titanium and steel alloys both exhibited the appearance of rate dependent effects at intermediate strain rates while the constitutive behavior of aluminum alloys remained independent of strain rate until strain rates beyond the intermediate range were encountered [38] [10].

Once yield occurs, plasticity begins to set into the ligament. This region is characterized by a higher rate of deformation than the elastic region which continues for the remainder of the test and is shown in region 3 of Figure 4.8. An important observation from the third region is that the rate of deformation or strain rate in this region does not remain constant throughout the remainder of the test. Instead the strain rate continuously decreases for the remainder of the test event. This phenomenon can be explained by analyzing the output of the tup velocity throughout the impact event from an ABAQUS solution of the impact event. The velocity output from one of the ABAQUS solutions is shown in Figure 4.17. In Figure 4.17 it can be seen that the velocity of the tup is decreasing at a constant rate after impact, and for the lower velocity tests the tup actually begins to rebound before the test is over. The constant deceleration of the tup results in a decreased magnitude of loading as the slotted beam test progresses, and a corresponding decrease in the strain rate as the test progresses. With this in mind, it was appropriate to determine the strain

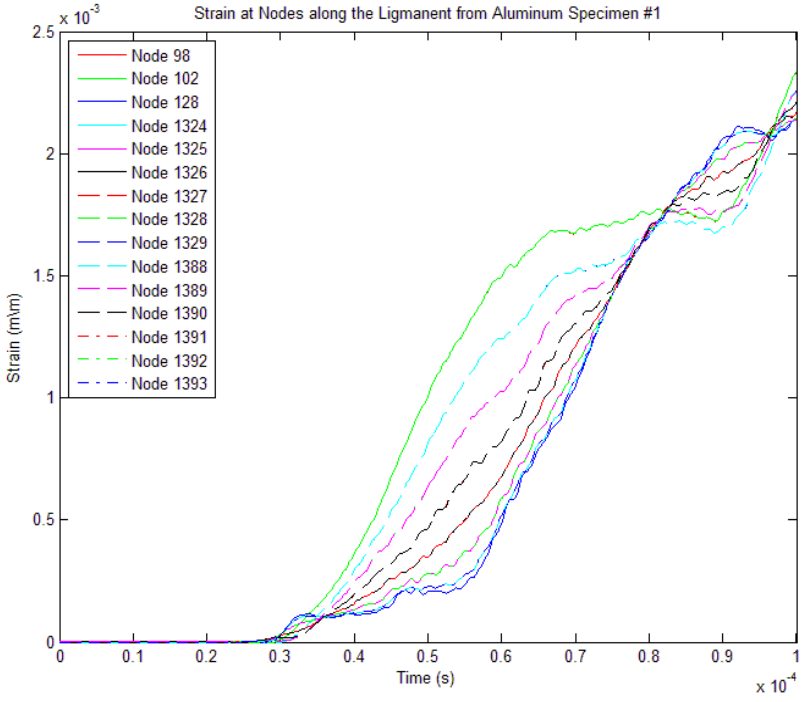

Figure 4.12: Investigation of Wave Behavior in Ligament for Aluminum Specimen #1

rates generated at the ligament to characterize each of the rates of loading. This was accomplished by fitting a first order polynomial to the third region of the strain history. Taking the slope of this line gives an approximation of the rate of change of the strain history and therefore the strain rate. Since different regions of deformation are exhibited in the strain history it would not be appropriate to fit the polynomial to the entire strain history, but rather fit the polynomial to one of the regions of deformation. Due to the brief duration and the fact that the strain rate in the elastic region appears to remain fairly constant between tests, the strain rate in the elastic region does not provide much information on the effect of increased rate of loading for each of the three materials. However, the region of plastic deformation in each strain history occurs for a much greater time period and appears to exhibit the effects of an increased rate of loading on the rate of plastic deformation. Accordingly, the plastic strain rate was chosen to characterize each test in an effort to examine how the

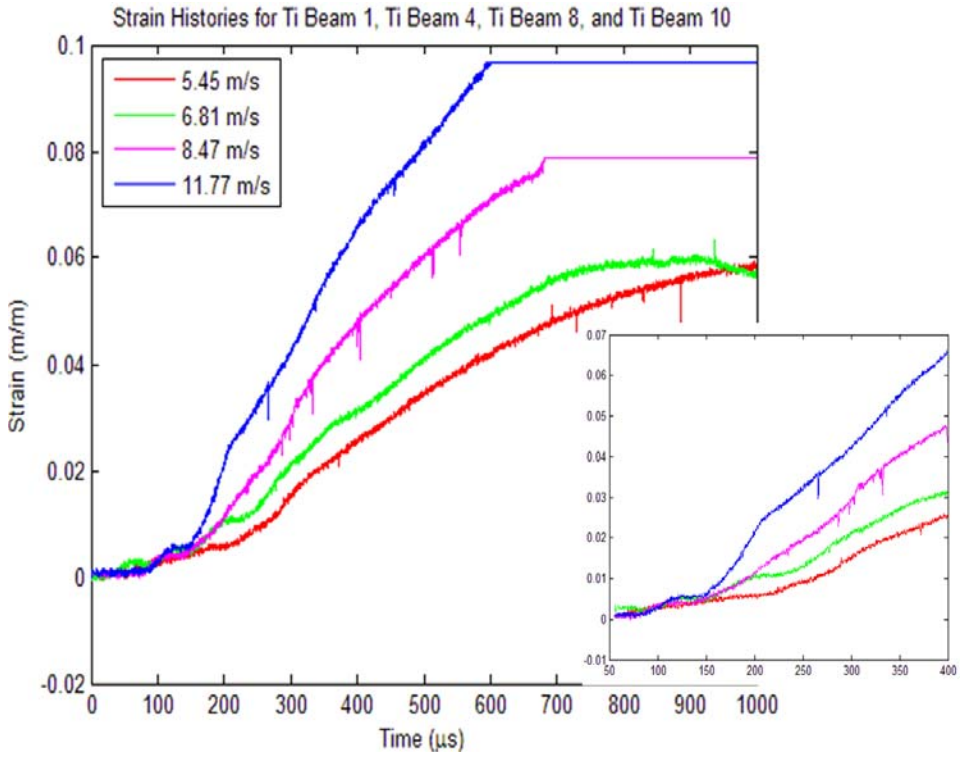

Figure 4.13: Strain Histories from Titanium Specimens #1, #4, #8, and #10

plastic strain rate at the ligament increases as the velocity of the tup increases. To determine the plastic strain rate for each test a first order polynomial was fit to each of the plastic regions of the strain histories reported in Figures 4.9, 4.10, and 4.11 and the slope of these lines taken as the plastic strain rate in each test. The results of this process are shown in Table 4.1. In determining the strain rate for these experiments, the fit for the first order polynomial began at the time where yield was estimated to occur for the lowest rate of loading and ended at 600 μs. This ending point was selected due to the fact the voltage signal was clipped at approximately this point on the highest rate of loading for the titanium tests. To retain consistency for all of the strain rate data reported, 600 μs was chosen as the end of the time region for the linear fit. A final comment on the plastic region of the strain histories reported is the appearance of a single 'hump' at the beginning of some of the strain histories as shown in Figure 4.16. This is believed to be the propagation of a plastic wave across the

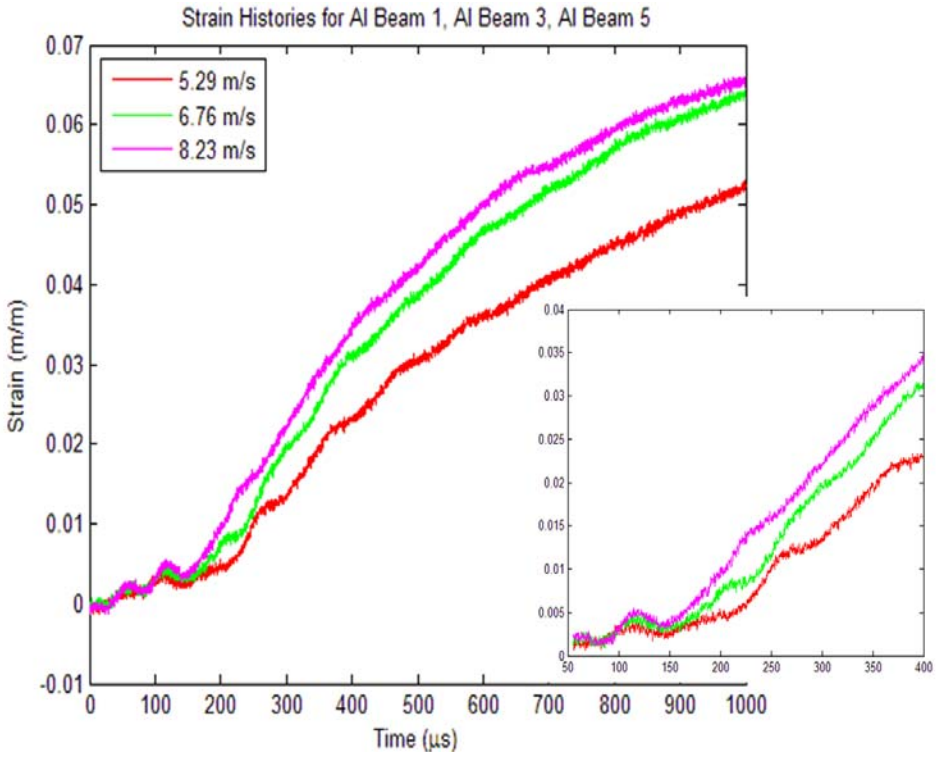

Figure 4.14: Strain Histories from Aluminum Specimens #1, #3, and #5

ligament and appeared in both the experimental and ABAQUS output. The location in the strain history of this 'hump' and the fact that it occurs at the onset of plasticity are consistent with the characteristics of a plastic wave as presented by Zukas, which indicate that the plastic wave travels at a slower velocity than the elastic wave and with a higher magnitude of stress [23]. Clearly the strain histories generated from the strain gage measurements at the ligament provide valuable information about the elastic deformation, yield point, and plastic deformation for each material and also indicate that the rate of loading in these tests may be approaching a level were wave propagation becomes important in analyzing the strain gage data.

4.1.4 Constitutive Modeling Results. After calculating the strain histories and plastic strain rates, it was necessary to attempt to converge on the coefficients in the Johnson-Cook constitutive equation. This was accomplished by running the ABAQUS model discussed in Appendix 2 at each test condition with the Johnson-

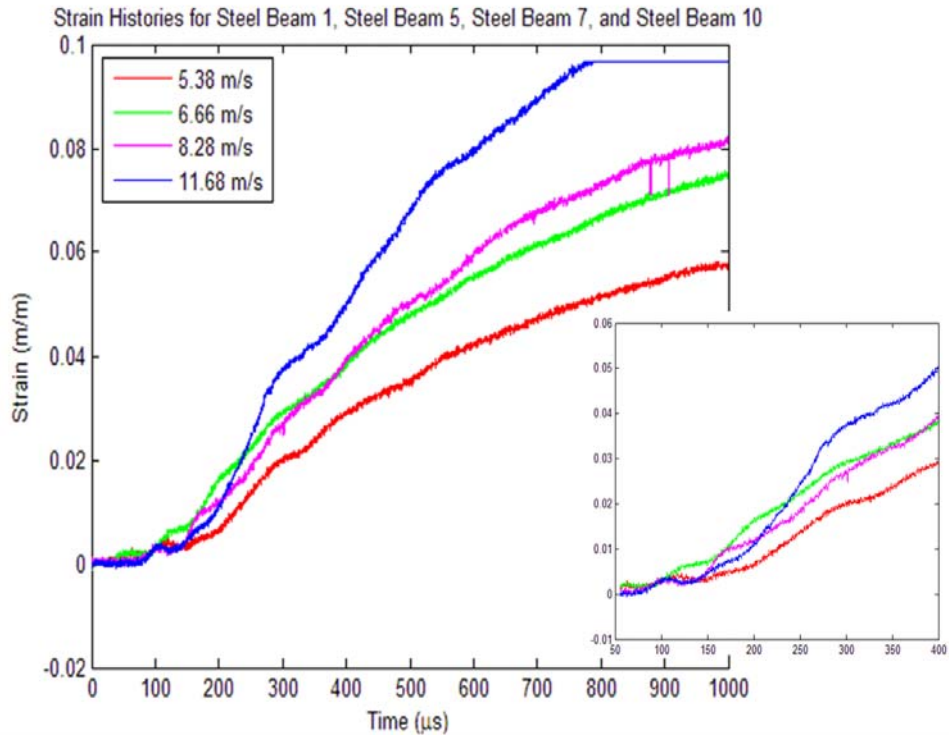

Figure 4.15: Strain Histories from Steel Specimens #1, #5, #7, and #10

Cook constitutive equation as the plasticity model used to define the constitutive behavior of the specimen material. The first step in this process was to input the initial estimates for the Johnson-Cook coefficients determined using the process described in section 3.3.1 into the ABAQUS materials menu. It is important to note that this process was attempted for all of the materials however the quasi-static data available for the aluminum and steel alloys and the potential variance between these mechanical properties and the mechanical properties of the materials led to coefficients which provided very poor initial agreement with the experimental results. In an attempt to approve the initial agreement between the experimental and numerical results, published Johnson-Cook coefficients were used for the aluminum and steel alloys which improved the agreement. The final values of the Johnson-Cook coefficients used for each material in the results reported in Figures 4.18 through 4.28 are included in Table 4.2.

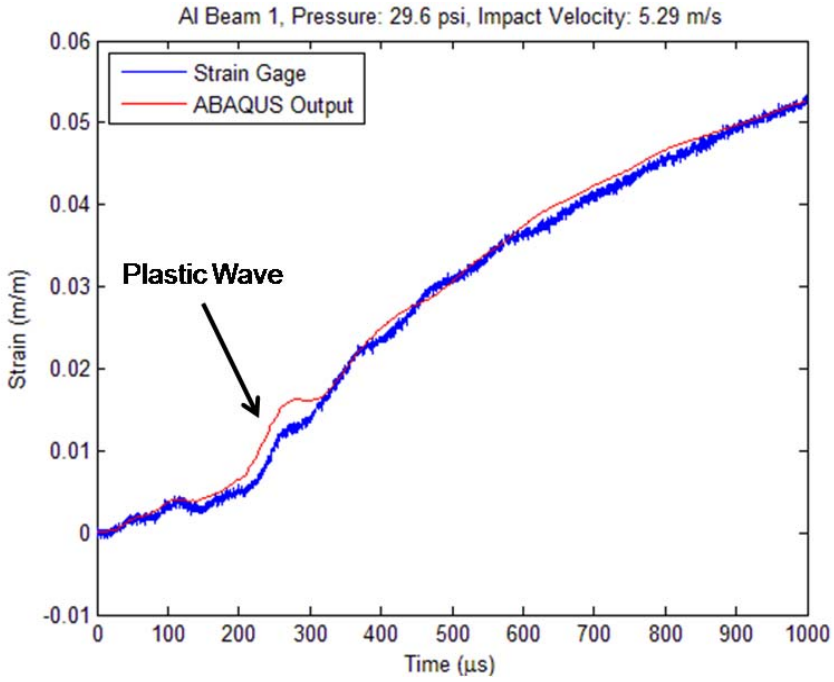

Figure 4.16: Appearance of Plastic Wave in Strain History

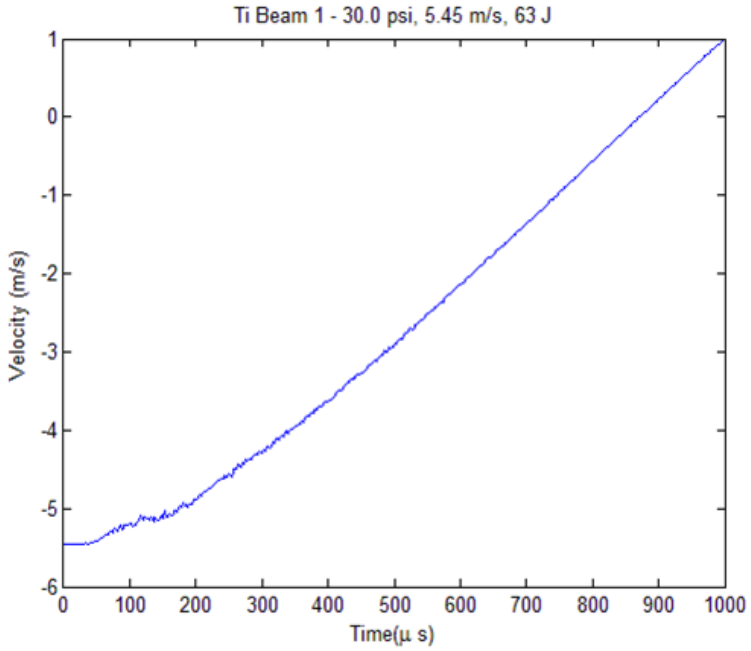

Figure 4.17: ABAQUS Tup Velocity Profile from Titanium Specimen #1

Table 4.1: Strain Rates and Velocities for all of the Specimens Reported

Material	Specimen #	Velocity (m/s)	Strain Rate (s^{-1})
CP Titanium	#1	5.45	95
	#4	6.81	102
	#8	8.47	152
	#10	11.77	206
2024-T3 Aluminum	#1	5.29	90
	#3	6.76	112
	#5	8.23	124
1018 Steel	#1	5.38	85
	#5	6.66	106
	#7	8.28	131
	#10	11.68	168

Table 4.2: Johnson-Cook Parameters for 1018 Steel, 2024-T3 Al, and CP Titanium

Material	A (MPa)	B (MPa)	n	C	$\dot{\varepsilon_0}$
1018 Steel [30]	350.52	275.31	.36	.022	1 s^{-1}
2024-T3 Aluminum [25]	368.986	683.974	.73	.0083	1 s^{-1}
CP Titanium	285.7	566.1	.5866	.0494	1 s^{-1}

Next, it was necessary to translate the tup in the ABAQUS assembly menu as described in Appendix 2. This was done on a case by case basis in an attempt to match the location of the tup in the ABAQUS FEM with the impact location documented on the actual beam specimen. The lengths in the longitudinal and transverse directions that the tup was translated for each ABAQUS model are contained in Table 4.3.

After the parameters to characterize both the material and the impact location were input into the ABAQUS model, it was necessary to create a loading condition in the ABAQUS model which would simulate the loading in the slotted beam experiments. The velocity measured from the Dynatup's velocity photodetector was used to accomplish this task. The velocity in (m/s), shown for each test case in Table 4.1, was input into the ABAQUS Predetermined Fields menu of the tup model. The ABAQUS model was then ready for solution and using a step of 1100 μs sampled 550 times, the model was sent to ABAQUS CAE, the ABAQUS explicit integration solver for

Table 4.3: Tup Translation Parameters for Titanium, Aluminum, and Steel Tests

Material	Specimen #	Longitudinal Translation (m)	Transverse Translation (m)
CP Titanium	#1	0	0
	#4	0.002	0
	#8	0.003	0
	#10	0.001	0.001
2024-T3 Aluminum	#1	0	0.0015
	#3	0.001	0.001
	#5	0.001	0
1018 Steel	#1	0	0.0005
	#5	0	0.002
	#7	0	0
	#10	0.005	0.001

processing. After the model was solved, it was necessary to collect the strain output at the ligament for comparison with the experimental results. The default strain output for ABAQUS is the true or logarithmic strain, which is the strain measurement associated with the Cauchy stress and not the strain measurement associated with engineering stress. The true strain measurement, LE, in ABAQUS, is more appropriate than the engineering strain measurement, E, for comparison in these experiments due to the large plastic deformations measured at the ligament. The true strain measurement takes into account the change in cross sectional area due to a large amount of deformation. A significant change in cross sectional area is characteristic of necking at the ligament as discussed in section 4.1.2, and therefore the true strain is the appropriate strain measure in this application. Furthermore, the strain measured by the strain gage at the ligament is over an area and not a single point such as the center node in the ABAQUS model. To take this into account, the strain in the direction of the length of the beam, LE22, at nine nodes over an area approximately the size of the strain gage was taken and averaged in an attempt to approximate the deformation measured by the strain gage. The nodes which were used for comparison on all three materials where nodes 128, 1325, 1355, 1362, 1392, 5119, 5161, 5236, and

5335. After collecting the strain output at these nodes, the outputs were averaged and the result was plotted against the experimental strain history. The results of this operation are shown in Figures 4.18 through 4.28. An important note in creating these plots is the fact that the ABAQUS model and experimental data do not begin at the same time in the impact event. To adjust for this and improve the agreement between the ABAQUS results and the experimental results, it was necessary to match the initiation of both outputs by horizontally shifting the ABAQUS output to match the experimental output. This involved removing the first 20-40μs of the ABAQUS output so that the initiation of strain at the ligament began at the same time. This was the primary purpose for using a step of 1100 μs for each ABAQUS model instead of 1000 μs.

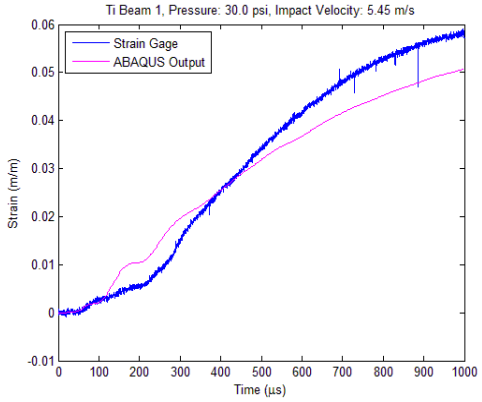

(a) Strain Gage and ABAQUS Output

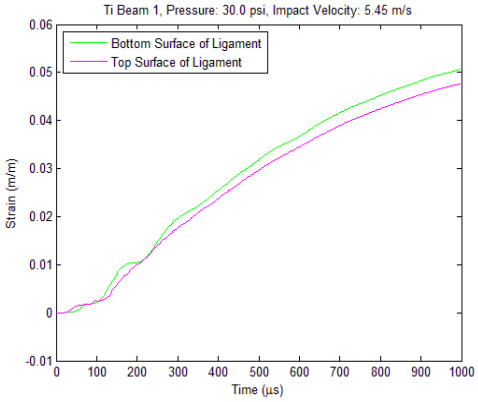

(b) ABAQUS Output at Top and Bottom Surfaces of Ligament

Figure 4.18: Comparison of ABAQUS and Experimental Results of Titanium Specimen #1

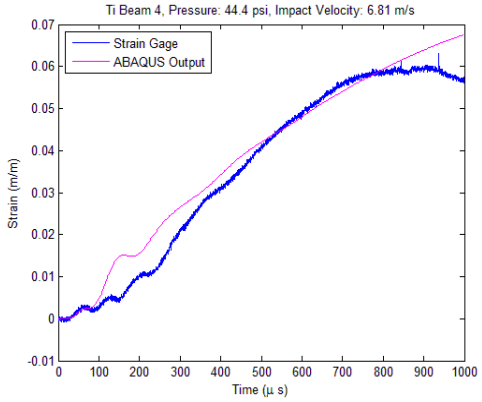

(a) Strain Gage and ABAQUS Output

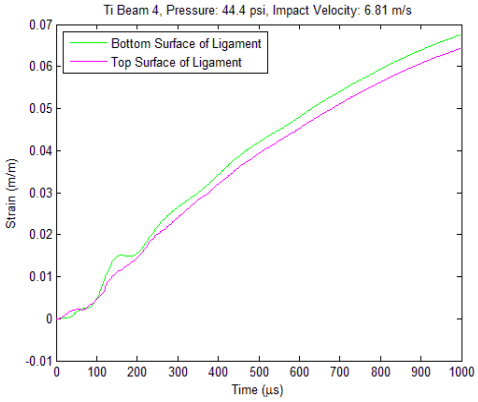

(b) ABAQUS Output at Top and Bottom Surfaces of Ligament

Figure 4.19: Comparison of ABAQUS and Experimental Results of Titanium Specimen #4

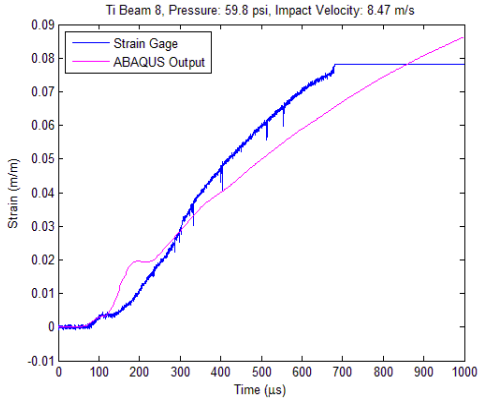

(a) Strain Gage and ABAQUS Output

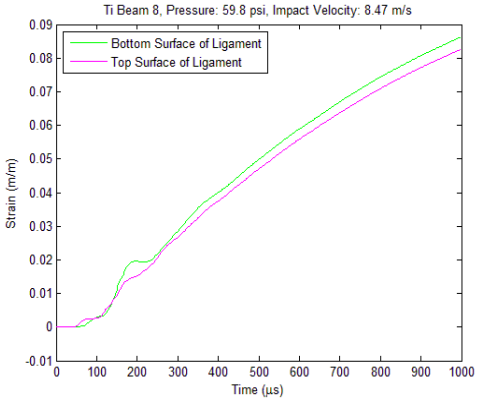

(b) ABAQUS Output at Top and Bottom Surfaces of Ligament

Figure 4.20: Comparison of ABAQUS and Experimental Results of Titanium Specimen #8

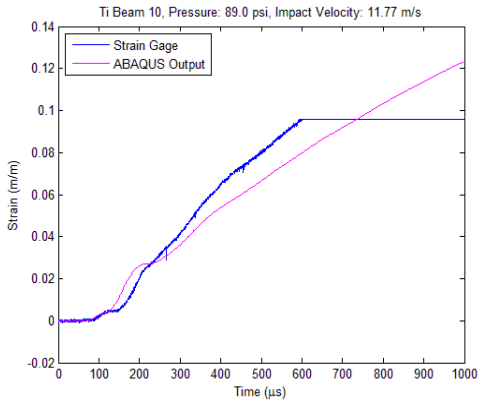

(a) Strain Gage and ABAQUS Output

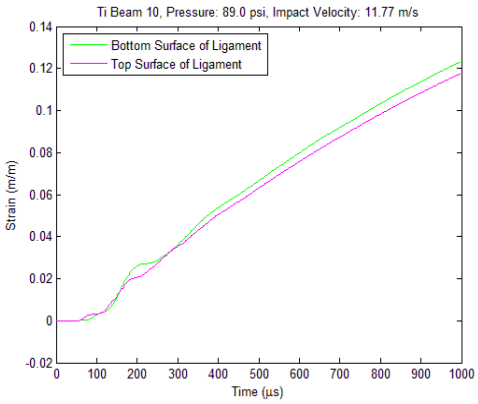

(b) ABAQUS Output at Top and Bottom Surfaces of Ligament

Figure 4.21: Comparison of ABAQUS and Experimental Results of Titanium Specimen #10

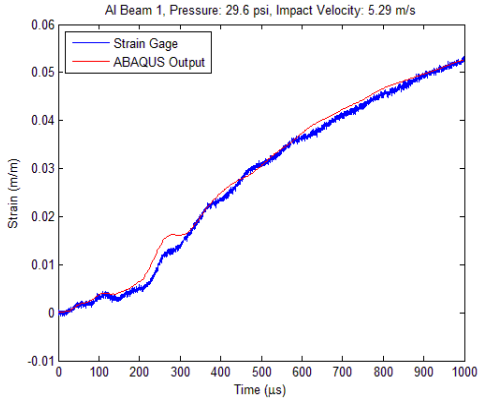

(a) Strain Gage and ABAQUS Output

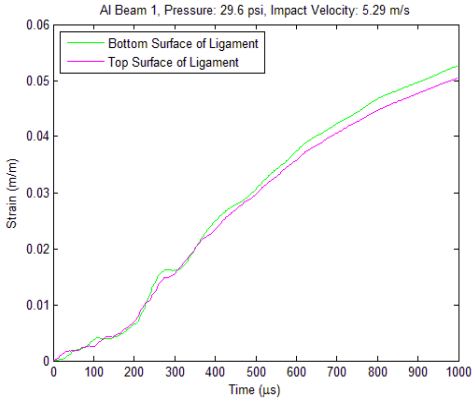

(b) ABAQUS Output at Top and Bottom Surfaces of Ligament

Figure 4.22: Comparison of ABAQUS and Experimental Results of Aluminum Specimen #1

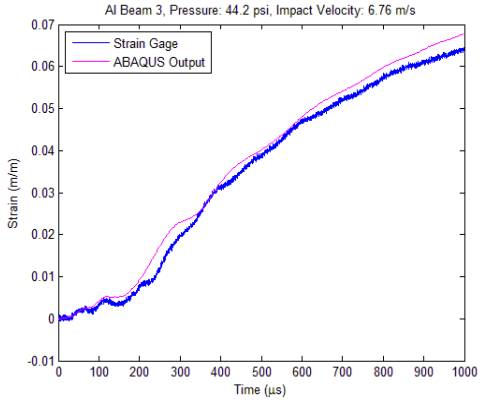

(a) Strain Gage and ABAQUS Output

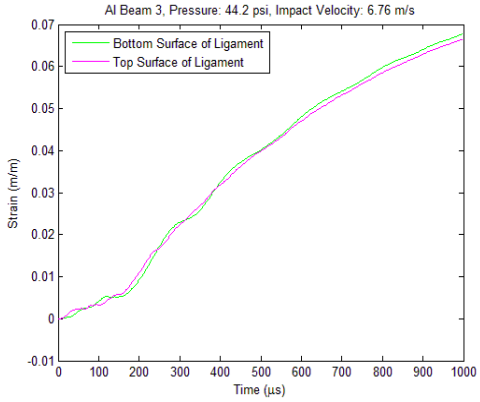

(b) ABAQUS Output at Top and Bottom Surfaces of Ligament

Figure 4.23: Comparison of ABAQUS and Experimental Results of Aluminum Specimen #3

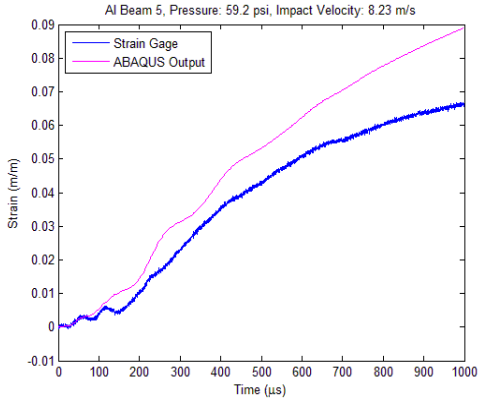

(a) Strain Gage and ABAQUS Output

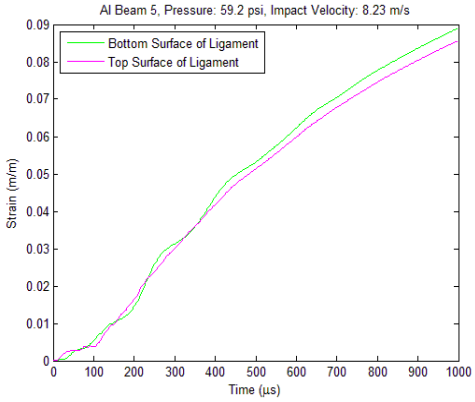

(b) ABAQUS Output at Top and Bottom Surfaces of Ligament

Figure 4.24: Comparison of ABAQUS and Experimental Results of Aluminum Specimen #5

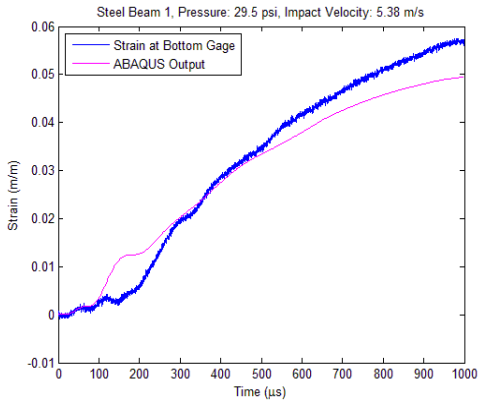

(a) Strain Gage and ABAQUS Output

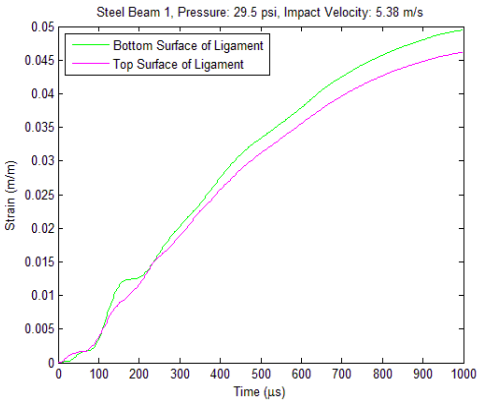

(b) ABAQUS Output at Top and Bottom Surfaces of Ligament

Figure 4.25: Comparison of ABAQUS and Experimental Results of Steel Specimen #1

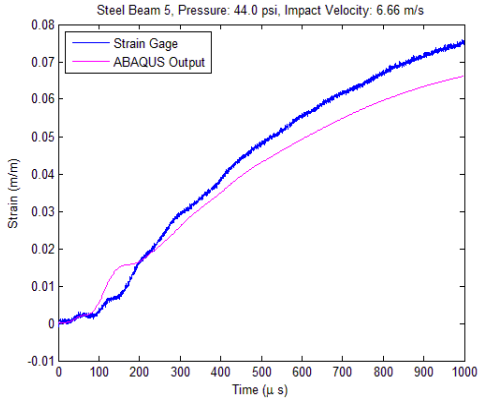

(a) Strain Gage and ABAQUS Output

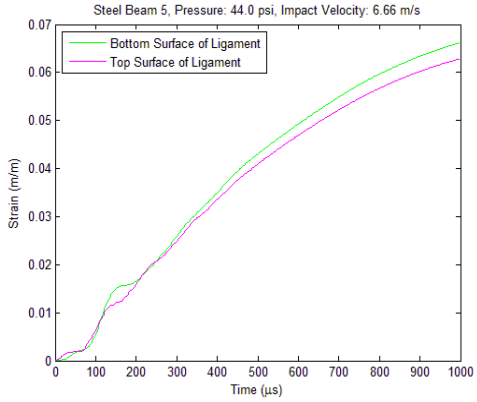

(b) ABAQUS Output at Top and Bottom Surfaces of Ligament

Figure 4.26: Comparison of ABAQUS and Experimental Results of Steel Specimen #5

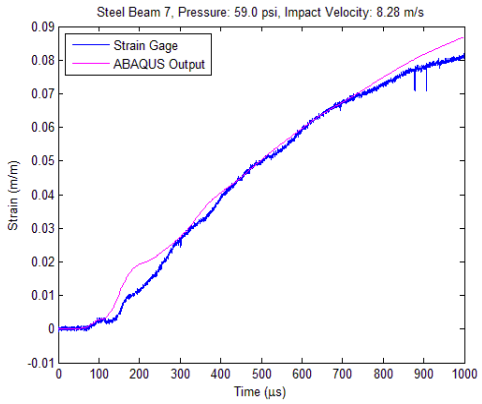

(a) Strain Gage and ABAQUS Output

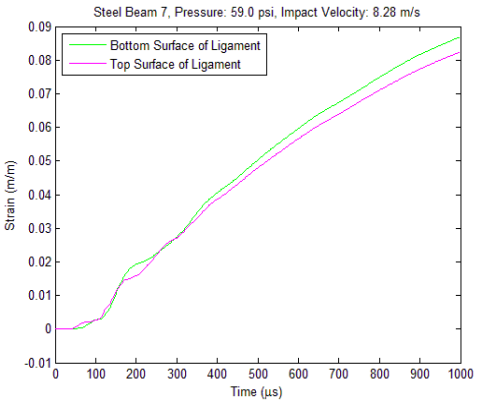

(b) ABAQUS Output at Top and Bottom Surfaces of Ligament

Figure 4.27: Comparison of ABAQUS and Experimental Results of Steel Specimen #7

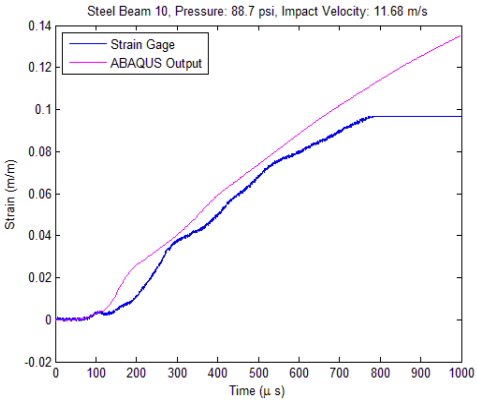

(a) Strain Gage and ABAQUS Output

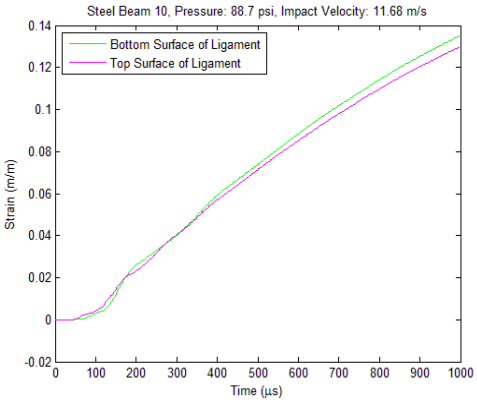

(b) ABAQUS Output at Top and Bottom Surfaces of Ligament

Figure 4.28: Comparison of ABAQUS and Experimental Results of Steel Specimen #10

Once this process was completed and the results were analyzed it was necessary to modify the Johnson-Cook coefficients in an attempt to improve the agreement between the ABAQUS and experimental results. This was done through an iterative trial an error process modifying the strain rate sensitivity factor, C. Unfortunately, a discernible improvement in agreement was not achieved by modifying this constant and it is clear that to improve agreement between the two outputs all four of the coefficients should be modified simultaneously. This is not realistic using the current method due to the limited time frame to complete this stage of the slotted beam research. Future attempts to improve the agreement would benefit from an automated process which varies all four coefficients simultaneously to improve agreement. The agreement achieved with the initial attempt showed very good results for the 2024-T3 Al samples except for the sample tested at 8.23 m/s. This was believed to be due to a difference in the material properties of the 2024-T3 Al samples. The difference stemmed from a machining problem at the AFIT lab which resulted in the manufacture of additional aluminum specimens from a different stock of 2024 Al. The agreement for the steel samples showed some signs of good agreement but indicated that more work was necessary to converge on Johnson-Cook coefficients for this particular material. The titanium results also showed that more work was necessary to determine the Johnson-Cook coefficients.

With this in my mind, an attempt was made to investigate the ability of each material's set of coefficients to predict the strain response at the top of the beam. In this analysis the Johnson-Cook coefficients provided in Table 4.2 were used for each material. The analysis was accomplished by running the ABAQUS model for the test conditions were two additional strain gages were applied to the beam specimen. Then in the same manner as described above but with different nodes to approximate the left and right strain gages the strain output was collected and compared with the experimental results. For this comparison nodes 135, 1434, 1435, 1444, 1449, 5426, 5427, 5468, and 5469 and nodes 134, 1426, 1430, 1431, 1455, 5406, 5410, 5502, and 5506 were chosen. The results of this attempt are shown in Figures 4.29 and 4.31.

Fair agreement is shown in all three cases, which indicates that the model may be able to predict the response at the top of the beam if further work is done to converge on Johnson-Cook coefficients. It is also worth noting the sensitivity of these strain gage locations to the impact location, and Figure 4.29 presents an excellent example of this sensitivity. In this plot, the ABAQUS outputs are the same due to the concentric impact in the model. However the experimental results make it clear that the impact was not concentric with the center between the two strain gages. Unfortunately any difference between the center of the beam, the impact location, and the equidistant point between the two strain gages was not visibly discernible.

In addition to investigating the agreement between the experimental and FEM results at the top surface of the beam, it was also necessary to investigate the state of stress in the ligament during both a concentric and eccentric impact. This was accomplished by additionally collecting the strain at the nodes 127, 1334, 1354, 1369, 1401, 5095, 5185, 5260, 5359, which are the nodes directly above the nodes at the bottom surface of the ligament. The strain at these nodes were collected so that any differences in the strain at the top and bottom surfaces of the ligament could be observed. Differences in the strain would indicate that stress components other than uniaxial tension were involved in the deformation of the ligament. The plot of the strains at these two locations for each case are shown in b of Figures 4.18 through 4.28.

It can be seen that while there is a difference between the strains at the top and bottom surfaces of the ligament for all of the test cases, this difference is no more than 5 percent in any of the cases. This indicates that the largest stress component in the ligament is uniaxial tension and the slot design was successful in generating a state of predominantly plastic uniaxial tension in all of the materials. Furthermore, these results also show that while a concentric impact is desired for all of the slotted beam tests, there was not a severe effect on the state of stress in the ligament from the impact locations observed in the slotted beam tests.

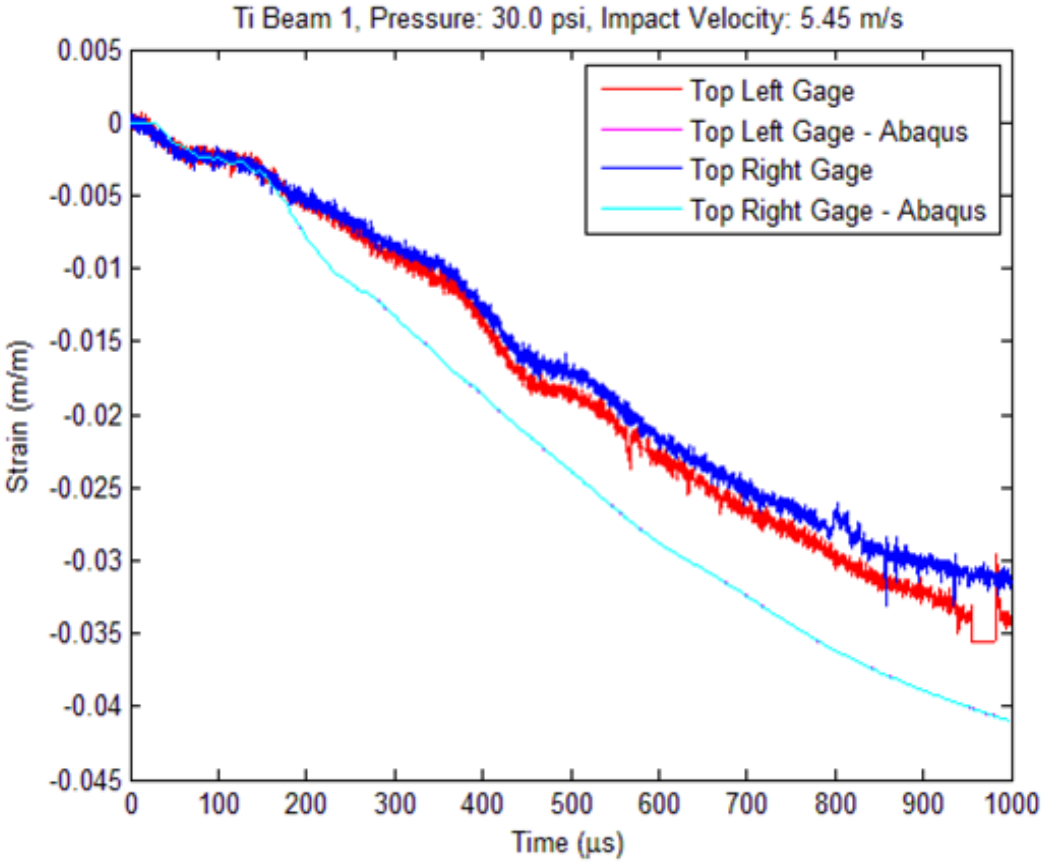

Figure 4.29: Strain Gage and ABAQUS Output from Top Surface of Titanium Specimen #1

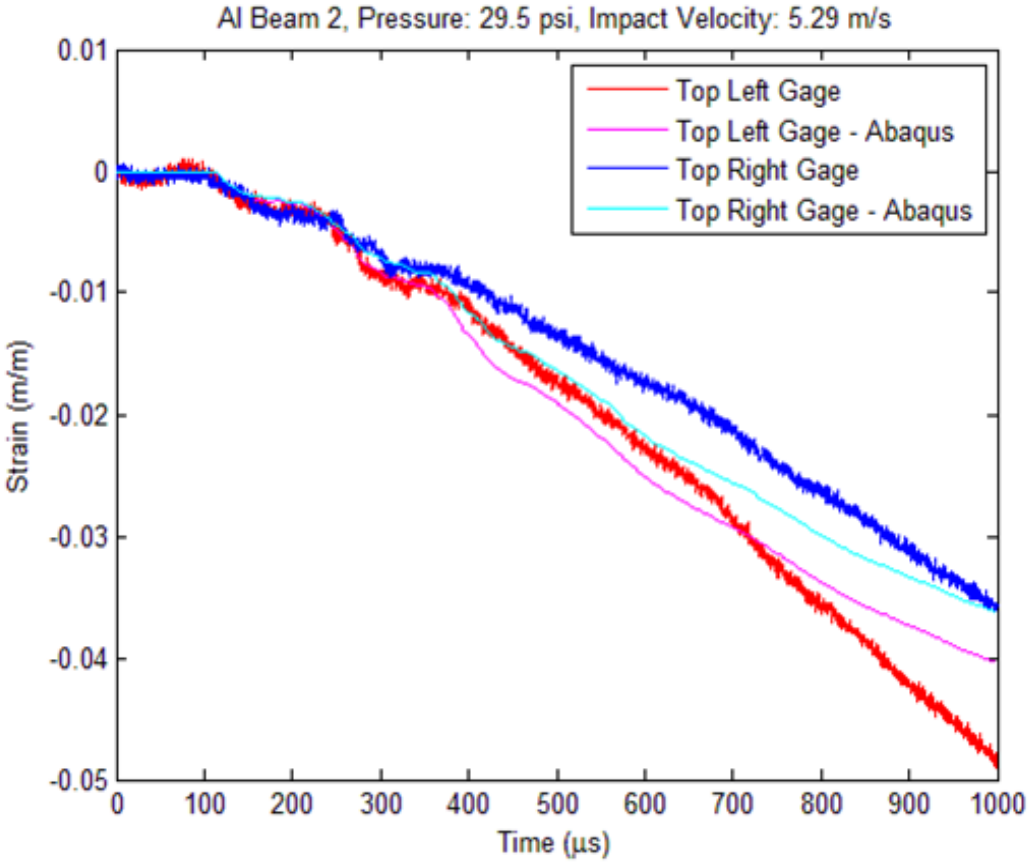

Figure 4.30: Strain Gage and ABAQUS Output from Top Surface of Aluminum Specimen #2

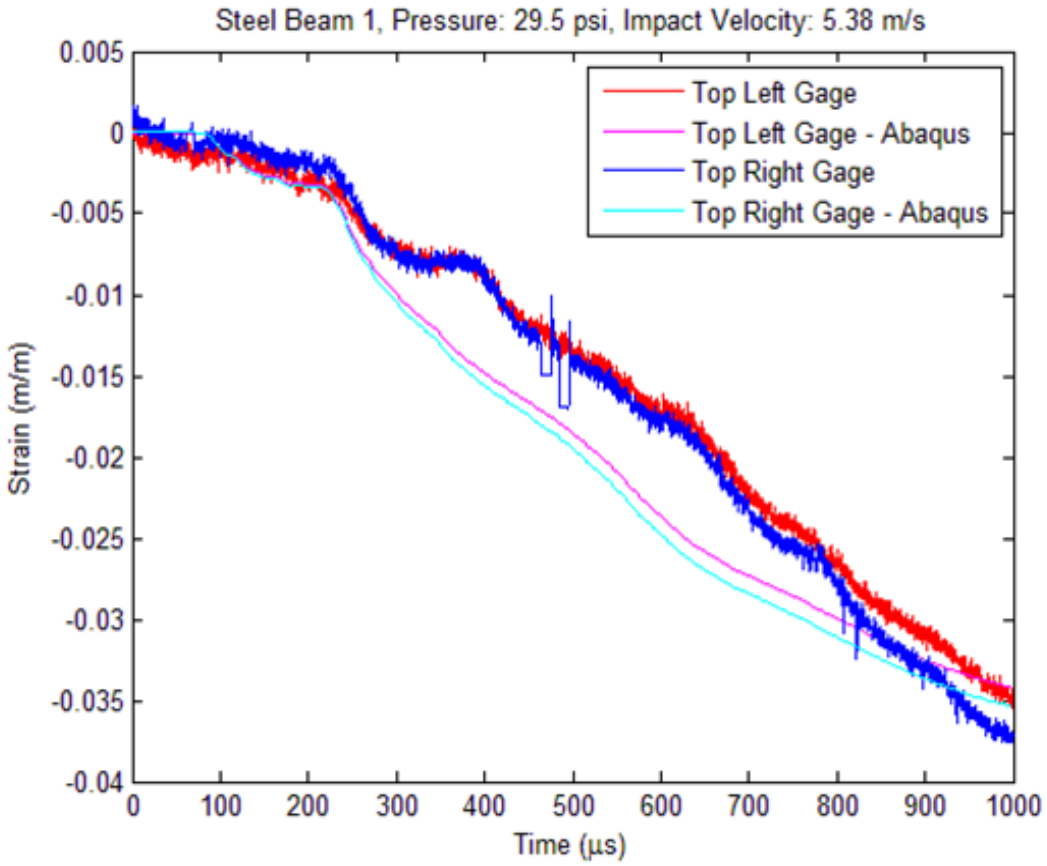

Figure 4.31: Strain Gage and ABAQUS Output from Top Surface of Steel Specimen #1

4.1.5 Results of Analysis. The results of the analysis of the strain histories, determination of the strain rates, and constitutive modeling indicate that the slotted beam test was successful in creating uniaxial tension in the slot, generating plastic strain rates in the intermediate strain rate range and providing a method to determine the Johnson-Cook coefficients of a material tested. The method of impacting the slotted beam and measuring the specimen response proved to be successful and valuable material data was collected during the deformation of the specimen. Attempts to develop a unique constitutive for each material showed promising results and future work should concentrate on refining the modeling process to make subsequent attempts more successful. The general trends and major conclusions which can be made from these results and this research are addressed in Chapter 5.

V. Conclusions

It is now appropriate to discuss the major trends and conclusions which can made from this stage of the slotted beam research and identify areas for future research. There were nine major conclusions which can be drawn from the slotted beam experiments and they include:

1. **The slotted beam specimen works for generating a tensile response in ductile metals.**
2. **The location of impact and slot design play a large role in global deformation.**
3. **The slotted beam test is a relatively simple and low cost test to perform.**
4. **The strain gages and associated measurement system work well for measuring the specimen response.**
5. **Plastic strain rates from 50 to 200 s^{-1} can be developed at the ligament using this technique.**
6. **The strain history provides important data about the elastic and plastic deformation along with yield point of the material tested.**
7. **The current FEM model provides good agreement for some of the experimental results.**
8. **Additional material and test data will be required to improve the experimental and FEM agreement.**
9. **Constitutive modeling can be accomplished with further development of matching technique.**

All of these conclusions will be discussed in detail to illustrate the strengths and weaknesses of the slotted beam technique. Furthermore, areas for further research in relation to each conclusion will be identified in an attempt to improve the capabilities of the slotted beam technique as it is developed in the future.

5.1 Major Trends and Conclusions

5.1.1 Conclusion 1: Slotted beam specimen works for generating tensile response in ductile metals. The slotted beam design was the primary mechanism in creating the uniaxial state of stress in the ligament, and therefore the most important factor in the success of this experimental method. The design of the slot as described in Appendix 1 provided a design which created both, a state of stress which is predominantly uniaxial in the ligament and at the same time was easily manufacturable. Furthermore, the design process can easily be reproduced for materials other than titanium using the design of experiments (DOE) and plane strain FEM technique described in Appendix 1. This design technique is a powerful tool for determining the slot dimensions in other materials. Future work should focus on investigating how the slot dimensions are affected by material properties. In addition, work should be accomplished to investigate if there are other slot dimensions which could be used in titanium or other materials which would further reduce the stress components other than the component of uniaxial tension.

5.1.2 Conclusion 2: Location of impact and slot design play large role in global deformation. From the results of the slotted beam tests, it is clear that the impact location in relation to both the center of the beam and the slot played a major role in the global deformation of the beam as illustrated in section 4.1.1. A concentric impact and symmetrical deformation was shown to be mildly important for maintaining a uniform state of stress in the ligament. In the future, the probability of a central impact of the specimen can be improved through several different actions. One of these actions is ensuring that the dimensions of the beam and slot remain in tolerances and the slot is machined off the center of the beam. This is important for centering the specimen and therefore the slot in the fixture before testing. The tolerances used in this stage of slotted beam tests proved appropriate, but improvements could be made for future work by either reducing the tolerances or using a more precise machining method such as EDM for the entire specimen and not just the slot. If the

manufacturing tolerances are exceeded or the slots are manufactured improperly, the likelihood of an off center impact is increased which may complicate the state of stress in the ligament and the analysis of the specimen response.

5.1.3 Conclusion 3: Relatively simple and low cost test to perform. The slotted beam technique was a relatively simple test to perform, and did not require an extensive test setup to perform. All of the test equipment used in this test method is commonly used in impact testing, and through the use of an instrumented drop weight machine the need for a complicated mechanism to accelerate an impactor was avoided. The strain gage is a relatively simple and widely used transducer which decreases the cost of these experiments. It is important to note that significant effort was required to prepare each specimen, and this must be taken into consideration for the planning of a successful slotted beam experiment. Furthermore, the machining technique used to create the slot in the beam, EDM, is widely used and reduces the complexity and cost of performing these experiments. The use of a slotted beam specimen also reduced the complexity of manufacturing the specimen since it was not a complicated design and can be easily manufactured. Future work in this area could focus on analyzing preparation methods and test procedures, which reduce the time required to perform the test. This could include analysis of the surface preparation steps used to achieve an optimum bond between the ligament and the strain gage or the actual procedure involved with installing and calibrating a specimen before testing.

5.1.4 Conclusion 4: Strain gages and associated measurement system work well for measuring the specimen response. Both the strain gages and the measurement system designed to collect the response from the strain gages worked well in these experiments. While section 4.1.1 showed that the majority of the tests resulted in at least partial disbonding of the gages and terminal pads, strain gage signals were collected for the entire test duration for many of the tests. The triggering system developed for the slotted beam tests was an essential component in consistently collecting data

from the impact of the specimen. Before a triggering system was developed, the data acquisition system was susceptible to inadvertent triggering from noise and Dynatup electrical signals. The inadvertent triggering resulted in less than a 50% success rate if success was judged by any strain data being collected during a test event. After the triggering system was developed, the success rate of data collection increased above 90%, which was directly related to the addition of the triggering system. Future work could focus on improving the reliability of the strain gages and reducing the time required to install the trigger system between each test. The reliability of the strain gage is an area where significant improvement could be made with the selection of smaller strain gages and smaller gauge wire. The strain gages used in these tests were selected to accommodate the large strains expected, and while a significant amount of strain was experienced at the ligament a smaller strain gage should be able to handle the strains experienced. Furthermore, the wires used in these experiments were relatively large compared to the wires which would typically be used in an experiment of this sort, and in future experiments the twisted wires used should be no larger than 20 AWG. The advantage of a smaller strain gage and wire is the reduced mass of the transducer system, which is the second most important factor behind surface preparation in preventing disbonding during the test window. Future improvements for the trigger design could include a redesign of the brackets, which secure the fiber optic cables, so that they are more quickly removed in between tests.

5.1.5 Conclusion 5: Plastic strain rates from 50 to 200 s^{-1} can be developed at the ligament. The determination of the strain rate for each loading condition showed that a range of plastic strain rates are possible with the velocities the Dynatup is capable of generating. While these strain rates were not constant, they were taken over a large portion of the plastic strain data collected and are therefore an appropriate characterization of the rate of loading for each test. In future tests, the plastic strain rate could be measured over the entire plastic strain region if none of the voltage signals are clipped or none of the strain gages appear to have disbonded prematurely.

The capability to generate strain rates in this range is important in bridging the gap between the quasi-static test and tests like the SHPB test. However, the capability to generate a wider range of strain rates which approach the strain rates possible with the SHPB test would remove the gap between test methods and should be a primary goal for future research. Therefore, further work should focus on generating larger plastic strain rates at the ligament. This may be accomplished by generating higher impact velocities or by modifying the beam and slot design. All of these areas of the slotted beam technique and design should be investigated in an attempt to increase the plastic strain rates at the ligament.

5.1.6 Conclusion 6: Strain history provides important data about elastic and plastic deformation along with yield point. Each strain history collected from a slotted beam test provided valuable information on the amounts and rates of elastic and plastic deformation occurring at the ligament. The results of the analysis showed that these amounts and rates of deformation were affected both by the material properties and the rate of loading. By measuring the material response, estimating the strain at which yield occurred, and comparing this strain to the strain at which yield occurs for quasi-static data, it was possible to observe strain rate sensitivity or visco-plastic behavior in both the titanium and steel samples. This was to be expected since both titanium and steel have shown signs of strain rate effects in the strain rate ranges generated during these tests in previous impact testing. These results show that the slotted beam technique can be used to investigate the strain rate sensitivity of the materials and structural metals. In future work, additional methods for estimating and quantifying the different regions of deformation in the strain history should be explored. This would include a method for estimating the yield of each material at each rate of loading so that any difference in the yield between slotted beam loading rates could be quantified.

5.1.7 Conclusion 7: Current FEM model provides good agreement for some of the tests. The agreement between the ABAQUS results and the experimental

results illustrated that Johnson-Cook coefficients could be determined for a material tested using the slotted beam technique. Analyzing the results from the aluminum and steel comparisons, show that good agreement was achieved while the titanium comparisons make it clear more work is needed to improve this method. Future work to improve the agreement between the model and the experiment should include the refinement of the ABAQUS model discussed in detail in Appendix 2. Additional work could focus on improving the contact law used between the tup and the specimen. Also further attempts to collect load cell data should be made to provide data which can increase the fidelity of the model of the impact condition.

5.1.8 Conclusion 8: Additional material and test data will be required to improve experimental and FEM agreement. One of the reasons believed to cause the differences between the ABAQUS results and the experimental data was the lack of quasi-static data for the actual materials tested. The constitutive modeling process described in section 3.3.1 relies on data from quasi-static material testing. The differences in mechanical properties between the actual material tested and published data may have been significant and resulted in the poor agreement for some of the test results. This added to the uncertainty in trying to match the experimental strain history and the ABAQUS output since the mechanical properties of the actual material tested are not known, and made it difficult to use a manual iteration technique to determine the Johnson-Cook coefficients. In future work, quasi-static tests should be performed prior to the slotted beam tests to characterize the quasi-static material properties. Obtaining the material properties at quasi-static strain rates is an essential part of the material characterization process since it allows the accurate determination of the first three Johnson-Cook constants, A, B, and n.

5.1.9 Conclusion 9: Constitutive modeling can be accomplished with further development of technique. The initial slotted beam test results presented in section 4.1.3 showed that the slotted beam test is viable for generating and measuring the mechanical response of ductile materials at elevated strain rates. A comparison of the

experimental data with the ABAQUS model showed good agreement for some tests but poor agreement for other tests. The lack of agreement could have been caused for several reasons and trying to improve agreement through the manipulation of one Johnson-Cook constant proved to have very little affect on improving the agreement. The good agreement that was shown was due to the fact that the initial estimates for the Johnson-Cook coefficients were already close to what could be considered the final values. This shows that good agreement can be achieved, but that the present method in not appropriate for future tests. In future work, an inverse modeling technique using optimization techniques should be developed so that all four coefficients can be modified simultaneously in an attempt to improve the agreement. This will improve the efficiency of this constitutive modeling method.

Appendix A. Slotted Beam Specimen Design

A.1 Specimen Design

The most important aspect of the slotted beam specimen was the slot placed in the beam specimen. The removal of material in the middle of the beam in the form of a slot was the primary mechanism in creating a state of uniaxial stress in the specimen ligament which could be measured. However the slot dimensions which would promote the most uniform state of tensile stress in the ligament had to be determined if the slotted beam technique was going to be successful. This required an analysis of various slot dimensions and locations in order to determine the slot design which created a most uniform state of tensile stress and at the same time was easily manufactured. The following is a description of this analysis and the slot design process.

A.1.1 Influences on Uniaxial State of Stress. Elementary beam theory can be used to predict the development of uniaxial tension at elevated strain rates in the slotted beam specimen. In this theory, it is well-known that a beam fixed at its ends with a concentrated force at mid-span on its top surface will induce a moment load that will cause the top surface of the beam to be in a state of compression while the bottom surface will be in a state of tension. In this case, if a small amount of volume in the form of a slot is removed from a location at and around the mid-span of the beam, three beam characteristics will be affected. These three characteristics include the relocation of the neutral axis of the beam at the location of the slot, the reduction of the cross-sectional area of the beam at the center of the beam, and the reduction of the beam's moment of inertia. This means that the slot will result in a redistribution of the stresses in the beam from the original beam configuration. The removal of material in the form of a slot also results in a maximum tensile stress in the ligament of material directly below the slot which is a higher magnitude of stress than in the unslotted beam. This is important to the slotted beam specimen since in an isotropic, plastic material with the same behavior in tension or compression, the ligament will exhibit the first signs of plasticity given the transverse loading condition. The flexure

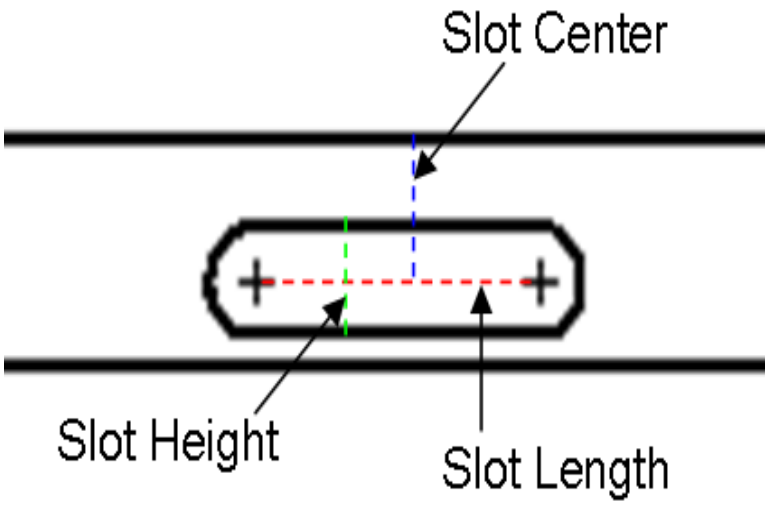

Figure A.1: Dimensions Used to Design the Slot

of the beam and the development of plasticity in the ligament will result in a state of nearly uniform state of tensile stress throughout the ligament cross-section. Clearly the slot dimensions will influence the plasticity generated in the ligament and the uniformity of the state of stress in the ligament. In an initial attempt to design the slot in the beam specimen, the development of uniaxial tensile stress in the slotted beam specimen was assumed to be a function the slot length, the slot height, and the location of the slot center. The slot length was measured as from the center of the radii on each enter of the slot. The slot height was measured from the top of the slot to the bottom of the slot. The slot center was measured from the top surface of the beam to the center of the slot. To impact the specimen in a manner where a state of uniaxial tension was developed at the ligament it was first necessary to determine the dimensions of the test specimen. Figure A.1 shows a drawing of the slot and each of the dimensions which were assumed to influence the state of stress in the ligament.

A.1.2 Design of Experiments, FEM, and Matlab. To design the slot, the factors which were believed to influence the state of stress in the ligament, slot height, slot length, and slot center, were taken and a 3 level 3 factor design of experiments

Test Number	Factor 1 Hole Length (m)	Factor 2 Hole Height (m)	Factor 3 Hole Center (m)	Max Diff. in S11 Stress (Pa)
1	0.020	0.004	0.006350	1.7279E+08
2	0.030	0.004	0.006350	3.1303E+08
3	0.040	0.004	0.006350	9.4271E+07
4	0.020	0.005	0.006350	1.5920E+08
5	0.030	0.005	0.006350	1.7618E+08
6	0.040	0.005	0.006350	7.7491E+07
7	0.020	0.006	0.006350	2.4566E+08
8	0.030	0.006	0.006350	7.7491E+07
9	0.040	0.006	0.006350	2.8365E+07
10	0.020	0.004	0.007232	3.4159E+07
11	0.030	0.004	0.007232	8.1670E+07
12	0.040	0.004	0.007232	2.0411E+08
13	0.020	0.005	0.007232	7.6353E+07
14	0.030	0.005	0.007232	9.4612E+07
15	0.040	0.005	0.007232	1.4009E+08
16	0.020	0.006	0.007232	1.3292E+07
17	0.030	0.006	0.007232	9.4616E+07
18	0.040	0.006	0.007232	1.5092E+08
19	0.020	0.004	0.008113	6.3810E+06
20	0.030	0.004	0.008113	8.6820E+07
21	0.040	0.004	0.008113	6.8504E+07
22	0.020	0.005	0.008113	1.1623E+07
23	0.030	0.005	0.008113	1.5190E+07
24	0.040	0.005	0.008113	4.9920E+07
25	0.020	0.006	0.008113	7.0700E+05
26	0.030	0.006	0.008113	2.1152E+07
27	0.040	0.006	0.008113	2.0447E+08

Figure A.2: Three Level, Three Factor Design of Experiments for Slot

was developed. The slot dimensions were used as the three factors in this design of experiments and three levels for each dimension was assigned to complete the design of experiments. This resulted in 27 experiments and Figure A.2 shows an image of the design of experiments used to determine the slot dimensions. The objective of this design of experiments was to quantify the effect of various slot dimensions on the state of stress in the ligament. This was accomplished using the plane strain FEM shown in Figure A.3. Using this FEM, run at an impact energy of 62.5 J or 5kg at 5 m/s due to the assumption that this would be approximately the lowest magnitude impact condition run during the slotted beam tests, the stress in the longitudinal direction of the beam at the the three nodes in the center of the ligament were measured. For each test run, the maximum difference between the stresses at these three nodes was calculated and used to develop a second order model for the maximum difference in stress, y defined as,

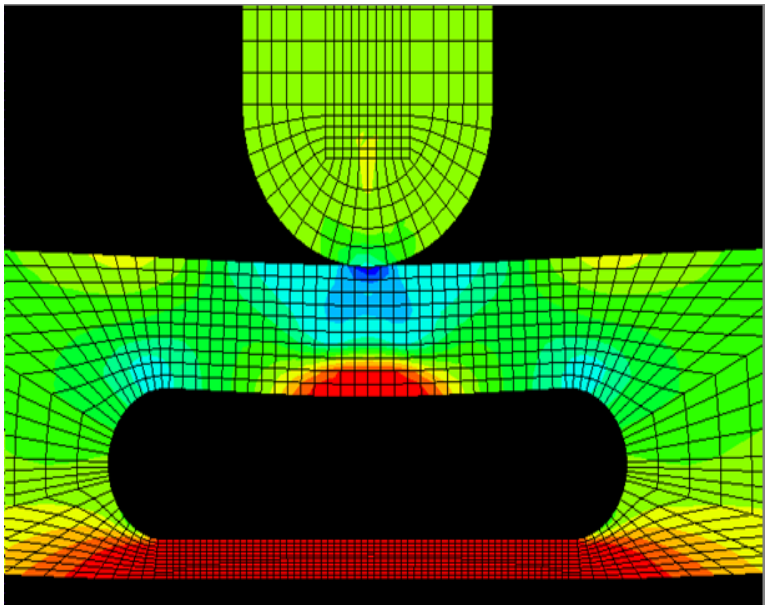

Figure A.3: Plane Strain FEM

$$y = (5.3134 - 0.5144x_1 - 1.2257x_2 - 2.1780x_3 - 0.1017x_1^2 + 0.1657x_2^2 \\ +0.0163x_3^2 - 0.0249x_1x_2 + 0.5679x_1x_3 + 0.2439x_2x_3) * 10^8 Pa \qquad \text{(A.1)}$$

where x_1, x_2, and x_3 are the three slot dimensions, slot length, slot height, and slot center respectively. It is important to note that equation (A.1) is developed for coded values and not for the actual values of x_1, x_2, and x_3 and was done to avoid any confusion between units. Once the model was developed, it was input into Matlab and using the *fmincon* function, a constrained minimization was performed.

A.1.3 Final Dimensions. Several sets of dimensions were found which created a minimum in the difference in the longitudinal stresses at the center of the ligament. However one set of dimensions, shown in Figure A.2 as experiment 25, was in close proximity to several local minimums. Furthermore, this set of dimensions was easily manufacturable into a beam specimen due to the relatively large dimensions and common sizes. These dimensions were a slot length of 2 cm, a slot height of 6

mm, and a slot center of 8.113 mm and were selected as the slot dimensions for these experiments. It is important to note that these dimensions were determined using the material properties of CP titanium and the slot dimensions for other materials would be different. In these experiments the same slot dimensions were used in all of the experiments to observe the effect of these slot dimensions on other materials.

Appendix B. Slotted Beam Finite Element Model

B.1 FEM User Manual

The ABAQUS FEM, developed by Capt Reid Larson and used for a large portion of the analysis of the slotted beam data, was developed in an attempt to determine the constitutive relationship of the material tested with the slotted beam technique. The ABAQUS FEM was required due to the fact that the stress at the ligament can not be measured experimentally. Further, the ABAQUS model was also used to investigate certain phenomenological aspects of the slotted beam including the state of stress in the ligament and the velocity of the impactor. The purpose of this appendix is to provide information about the model and instructions for the use of this model for future slotted beam experiments.

B.1.1 Model Components, Nodes, and Elements. The FEM of the slotted beam test is broken into several components to provide a realistic model of the impact event, while at the same time creating a model which is relatively quick to solve. From the results presented in Chapter 4 of this document it can be seen that good agreement is achieved with several of the materials. At the same time the model only takes approximately 15 minutes to solve in ABAQUS CAE, the ABAQUS explicit-integration solver.

The slotted beam FEM is comprised of three primary components, the beam fixture, the slotted beam specimen, and the model of the Dynatup tup, load cell, and crosshead. The beam fixture is broken up into several components including the bottom plate, spacer plate, top plate, Dynatup attachment screws, and plate fasteners. The total number of nodes and elements for all of these components is 40714 and 30304 respectively. The properties of 304 Stainless Steel are used to model all of these components. The slotted beam specimen is modeled as one component with 10725 nodes and 8640 elements. The constitutive properties of the slotted beam specimen are defined by the Johnson-Cook constitutive relationship which was developed as part of the slotted beam research. Finally, the simplified model of the Dynatup tup and

load cell is modeled in two parts with 5579 nodes and 4960 elements total. The first part of this simplified model is the tup, which is configured with the same geometry as the 1" hemispherical impactor used on the Dynatup. This part of the impactor is modeled with the material properties of 4340 Alloy Steel, which is a hardened steel alloy typically used in impact tests. The second part of this simplified model is used to represent the mass contained in the crosshead above the tup and load cell in addition to the mass of the tup and load cell assembly. This is accomplished with a cylinder 1/2 inch in height and 1 inch in diameter. To model the mass contained in the crosshead and the stiffness of the assembly, a rigid material is used that has a large stiffness, 5000 GPa and a mass density of 663963 kg/m^3. One section is configured in the same geometry of tup attached to the load cell. It is important to note that all components in this FEM are meshed with linear, 8-noded, 3-D brick elements. Images of each component are contained in Figure B.1.

B.1.2 Boundary Conditions. Another important aspect of the Slotted Beam FEM is the boundary conditions used to constrain and load the model. The particular boundary conditions described here were used in an attempt to model the actual constraints on the specimen and beam fixture. At the same time, the boundary conditions used in this model provide for the loading of the beam specimen in a realistic manner with the data collected from the Dynatup. The first boundary condition is used to constrain the surface under the bottom plate which is in direct contact with the base of the Dynatup. This surface is constrained from vertical displacement to reflect the rigid interface with the Dynatup base which is a thick steel slab. The next boundary conditions are used to represent the interfaces between individual plates in the fixture assembly. This is accomplished by assigning a rigid contact law in ABAQUS to prevent displacement between each plate. To represent the contact between the tup and the impact site on the top surface of the beam specimen and the surfaces of the slotted beam specimen in direct contact with the top and bottom plates of the fixture, the same rigid contact law is assigned. Modeling the compressive force

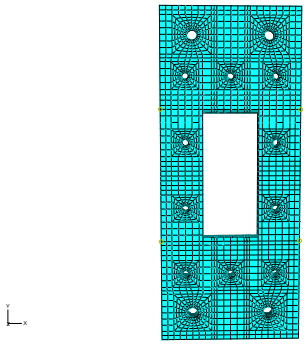

(a) bottom plate

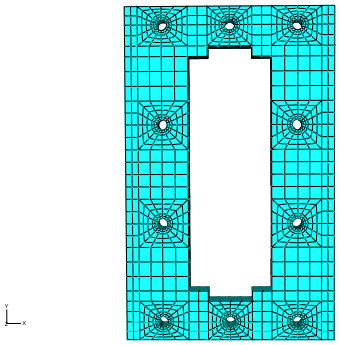

(b) spacer plate

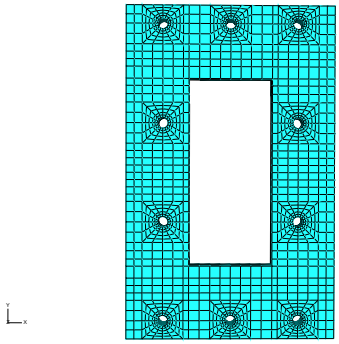

(c) top plate

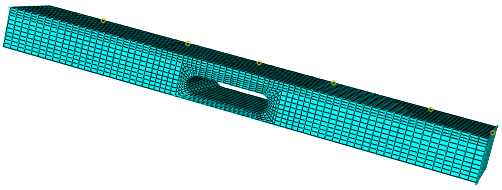

(d) slotted beam

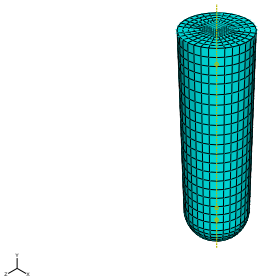

(e) tup

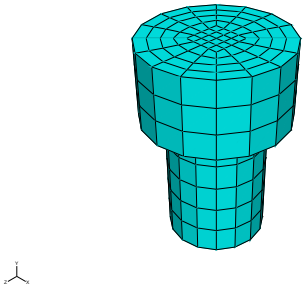

(f) attachment screw

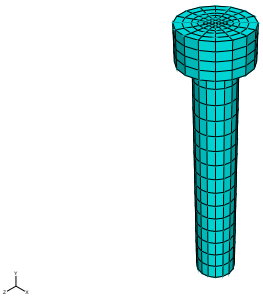

(g) fixture screw

Figure B.1: Components of ABAQUS Slotted Beam FEM

created by the fasteners when torqued into the fixture is accomplished by assigning a rigid contact law to the heads of the fasteners at the top of the plates. These fixture to fixture fasteners are only threaded through the fixture's bottom plate, and the top and spacer plates had through holes and were not tapped. To model this situation, the surfaces of the fasteners in the proximity of the fastener threads are tied to the displacements of the bottom plate at that location. The Dynatup attachment screws are constrained from vertical displacement in the same fashion as the bottom surface of the bottom plate. Loading the beam specimen is accomplished by applying a velocity to the simplified tup and load cell model. The velocity used in ABAQUS is the same as measured by the Dynatup's velocity photodetector, so that the same impact energy can be applied to the computer simulation as in the actual test.

B.1.3 Using the FEM. Included below is a list of instructions which detail how to run a slotted beam model.

1. Open the slotted beam model, File name: BeamFixture JC.cae making sure that the folder with the files for the Attachment Screws are contained in the same beam model folder
2. Define the impact location by translating the tup
   (a) In the Assembly Module
   (b) Select Instance
   (c) Select Translate
   (d) Select the tup model with the mouse
   (e) Select a point to define the start of the tup translation
   (f) Input the impact location in terms of the x and y components of the distance from impact location to the center of the beam specimen
   (g) Click OK to approve tup translation
3. Define the Beam Specimen's Constitutive relationship

(a) Expand the Materials menu in the Model Tree

(b) Double click on Aluminum 2024

(c) Input the Density, Elastic, Plastic, and Rate dependent Properties Estimates for the materials being tested

(d) Click OK after all Material Parameters have been input

4. Define the tup model's velocity

(a) Expand the Predefined Fields menu in the Model Tree

(b) Expand the Tup Velocity menu

(c) Expand the States menu

(d) Double click on Initial(created)

(e) Input tup velocity in (m/s) and click OK

5. Submit the job to ABAQUS for solution

(a) In the Job Module

(b) Select Job

(c) Select Manager

(d) Click on Submit and then OK

6. Collect the Strain Output at the Top and Bottom Surfaces of the Ligament

(a) In the Visualization Module

(b) Double Click on XYData

(c) Select ODB field output and then OK

(d) Click on Submit and then OK

(e) Select Unique Nodal in the Position menu and the Variable for Output, E22

(f) Select the Nodes for Output in the Viewport and Click OK

(g) Select Plot and then Select Save

(h) Select Report from the Top Menu

(i) Select XY and then Select the Data to Report to a File making sure to Unselect Append to File

Bibliography

1. "Piezoelectric Tups". www.instron.us, 2004.
2. "TDS 3034 Digital Phosphor Oscillosope Specification". www.tektronix.com, 2004.
3. Al-Mousawi, M.M. "Theoretical Studies on Flexural Wave Propagation in Beams: A Comprehensive Review Part 1". *The Shock and Vibration Digest*, 18(4), 1986.
4. Al-Mousawi, M.M. "Theoretical Studies on Flexural Wave Propagation in Beams: A Comprehensive Review Part 3". *The Shock and Vibration Digest*, 18(6), 1986.
5. Atkins, A. G. "Maximum Attainable Uniform Strain Rates with High-Speed-Crosshead Testing Machines: Theoretical Considerations". *Journal of Strain Analysis*, 5(4), 1970.
6. Benck, R. F. and D. A. DiBerardo. *Quasi-static Tensile Stress-Strain Curves for 2024-T3 Aluminum Alloy*. Technical report, USA Ballistic Research Laboratories, February 1976.
7. Board, Columbia Accident Investigation. *Columbia Accident Investigation Board, Volume 1*. Technical report, National Aeronautical and Space Administration, 2003.
8. Brar, Singh. *Inertial Effects on Strain Gages and Wave Propagation through Slotted Beam*. University of Dayton Research Institute, 2008. Personal correspondence.
9. Brendin, Harold. "Measuring Shock and Vibration". *Mechanical Engineering*, February 1983.
10. Campbell, J.D. "Dynamic Plasticity: Macroscopic and Microscopic Aspects". *Materials Science and Engineering*, 12:3–21, 1973.
11. Center, Mechanical Properties Data. *Aerospace Structural Metals Handbook*. Technical report, Battelle Columbus Laboratories, 2003.
12. Chalmers, G.F. *Strain Gauge Technology*. Applied Science Publishers, 1982.
13. Cooper, R.H. and J.D. Campbell. "Testing of Materials at Medium Rates of Strain". *Journal of Mechancial Engineering Science*, 9(4), 1967.
14. Dennis C. Krinke, John P. Barber and Theodore Nicholas. *The Charpy Impact Test as a Method for Evaluating Impact Resistance of Composite Materials*. Technical report, University of Dayton Research Institute, 1978.
15. Dowling, Norman E. *Mechanical Behavior of Materials*. Prentice Hall, second edition, 1999.

16. DSS Simulia. *ABAQUS Version 6.7 Documentation*.

17. Dunn, Patrick F. *Measurement and Data Analysis for Engineering and Science*. McGraw-Hill, 2005.

18. Fujan, David. *Capabilities of Fiber Optic Equipment*. Banner Engineering Application Engineer, 2008. Personal correspondence.

19. Goldsmith, Werner. *Impact: The Theory and Physical Behaviour of Colliding Solids*. Edward Arnold LTD, 1960.

20. Ho K.H., Newman S.T. "State of the art electrical discharge machining (EDM)". *International Journal of Machine Tools and Manufacture*, 43(13), 2003.

21. Instron/General Research, 5383 Hollister Ave./Santa Barbara, CA 93111. *GRC 8250 Impact Test Machine*.

22. Ireland, D.R. "Procedures and Problems Associated with Reliable Control of the Instrumented Impact Test". *ASTM STP 563*, 1974.

23. J. Zukas, H.F. Swift L.B. Greszczuk D.R. Curran, T. Nicholas. *Impact Dynamics*. Kreiger Publishing Company, 1992.

24. Jones, Norman. *Structural Impact*. Cambridge University Press, 1989.

25. Kay, G. *Failure Modeling of Titanium-61-4V and 2024-T3 Aluminum with the Johnson-Cook Material Model*. Technical report, Lawerence Livermore National Laboratory, 2002.

26. Keenan, Zachary. *Determination of the Constitutive Equations for 1080 Steel and Vascomax 300*. Master's thesis, Air Force Institute of Technology, 2005.

27. Khazan, Alexander. *Transducers and Their Elements*. Prentice Hall, 1994.

28. Larson, Reid. *Slotted Beam Fixture*. Air Force Institute of Technology, 2008. Personal correspondence.

29. Larson, Reid A. *A Novel Method For Characterizing the Impact Response of Functionally Graded Circular Plates, Dissertation Prospectus*. Air Force Institute of Technology, 2007.

30. M. Vural, D. Rittel and G. Ravichandran. "Large Strain Mechanical Behavior of 1018 Cold-Rolled Steel over a Wide Range of Strain Rates". *Metallurgical and Materials Transactions*, 2003.

31. Mathworks. "Matlab Help". http://www.mathworks.com/.

32. Meier, Mike. "The Ductile to Brittle Transition". http://www.matsci.ucdavis.edu, September 2004.

33. Meyers, Marc Andre. *Dynamic Behavior of Materials*. John Wiley and Sons, 1994.

34. Mordan, G. C. *Adhesives and Installation Techniques.* Applied Science Publishers, 1982.

35. Nettles, A.T. and M.J. Douglas. *A Comparision of Quasi-Static Indentation to Low-Velocity Impact.* Technical report, National Aeronautical and Space Administration, 2000.

36. Nicholas, Ted. "Class Handout, AERO 899, High Velocity Impact", Fall Quarter 2004.

37. Nicholas, Theodore. "Strain rate and strain-rate-history effects in several metals in torsion". *Experimental Mechanics*, 1971.

38. Nicholas, Theodore. "Tensile Testing of Materials at High Rates of Strain". *Experimental Mechanics*, 1981.

39. Oi, K. "Transient response of bonded strain gauges". *Experimental Mechanics*, 6(9):463, 1966.

40. P. Landrien, L. Guillaumat, T. Lorriot. "Influence of some test parameters on specimen loading determination methods in instrumented Charpy impact tests". *Engineering Fracture Mechanics*, 2001.

41. Perry, C.C. and H.R. Lissner. *The Strain Gage Primer.* McGraw-Hill Book Company, second edition, 1962.

42. Poormon, Kevin. *Measurement Equipment for Impact Testing.* University of Dayton Research Institute, 2007. Personal correspondence.

43. P.R. Sreenivasan, S.L. Mannam P. Rodriquez, S.K. Ray. "Dynamic fracture toughness and Charpy Impact properties of an AISI 403 martensitic stainless steel". *Journal of Nuclear Materials*, 1996.

44. Reid Larson, Rachel DeRoche. *Slot Design for Slotted Beam Specimen.* Air Force Insitute of Technology, 2007. Personal correspondence.

45. Richard S. Figliola, Donald E. Beasley. *Theory and Design for Mechanical Measurements.* John Wiley and Sons, Inc., third edition, 2000.

46. Saada, Adel S. *Elasticity: Theory and Applications.* Krieger Publishing Company, 1993.

47. Sahraoui, S. and J.L. Lataillade. "Analysis of load oscillations in instrumented impact testing". *Engineering Fracture Mechanics*, 1998.

48. Scott, K. and A. Owens. *Strain Gauge Technology.* Applied Science Publishers, 1982.

49. Shames, Irving H. and Francis A. Cozzarelli. *Elastic and Inelastic Stress Analysis.* Taylor and Francis, 1997.

50. Soboyejo, Wole. *Mechanical Properties of Engineered Materials.* Marcel Dekker, Inc, 2003.

51. Sturges, J.L. and B.N. Cole. "The flying wedge: A method for high-strain-rate tensile testing. Part 1. Reasons for its development and general description". *International Journal of Impact Engineering*, 2001.

52. Ulicny, Tom. *Errors due to Gage Transverse Sensitivity*. Stress Analysis Services, 2007. Personal correspondence.

53. Vishay Micro-Measurements. *The Proper Use of Bondable Terminals in Strain Gage Applications, Application Note TT-603*, April.

54. Vishay Micro-Measurements. *Strain Gage Soldering Techniques, Application Note TT-609*, March.

55. Vishay Micro-Measurements. *High-Elongation Strain Measurements Elongation Technical Note 605*, April 2007.

56. Vishay Micro-Measurements. *Errors due to Transverse Sensitivity in Strain Gages, Technical Note 509*, 9 April 2007.

57. Vishay Micro-Measurments. *Introduction to Digital Signal Processing, Technical Note 517*, August 2007.

58. Vishay Micro-Measurments. *Strain Gage Selection: Criteria, Procedures, Recommendations, Technical Note 505*, April 2007.

59. Wen Huang, Xu Nie Ming Gong Yang Wang Yuanming Xia, Xiang Zan. "Experimental study on the dynamic tensile behavior of a poly-crystal pure titanium at elevated temperatures". *Material Science & Engineering*, 2006.

Vita

Hugh Gardenier was born in Houston, TX and raised in The Woodlands, TX until 1997, when he graduated from The Woodlands High School. Having earned a scholarship, he attended New Mexico Military Institute, where he applied and was accepted to the United States Air Force Academy. At the Academy he earned his Bachelors of Science in Engineering Mechanics with a minor in Mathematics. Upon graduation from the Air Force Academy, he was commissioned into the United States Air Force as a Second Lieutenant with the Air Force Specialty Code of Developmental Engineer. He reported to Wright-Patterson AFB for his first assignment in the Summer of 2002, where he began work in the Propulsion SPO on the USAF Reliability Centered Maintenance Program. In the Summer of 2004, he moved to the Training System SPO where he took on the responsibilities of Test Engineer for the B-1 and B-2 Training Systems Programs. In 2006, he applied and was accepted to the Air Force Institute of Technology to earn his master's degree in Aeronautical Engineering. After graduating from AFIT, Capt Gardenier will be moving to Kirtland AFB to begin work at the Air Force Research Laboratory.

Permanent address: 2950 Hobson Way
Air Force Institute of Technology
Wright-Patterson AFB, OH 45433

REPORT DOCUMENTATION PAGE

Form Approved
OMB No. 0704–0188

1. REPORT DATE (DD–MM–YYYY)	2. REPORT TYPE	3. DATES COVERED *(From — To)*
17–03–2006	Master's Thesis	Mar 2007 — Mar 2008

4. TITLE AND SUBTITLE

An Experimental Technique for Developing Intermediate Strain Rates in Ductile Metals

5a. CONTRACT NUMBER

5b. GRANT NUMBER

5c. PROGRAM ELEMENT NUMBER

6. AUTHOR(S)

Hugh E. Gardenier IV, Capt, USAF

5d. PROJECT NUMBER

5e. TASK NUMBER

5f. WORK UNIT NUMBER

7. PERFORMING ORGANIZATION NAME(S) AND ADDRESS(ES)

Air Force Institute of Technology
Graduate School of Engineering and Management (AFIT/EN)
2950 Hobson Way
WPAFB OH 45433-7765

8. PERFORMING ORGANIZATION REPORT NUMBER

AFIT/GAE/ENY/08-M10

9. SPONSORING / MONITORING AGENCY NAME(S) AND ADDRESS(ES)

AFRL/RBSM
2790 D Street, Bldg 65
WPAFB, OH 45433

10. SPONSOR/MONITOR'S ACRONYM(S)

11. SPONSOR/MONITOR'S REPORT NUMBER(S)

12. DISTRIBUTION / AVAILABILITY STATEMENT

APPROVED FOR PUBLIC RELEASE; DISTRIBUTION UNLIMITED

13. SUPPLEMENTARY NOTES

14. ABSTRACT

Quantifying the strain-rate sensitive dynamic properties of structural materials is an important area of research in the solid mechanics field. Property evaluation is typically accomplished using dynamic tests which involve rapid loading or impact of specimens. In these tests, inertial forces and wave propagation make it difficult to accurately record the material response to a loading condition at an equivalent location. Furthermore, these tests typically generate high strain rates (in excess of 10^3 s^-1 and an experimental method for generating rates of strain in the intermediate strain rate regime which is relatively simple, low cost, and reliable is still lacking. This research effort develops an experimental technique for generating tensile plastic strain rates up to 10^2 s^-1 in ductile metals. The technique relies on an impact from a load cell instrumented drop weight machine capable of delivering a suitable impact velocity and energy to globally deform a slotted beam specimen. At impact, a state of plastic uniaxial tensile stress is created in the ligament underneath a slot. The ligament is instrumented with an electrical-resistance strain gauge, and the strain history from the gauge is measured and stored in a digital oscilloscope. The Johnson-Cook constitutive equation is assumed to reflect the material behavior and its parameters are determined through a matching of the experimental strain history with a finite element simulation.

15. SUBJECT TERMS

Impact, Elastic-Viscoplasticity, Elevated Strain Rates, Strain Gage, Transverse Impact of Beams, Ductile Metals, Wave Propagation, Drop Weight Impact Testing, Constitutive Modeling, Finite Element Modeling

16. SECURITY CLASSIFICATION OF:			17. LIMITATION OF ABSTRACT	18. NUMBER OF PAGES	19a. NAME OF RESPONSIBLE PERSON
					Dr. Anthony N. Palazotto
a. REPORT	b. ABSTRACT	c. THIS PAGE	UU	194	19b. TELEPHONE NUMBER (Include Area Code) (937) 255-3636, ext 4599; e-mail: Anthony.Palazotto@afit.edu
U	U	U			